The Design and Analysis of a Large Angular Range, Two-Axis Flexure Assembly

by

Barry A. Gin

SUBMITTED TO THE DEPARTMENT OF
MECHANICAL ENGINEERING
IN PARTIAL FULFILLMENT OF THE REQUIREMENTS
FOR THE DEGREES OF

MASTER OF SCIENCE IN MECHANICAL ENGINEERING

and

BACHELOR OF SCIENCE IN MECHANICAL ENGINEERING

at the

MASSACHUSETTS INSTITUTE OF TECHNOLOGY

February, 1988

Signature of Author_____
Department of Mechanical Engineering
February, 1988

Certified by_____
Professor Igor Paul
Thesis Supervisor

Accepted by_____
Professor Ain Ants Sonin
Chairman, Department Graduate Committee

Exhibit C

ENGINEERING INTERNSHIP PROGRAM

SCHOOL OF ENGINEERING

MASSACHUSETTS INSTITUTE OF TECHNOLOGY

Cambridge, Mass. 02139

THESIS REVIEW LETTER

Attention: John R. Martuccelli, Director, Room 1-211

Subject: Master's Thesis of Barry A. Gin
(student name)

The attached thesis, The Design and Analysis of a Large Angular Range, Two-Axis Flexure Assembly.
(Title)

has been reviewed by the undersigned Hughes Aircraft Company
(company name)

representatives and confirmed that it does not contain details objectionable from the standpoint of Hughes Aircraft Company.
(company name)

In addition, we understand that the aforementioned thesis report becomes the permanent property of M.I.T., will be placed in the M.I.T. Library within one month of the date of submission and may not be published wholly or in part except by authorization of the Department of Mechanical Engineering,
(department name)

in which the student is enrolled. (It is understood that authorization is granted to the Company for such limited publication as the Company's prior contractual obligations may require.)

Hughes Aircraft Company

Company Name

Direct Company Supervisor of Student

Student Name

Approved By (for company)

Title:

Date: 1/25/88

Date:

Date: 25 JAN 1988

The Design and Analysis of a Large Angular Range, Two-Axis Flexure Assembly

by

Barry A. Gin

Submitted to the Department of Mechanical Engineering in partial fulfillment of the requirements for the degrees of Bachelor of Science and Master of Science in Mechanical Engineering

ABSTRACT

A new concept for a large angular range, two-axis flexure assembly using a crossed-leaf approach was designed. It was to be a brazed assembly that would be able to have a high stiffness about its axial axis as well as in translation along all three axes, yet be rotationally soft about its radial axes. The flexure was to have an angular range of 87 mrad and was designed to meet the requirements of an application at Hughes Aircraft Company in El Segundo, California.

After a materials study, three prototypes were fabricated out of PH 13-8 Mo Stainless Steel, assembled using a two-step braze process and heat treated to obtain optimum strength and ductility.

The prototypes were tested for stiffnesses about the radial axes, hysteresis, and fatigue life and the results compared to the performance predictions. The stiffnesses ranged from 3.69 in-lbs/rad to 4.67 in-lbs/rad, compared to 4.21 in-lbs/rad theoretical stiffness. The maximum hysteresis obtained was approximately 2 mrad. The one flexure that was fatigue tested had one blade fail after 400,000 cycles, suggesting that there were either eccentricities in the test setup or deterioration of mechanical properties due to the heating and cooling cycles of the brazing and heat treating processes.

Thesis Supervisor: Prof. Igor Paul
Title: Associate Professor of Mechanical Engineering

Acknowledgements

There were many people who enabled me to complete this project. I would like to take this opportunity to give special thanks to the following:

- Robert Fairbanks of Scarrott Metallurgical Company, whose extreme generosity with his time and the facilities at Scarrott enabled me to get the flexures brazed and heat treated.
- John Harrell, my company thesis supervisor, whose guidance, ideas and advice was invaluable. Working with him was a great learning experience for me.
- Tom Pavliscak and Dave Hiley, the managers of the Mechanical Engineering Laboratory, for their encouragement and support. I would also like to thank Dave Hiley for the work he did in developing the equations in Chapter 3.
- Dave Goulding, Don Mannas, and Dave Bronson, engineers and scientists at Hughes, for their technical support and suggestions.
- Jeff Barina, a co-worker who was a great help in selecting the materials, coming up with ideas, and solving problems.
- Allison Sheridan, my officemate, who was always more than willing to offer her assistance with the project and the computer problems and questions I had.
- The guys down in the machine shop and the Precision Mechanisms laboratory, who machined all of the parts and were really helpful in getting the tests set up.
- My roommates, Nelson and Steve, who provided me a home away from home.
- Rich, Howard, Wallace, and Ron, who kept me spiritually minded during my time out here.
- Ivan, Dickson, Bob, Melissa, and Paul C., great friends who really reached out to me during the rough times.
- My parents, whose constant love, prayers and encouragement have always kept me going.
- My Lord and Savior Jesus Christ, who made all of this possible. This thesis is dedicated to Him and is for His Glory.

Table of Contents

List of Figures

List of Tables

CHAPTER 1
Introduction

1.1 Background

In many aerospace precision mechanisms, a variety of applications call for the use of flex pivots. These pivots basically are mechanisms which allow a driven mass to flex about one or more axes of rotation. Many kinds of springs would be able to serve this purpose about one axis of rotation. One such spring is the cross-leaf flexure, which consists of two leaves, or blades, arranged in an 'X' configuration. One side of the 'X' is connected to ground while the other side is attached to the flexing element, which theoretically pivots about the axis created by the intersection of the two blades. A significant advantage to using the cross-leaf spring is that there is no sliding or rubbing contact between the members. Because of this, there is absolutely no wear of parts due to friction, and no lubrication is necessary. Another advantage is the insensitivity of these flexures to contamination. In other types of assemblies where ball bearings are used, cleanliness and careful alignment are required in order for the flexure to operate properly. With the cross-leaf flexures, tolerances do not have to be as tight, and cleanliness of the parts and their operating environment are not as critical.

A single-axis flexural pivot bearing using the same principles as the cross-leaf spring has been developed and marketed by the Bendix Corporation. These pivots basically consist of concentric, cylindrical members interconnected by a cross-leaf spring (Fig. 1.1). It is a brazed assembly using a 410 CRES housing and 420 CRES blades. The blades

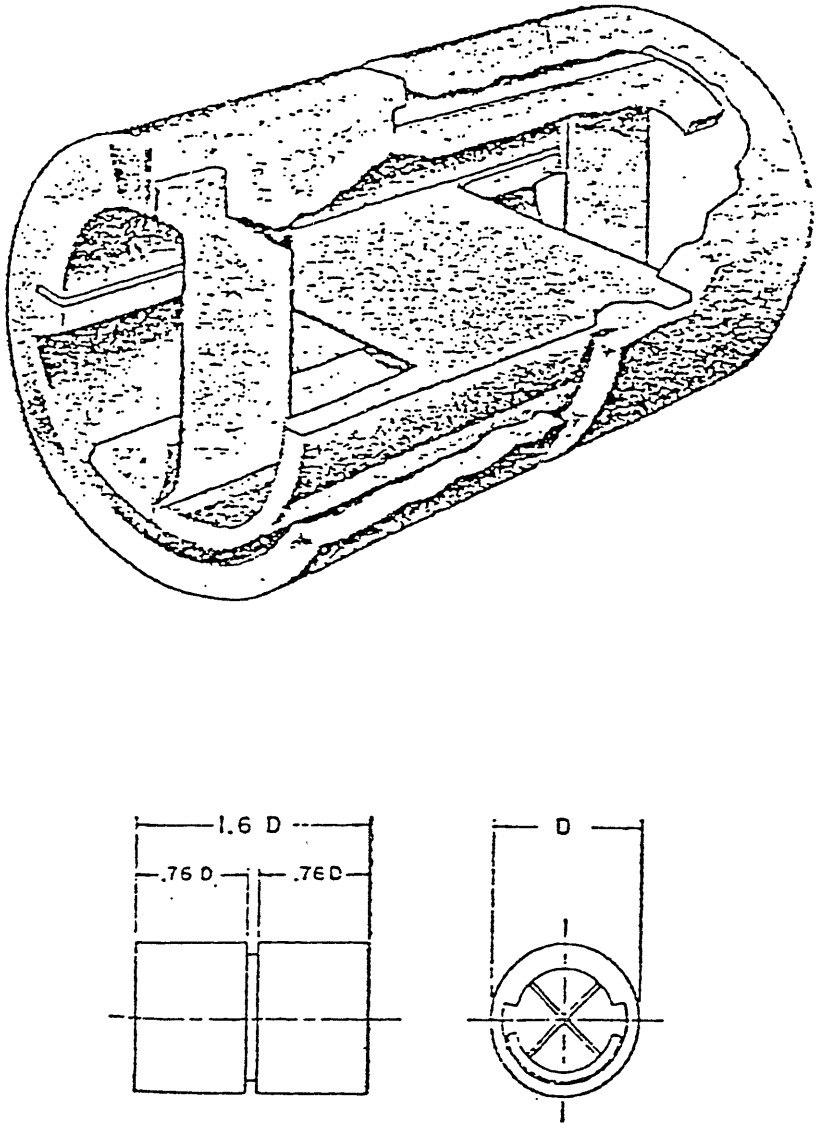

Figure 1.1 - Bendix Flex Pivot
(Reprinted from "Considerations in the Applications of Flexural Pivots," *Automatic Control*, November, 1962, p. 41

come in varying thicknesses, and thus, various spring rates can be attained. Depending on the blade thickness, these pivots can have an angular range as high as ±30° and an elastic deflection range of ±10°.

Because these springs are only capable of flexing about one axis of rotation, four of them must be used to construct a two-axis flexure, which is much more complicated than a single-axis flexure. A two-axis flexure, as the name implies, enables a driven mass to pivot about two axes. Many of the applications in the aerospace industry call for other requirements which are rather difficult to meet. These requirments include a sufficient angular range, a high axial stiffness while having a relatively low radial stiffness, high translational stiffnesses along all three axes, as well as certain natural frequency requirements, infinite fatigue life, and a high g-load carrying capacity. Four Bendix flexures would likely be able to meet most of these requirements of a two-axis flexure. This four flexural pivot design, however, would be quite expensive because it would require a number of parts that would have to be aligned and pinned with a high degree of precision. Fasteners for this type of arrangement would be rather bulky and take up space. Since aerospace precision mechanisms are required to be of minimal size and weight, this type of configuration would not be ideal.

The two-axis elliptical post flexure (Fig. 1.2) is one type of two-axis flexure which has been commonly used for several applications. Its main flexing element is a post machined out of titanium. An elliptical curve is machined out of this post such that the smallest cross-sectional area is in the middle. This is done to minimize any stress concentrations at the interfaces. The flexure is able to pivot in this middle section about two axes. An S-bar, which is a flat ring

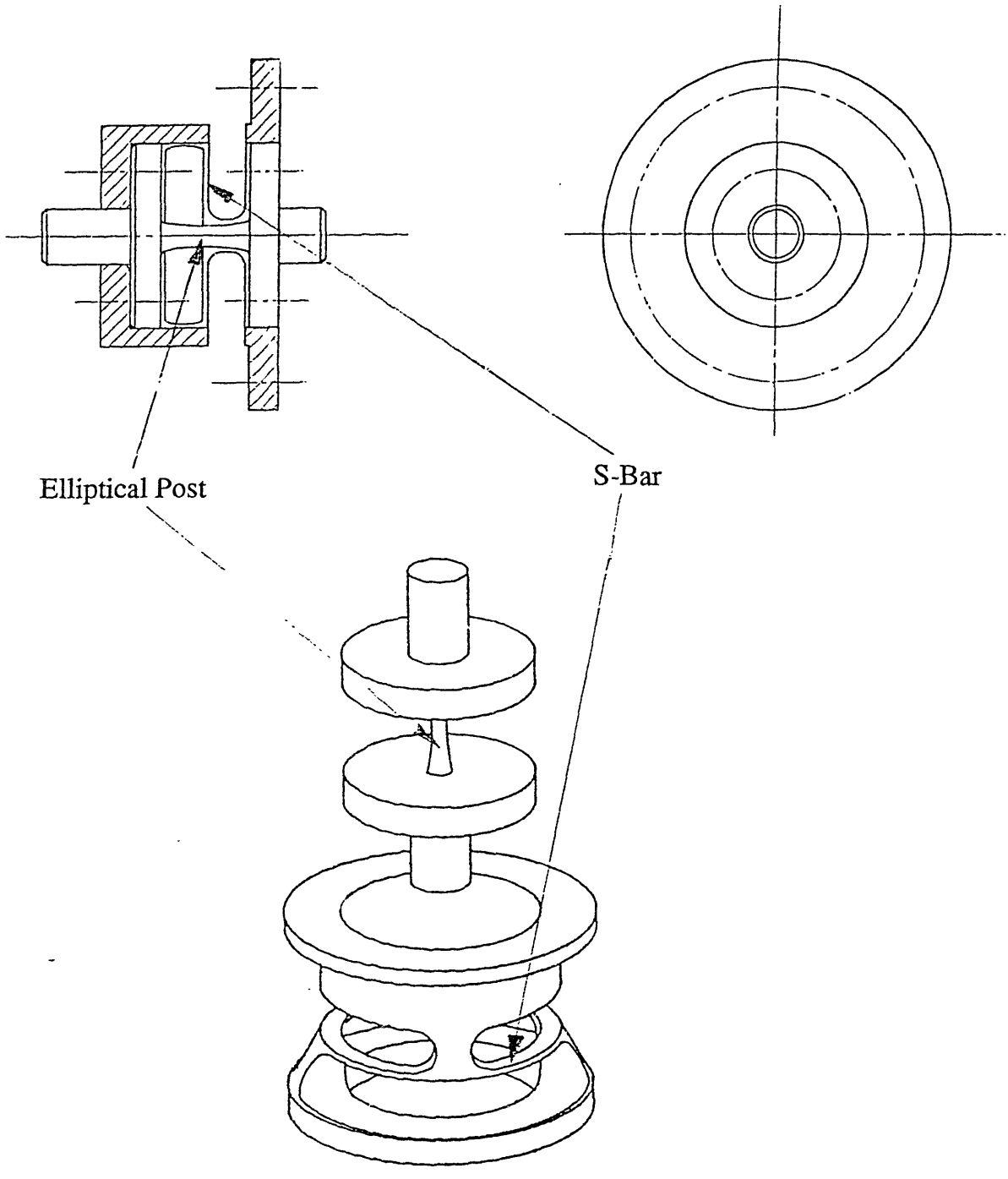

Figure 1.2 - Elliptical Post Flexure with S-Bar

circling the post and connected to the opposing elements, keeps the flexure from pivoting about the axial axis. This ring is thin so that it does not add significant stiffness to the axes about which the flexure is to pivot. The axial compressive strength of the post keeps the flexure stiff in translation along the axial axis, and both the S-bar and the post contribute to the stiffness along the radial axes. The elliptical post with S-bar has several advantages. Like the cross-leaf, single-axis flexures, it has low friction and hysteresis, a low predictable spring rate, a relatively simple design, and quantities such as stiffnesses and stresses which are easy to analyze.

There are, however, several disadvantages to the elliptical post flexure. First of all, it is quite limited in angular rotation, having a maximum angular travel of about ±5 mrad. Some applications require an angular travel of about ±90 mrad, almost 15 times the maximum travel of the elliptical post. Another major disadvantage is the manufacturing complexity and high cost. Because of its shape, the elliptical cross-section is rather difficult to machine. The assembly must be heat treated to give it maximum strength, and then hand polished to a very high finish because surface defects would shorten the fatigue life.

Because of the shortcomings of the four flexural pivot design and the elliptical post with S-bar flexure, as well as new applications being proposed requiring multi-degree angular travel, a new concept for a two-axis flexure is desired. Such a flexure would need to maintain the compact packaging of the elliptical post flexure, have the low stiffness capability and large angular range of the four flexural pivot design, yet still maintain simplicity in design and be inexpensive to manufacture.

A concept for a large angular range, two-axis flexure assembly meeting the above requirements has been proposed. It works basically on the same principle as the cross-leaf pivots, yet does not take up the large amount of space that would be needed if the Bendix flexure pivots were used. This concept should also have much better stiffness and natural frequency characteristics than do the previous concepts. Another advantage is that it should not be as difficult to manufacture as the elliptical post flexure.

A prototype of this concept was designed, fabricated, and tested to analyze its performance characteristics and ease of fabrication. Quantities such as stiffnesses, natural frequencies, and fatigue life were to be analyzed to see whether or not this new concept was practical and able to meet its intended requirements.

CHAPTER 2

A Description of the Design

2.1 Basic Concept

An isometric drawing illustrating the basic components of the design as initially proposed is shown in Figure 2.1. It is comprised of four basic elements; the top frame, the middle frame, the bottom frame, and the blades. The bottom frame is grounded to a stationary platform. The driven mass is attached by four bolts to the middle frame. This frame piece is the pivoting element of the flexure, and is able to flex about the x and y axes. Slots are cut into these two frame pieces, and two pairs of blades, which are the flexing elements, are brazed into these slots. The other ends of these blades are brazed into the top frame, which holds the entire assembly together.

The middle frame is able to pivot freely about the y axis using the set of blades which attach it to the top frame as the flexing elements. When this happens, the top frame is held stationary by the blades attaching it to the bottom frame. However, when the middle frame pivots about x, the blades attaching it to the top frame move the top frame along with it, and the blades attaching the top frame to the bottom frame are the flexing elements. Theoretically, the pivoting about x is independent of the pivoting about y.

Because of the arrangement of the blades in this configuration, the flexure should be rotationally soft about the x and y axes. It should, however, be quite stiff in rotation about the z axis as well as in translation. These quantities will be analyzed in a later section.

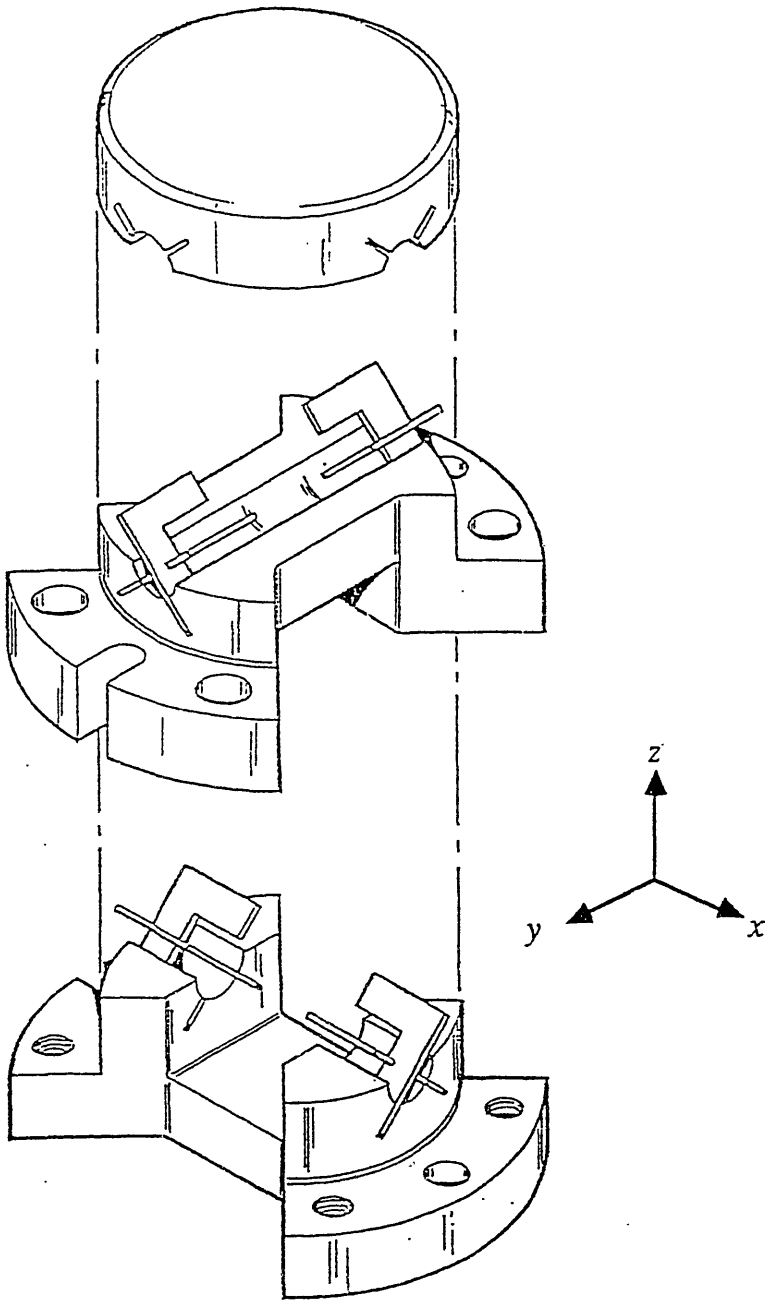

Figure 2.1 - Exploded Isometric View of the Concept

There are several advantages to this concept. First of all, it is simple in design. There are only four unique parts to the design, all which are rather simple in form and can be easily machined. Another advantage is that it can be made out of a low cost material, such as 410 CRES or another high strength stainless steel. Since it is a brazed assembly, it requires no mechanical fasteners, which tend to wear or loosen over a period of time. Like the elliptical post flexure, it is a very compact package, yet can have the large angular range that many of the new applications require. Because of these advantages, this new concept would be very superior to the existing flexures.

2.2 Basic Fabrication and Assembly

One major limitation to the initial concept illustrated in Fig. 2.1 was the difficulty in cutting the slots into which the blades were to be brazed. Since alignment of the blades with respect to the axis about which they flex as well as the alignment of the two opposing slots for each individual blade was very important, attaining the tolerances required in these slots would have been a rather slow, difficult, and expensive process. A solution to this problem was proposed and implemented. Instead of cutting these slots into the main frame pieces, these slots would be cut into a jigging tube, which is illustrated in Figure 2.2. A single pass with a slitting saw would be able to make the two slots necessary for one blade while another pass would make the two slots necessary for the other blade. Once this was done, the blades would be brazed into these slots as shown in Fig. 2.3. After this process, four of these blade and jig assemblies would be brazed into the frame pieces as illustrated in Fig. 2.4. Once the entire assembly was

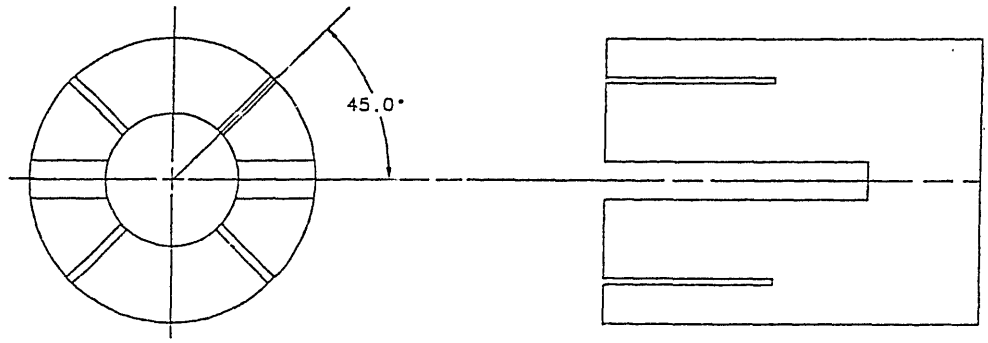

Figure 2.2 - Jigging Tube

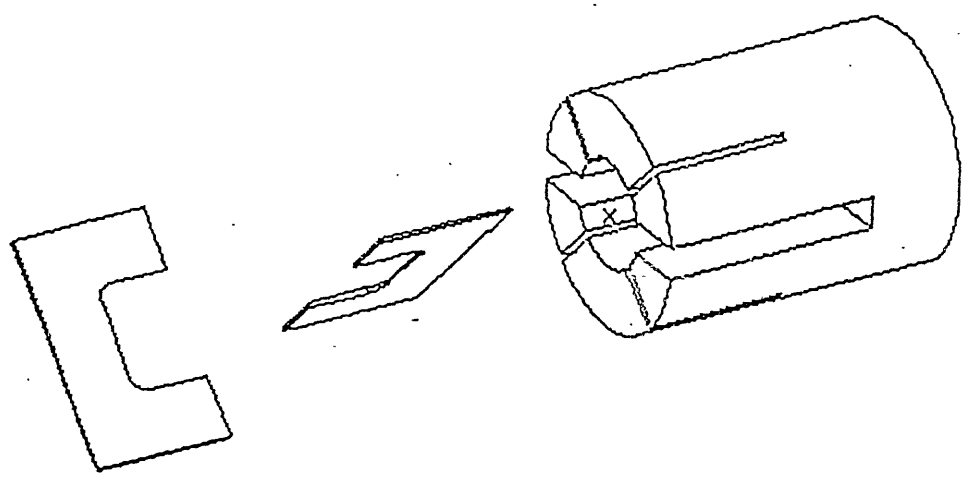

Figure 2.3 - Brazing of the Blades into the Jig

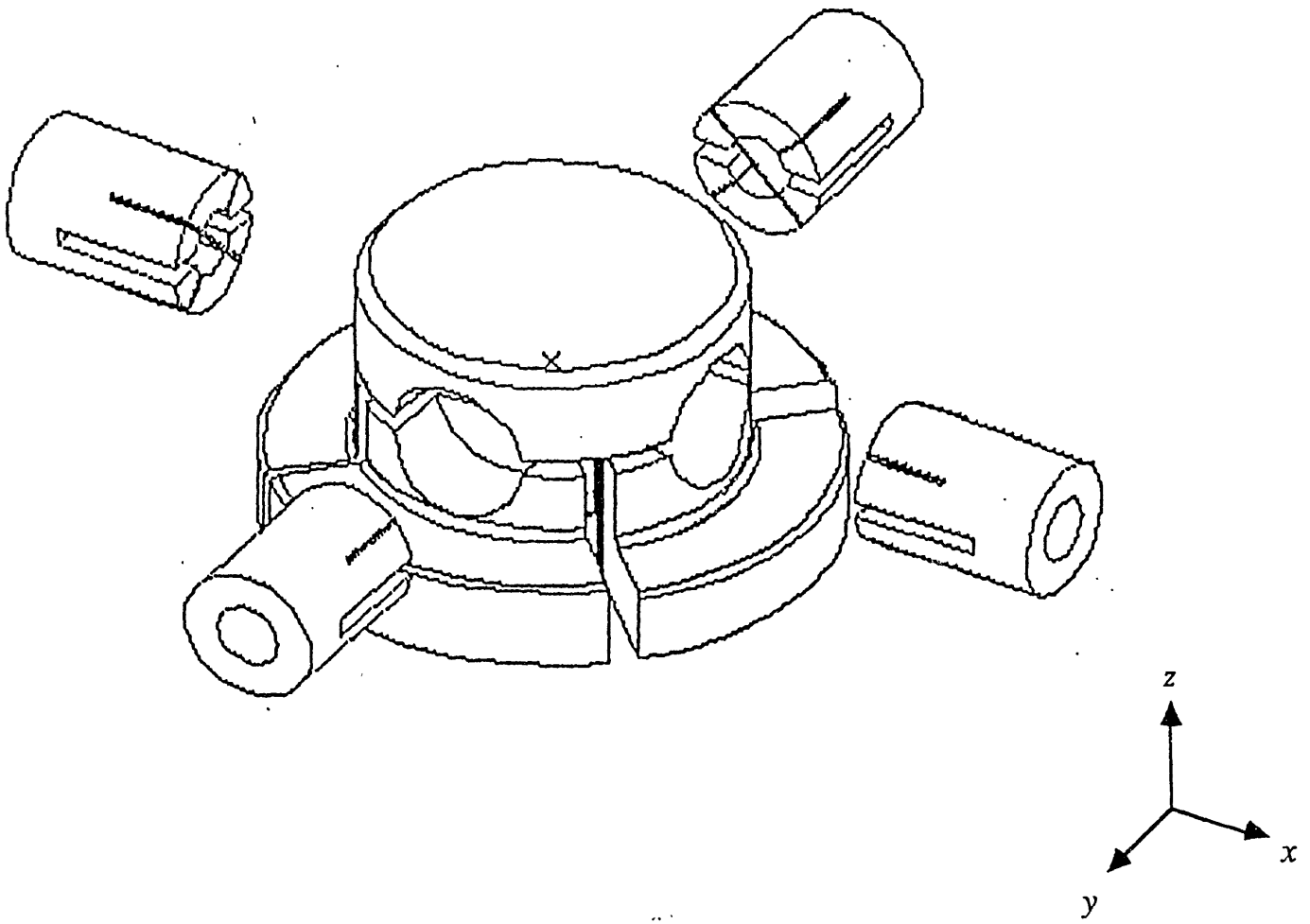

Figure 2.4 - Brazing of the Jig Assemblies into the Frame Pieces

heat treated, the protruding portion of the jigs would be machined off, resulting in the finished assembly (Fig. 2.5). The advantage of using such a two-step braze process was that should one of the blade and jig assemblies fail to align properly or obtain a good braze joint, the fault could be detected and the defective blade and jig assembly easily discarded and replaced without ruining the entire assembly. Hence, there would be a much better chance of getting quality flexures without any defects because good blade alignment and braze joints are assured.

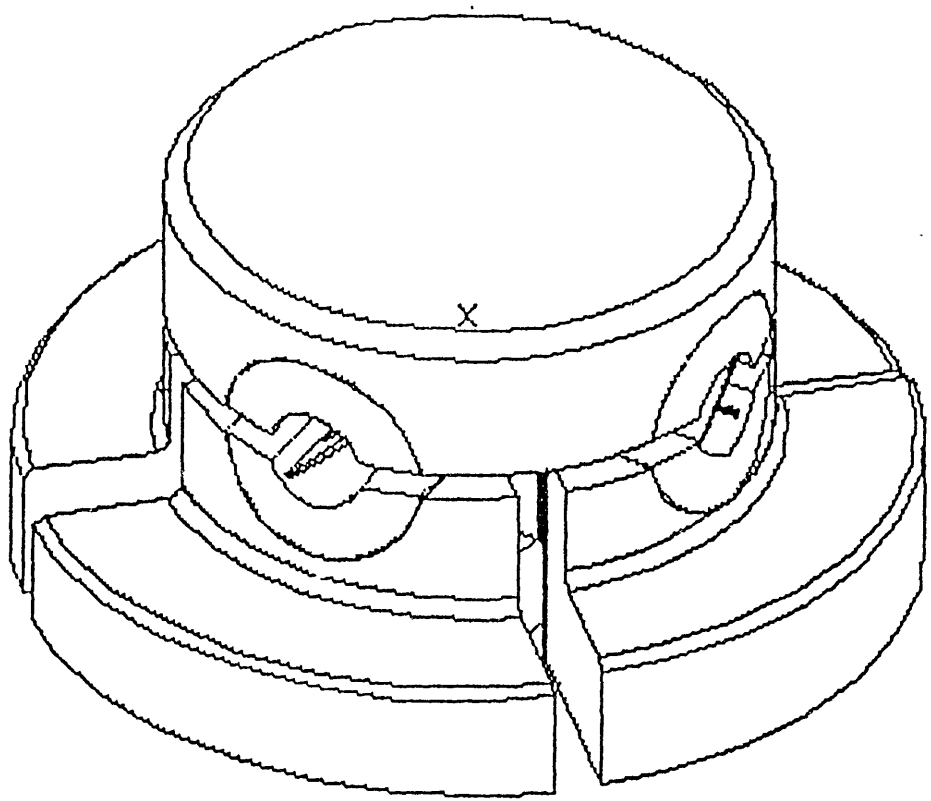

Figure 2.5 - Completed Assembly After Machining Off Protruding Ends of Tubes

CHAPTER 3

Cross-Leaf Flexure Theory

Most of the analysis for the two-axis cross-leaf flexure can be done using beam theory for small deflections. To obtain performance predictions for the two-axis flexure, the equations from beam theory can be applied to a single pair of leaves, or blades, then these results applied to a pair of springs about one axis, and finally, the results from a pair of springs used to obtain predictions on performance for two pairs of springs about two axes.

3.1 Single Pair of Blades About One Axis

For a single pair of blades, as shown in Figure 3.1, the rotational stiffness about the x axis is determined by the following equation:

$$k_{\theta x} = \frac{2EI}{l} \tag{3.1}$$

where E is the elastic modulus of the material, I is the moment of inertia ($bt^3/12$), and l is the length of the leaf. By substituting in for the moment of inertia, the following expression is obtained:

$$k_{\theta x} = \frac{Ebt^3}{6l} \tag{3.2}$$

where b is the width of the blade and t is its thickness.

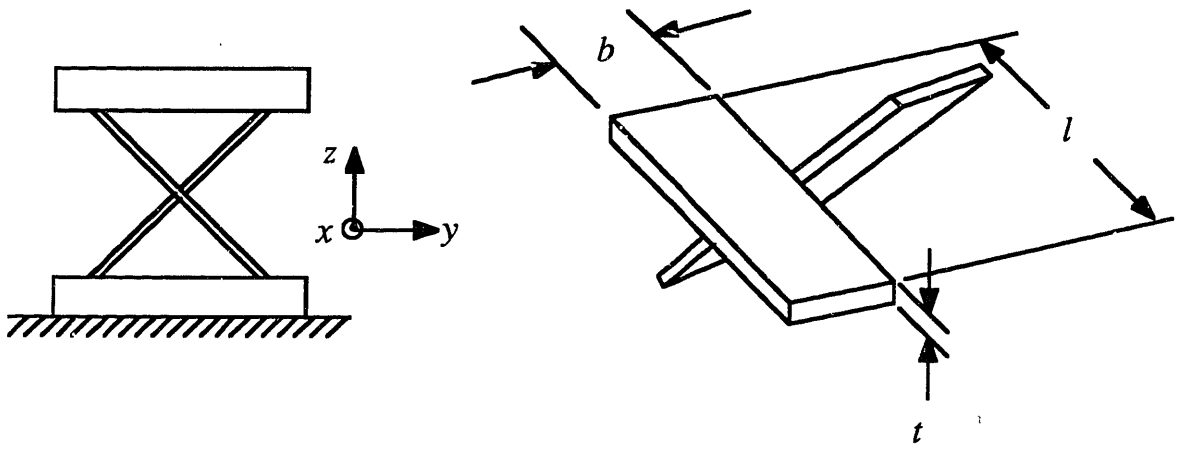

Figure 3.1 - A Single Pair of Blades

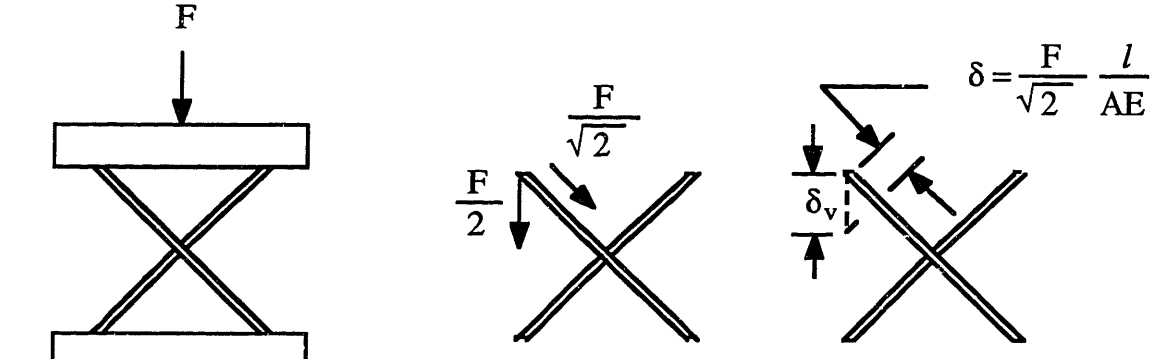

$$\delta_v = \sqrt{2}\,\delta = \frac{Fl}{AE}$$

$$k_v = \frac{F}{\delta_v} = \frac{AE}{l}$$

$$k_v = \frac{Ebt}{l}$$

Figure 3.2 - Vertical Translational Stiffness Assuming Small Deflections

By assuming small deflections, the translational stiffness along the z axis is found to be (Fig. 3.2):

$$k_z = \frac{Ebt}{l} \tag{3.3}$$

When determining the stiffness of the pair of blades along the x axis, both the shear stiffness of the blades as well as their bending stiffness must be taken into account. By combining equations for shear stress and strain, the shear displacement along the x axis due to a load F applied on the top of the blades in the x direction is:

$$\delta_s = \frac{Fl}{Gbt} \tag{3.4}$$

where G is the shear modulus of the blade material. The bending displacement due to the same applied force is:

$$\delta_b = \frac{Fl^3}{Etb^3} \tag{3.5}$$

By combining these displacements, the total stiffness along the x axis for two blades becomes:

$$k_x = \frac{2Gbt}{l}\left[\frac{1}{1 + \frac{G}{E}\left(\frac{l}{b}\right)^2}\right] \tag{3.6}$$

The critical buckling load due to a force in the z direction can be determined using the model for a simple cantilever beam with both ends fixed. This quantity is determined by the following:

$$F_{cr} = 4\pi^2 \frac{EI}{l^2} \tag{3.7}$$

A force F in the z direction gives a resultant compressive force of $F/\sqrt{2}$ along the axis of the blade. A force in the y direction will result in this same force acting on one of the blades. Therefore, by substituting this into Eq. 3.7 and substituting in the variables for the moment of inertia, the critical buckling load along the z axis becomes:

$$F_{cr_{y\,z}} = \frac{\sqrt{2}\pi^2 E b t^3}{3l^2} \tag{3.8}$$

The critical load along the x axis can be determined using the lateral buckling load for a beam in bending under the condition that both ends are fixed. This equation can be found in *Strength of Materials* by F. R. Shanley. For one beam, the critical lateral buckling load is:

$$F_{x\,cr} = 0.6413 \frac{E b t^3}{l^2} \; * \tag{3.9}$$

If we assume that the loads are equally shared by both blades in the spring, then the critical load can be doubled. Therefore, the critical

---

* F. R. Shanley, *Strength of Materials*, McGraw-Hill Book Company, Inc., New York, 1957, pp. 624-626.

load for a pair of blades becomes:

$$F_{x\,cr} = 1.2826\,\frac{Ebt^3}{l^2} \tag{3.10}$$

Another important quantity in the analysis of the flexure is the bending stresses due to flexing. If the top component of the flexure blades flexes an angle ϕ, then the resulting maximum bending stress at the middle of the blade is:

$$\sigma = \frac{\phi E t}{2l} \tag{3.11}$$

3.2 Two Pairs of Blades About One Axis

Since the equations for a single pair of blades about one axis have already been derived, the equations for two pairs of blades about the same axis is a rather simple process. One can obtain the stiffnesses of this system by treating the two pairs of blades as two springs in parallel. Since the stiffnesses of two springs in parallel add, the resultant stiffnesses of this two pair configuration are double the stiffnesses of a single pair of blades. Assuming symmetry of loading, the buckling loads are also doubled because there are twice as many members resisting the forces applied. The only quantity that does not change is the bending stress due to rotation about the x axis, which is only dependent upon ϕ and independent of the number of blades used. Hence, for a single axis pair of springs, the performance characteristics are governed by the following equations:

Stiffness about the x axis:

$$k_{\theta x} = \frac{Ebt^3}{3l} \tag{3.12}$$

Translational stiffness along the x axis:

$$k_x = \frac{4Gbt}{l}\left[\frac{1}{1 + \frac{G}{E}\left(\frac{l}{b}\right)^2}\right] \tag{3.13}$$

Translational stiffness along the y and z axis:

$$k_{y,z} = \frac{2Ebt}{l} \tag{3.14}$$

Critical load along the x direction:

$$F_{x\,cr} = 2.56\,\frac{Ebt^3}{l^2} \tag{3.15}$$

Critical loads along the y and z directions:

$$F_{cr_{y\,z}} = \frac{2\sqrt{2}\pi^2 Ebt^3}{3l^2} \tag{3.16}$$

Bending stress due to rotation about the x axis:

$$\sigma = \frac{\phi Et}{2l} \tag{3.17}$$

3.3 Two Pairs of Springs About Two Axes

For the two-axis flexure using two pairs of springs (or four pairs of blades) in the configuration shown in Fig. 2.1, the system can be modeled as two springs in series when determining the translational stiffness along the x or y axis. The reasoning behind this is that a force acting on the middle frame is transmitted first to the top frame by the blades connecting these two pieces. This in turn is transmitted to the bottom frame by the blades connecting the top to the bottom frame. Therefore, the translational stiffness of two pairs of blades along the x axis (Eqn. 3.13) is put in series with the translational stiffness of two pairs of blades along the y axis (Eqn. 3.14). The resulting translational stiffness of the flexure along the x and y axis becomes:

$$k_x = k_y = \frac{4Ebt}{l}\left[\frac{1}{2 + \frac{E}{G} + \left(\frac{l}{b}\right)^2}\right] \tag{3.18}$$

For the rotational stiffness about the z axis, the system can also be modeled as two springs in series. This quantity is found by using the translational stiffness in the y direction from Eqn. 3.14, which will now be called the lateral stiffness k_l. By definition, the stiffness about the z direction is:

$$k_{\theta z} = \frac{M}{\theta} = \frac{Fa}{\theta} \tag{3.19}$$

where M is the applied moment, which is equal to the applied force F times the nominal distance from the center a, and θ is the angular

deflection about z. For small deflections:

$$\theta = \frac{\delta}{a} \tag{3.20}$$

and by substituting this into Eqn. 3.19, the following is obtained:

$$k_{\theta z} = \frac{F}{\delta} a^2 \tag{3.21}$$

In linear translation, F/δ is the lateral stiffness k_l. Therefore, by substituting this into Eqn. 3.21 and taking two of these springs in series, the rotational stiffness about the z axis is:

$$k_{\theta z} = \frac{Ebta^2}{l} \tag{3.22}$$

Similarly, the translational stiffness of the entire assembly along the z axis can also be determined by modeling the system as two springs in series, using the translational stiffness in the z direction. Thus, for the entire assembly, the translational stiffness along this axis is:

$$k_z = \frac{Ebt}{l} \tag{3.23}$$

Table 3.1 is a summary of all the equations described above for a two-axis flexure. From these equations, all of the quantities necessary in predicting the performance of this two-axis flexure can be obtained.

Table 3.1 - Performance Equations for a Two-Axis Flexure Assembly

Rotational Stiffness About x and y	$k_{\theta x} = k_{\theta y} = \frac{Ebt^3}{3l}$
Rotational Stiffness About z	$k_{\theta z} = \frac{Ebta^2}{l}$
Translational Stiffness Along x and y	$k_x = k_y = \frac{4Ebt}{l}\left[\frac{1}{2 + \frac{E}{G} + \left(\frac{l}{b}\right)^2}\right]$
Translational Stiffness Along z	$k_z = \frac{Ebt}{l}$
Critical Axial Load	$F_{cr_{yz}} = \frac{2\sqrt{2}\pi^2 Ebt^3}{3l^2}$
Critical Lateral Load	$F_{x\,cr} = 2.56\,\frac{Ebt^3}{l^2}$
Bending Stress Due to Rotation about x and y	$\sigma = \frac{\phi Et}{2l}$

CHAPTER 4

Design Development

4.1 Requirements Study

There were several projects at Hughes Aircraft Company which called for the use of these two-axis flexures. The angular range requirements of these applications ranged from ±13 to ±87 mrad, while the weight of the driven masses varied from 1.8 lbs. to 36 lbs. There were various other criteria that were given, including natural frequencies, critical loads, and size requirements. A comparison study was done to determine which application the prototype was to be designed. After some preliminary analysis, it was recommended that the prototype be designed to meet the requirements of the application that required the highest angular range. This application was chosen for several reasons. First of all, a high angular range was one of the most important features of this two-axis concept. Therefore, since the angular travel requirements of this application were roughly six times that of the others, designing the flexure to meet this requirments would give a much better picture of the capabilities of this design. Secondly, there were other shortcomings to the other applications which would have made the flexure more difficult to test or to assemble. One application had a driven mass weighing almost 40 lbs., which would have made the assembly and testing more difficult. Another application would have also been more difficult to assemble because it was determined that the blade lengths that would be required would have to be less than 0.10" in length.

Table 4.1 shows a summary of the parameters and requirements of the chosen application.

Table 4.1 - Application Parameters and Requirements

Flexure Diameter	1.00 in
Weight of Driven Mass	1.81 lbs
I_{xx} , I_{yy}	0.038 in-lbs-sec^2
I_{zz}	0.074 in-lbs-sec^2
Angular Travel	± 87 mrad (± 5°)
Natural Rocking Frequency About x and y	< 10 Hz
Natural Frequency about z	40 Hz
Lateral Natural Frequency	550 Hz
Axial Natural Frequency	550 Hz

4.2 Material Selection

The critical element of these flexures was the flexing elements, or the blades. It was important that these blades be made of a material that would be able to flex the required angles and have an infinite life when implemented. It also would have to be strong enough to support the weight of the driven mass as well as the middle and top frames.

Originally, these blades were intended to be made out of Type 420 Corrosion Resistant Stainless Steel (CRES). The main reasoning behind this was that this was the material that Bendix used in their flex pivots.

Type 420 is a high strength martensitic stainless steel with a tensile strength of up to 230 ksi and a yield strength of 195 ksi when hardened at a temperature between 1800-1900° F and tempered at 600° F.

Although Type 420 CRES seemed to be an ideal material, there appeared to be several potential problems. First of all, it did not appear that the material would respond favorably to a two-step braze process. If the blades were hardened before brazing, the brazing temperature would then have to be below the hardening temperature. It appeared that even the temperatures that the low-temperature braze alloys required could harm the heat treat properties. If the blades were brazed before hardening, they would have to be brazed at a temperature above the hardening temperature. At such high temperatures, there would probably be irreversible grain growth in the material. This would result in a deterioration of the mechanical properties, and ultimately, a premature failure of the blades.

Another potential problem with the 420 CRES that made the material incompatible with this design was the fact that water or oil quenching was required after the hardening treatment. This was potentially dangerous because the blades were so thin. Water or oil quenching could bring about a thermal shock on the blade which could cause a distortion of the blades as well as potential internal stresses within the blade, which were undesirable for this application.

The possibility of these potential problems warranted an investigation into other materials in order to find a material that was more suitable for this application. Such a metal would not require water or oil quenching in its heat treatment, would not be too sensitive

to cooling rates, and would be able to go through several heating and cooling cycles without severe deterioration of mechanical properties or irreversible grain growth. In addition, this metal would also have the ductility and fatigue properties which would enable it to meet the requirements of the flexure.

PH 13-8 Mo, a precipitation hardened, martensitic stainless steel manufactured by Armco, was a material which met these requirements. When compared to 420 CRES (Table 4.2), it had the same, if not better, mechanical properties. It could have a tensile strength of up to 230 ksi and a yield strength of 210 ksi. It had good ductility properties, and most, if not all, of its mechanical properties were irrespective of grain orientation. Another advantage was that its mechanical properties were not sensitive to cooling rates. Also, if the metal was brought to a temperature above the solution treatment temperature, as would be done in the flexure assembly, the grains could easily be refined by cooling the metal down to 60° F. Thus, the material could undergo several heating and cooling cycles without any significant deterioration of mechanical properties. Because of these advantages, it was decided to machine the whole assembly out of PH 13-8 Mo.

4.3 Blade Design Development

As was shown earlier in the theoretical development, the performance of this flexure was mainly dependent upon the material of the blades as well as its dimensions. Once the material was selected, the dimensions to obtain the desired performance were determined. This was done using the equations derived in Section 3.3 (Table 3.1).

Table 4.2 - Comparison of 420 CRES and PH 13-8 Mo

	420 CRES	PH 13-8 Mo
Ultimate Tensile Stress	230 ksi	215 ksi
2% Yield Stress	195 ksi	205 ksi
e (2 in) %	8	13
Density	.280 lb/cu. in	.271 lb/cu. in
Coef. of Thermal Expansion	5.7×10^{-6}	5.8×10^{-6}
Elastic Modulus	29.0×10^{6}	29.4×10^{6}

For PH 13-8 Mo, the fatigue limit is 90 ksi. For the initial analysis, the fatigue limit was taken to be 50 ksi in order to put in a margin of safety. Thus, by substituting this value into Eqn. 3.17 and substituting in for ϕ, the maximum ratio of thickness to length was obtained. By varying the four design parameters for the blades, which are the length l, thickness t, width b, and the nominal distance of the two blades from center a, various performance characteristics, such as stiffnesses and natural frequencies, can be obtained.

There were several limitations to these dimensions due to size requirements. A gap of 0.020" was desired between the blades to insure that they would not come in contact with each other during operation. Therefore:

$$a + b + .010" < .500" \tag{4.1}$$

A quick analysis was done to get a rough estimate of the size of the blades that would be needed to meet the requirements of the flexure. The most difficult requirement to meet was the lateral natural frequency along the x and y axis. Data showing the relationship between the length of the blade and the lateral natural frequency for various blade widths and nominal distances from center are shown in Table 4.3. Figure 4.1 shows the resulting graphs. From this information, it can be seen that in order to meet the lateral natural frequency requirement, the length of the blade would have to be between 0.1" and 0.3", and that the width of the blade would have to be between 0.090" and 0.140". The thickness of the blade would also have to be less than 0.010".

Table 4.3 - Lateral Natural Frequencies and Thicknesses for Various Blade Lengths and Nominal Distances from Center

For a=0.400 in, b=0.090 in:

Length of Blade in	Blade Thickness in	Natural Frequency Hz
0.112	0.004	596.0
0.125	0.005	579.4
0.150	0.006	545.7
0.200	0.008	480.9
0.250	0.010	423.9
0.500	0.020	250.7
0.750	0.030	173.7
0.832	0.033	157.5

For a=0.375 in, b=0.115 in:

Length of Blade in	Blade Thickness in	Natural Frequency Hz
0.100	0.004	721.5
0.125	0.005	695.1
0.150	0.006	666.5
0.200	0.008	607.0
0.225	0.009	577.8
0.250	0.010	549.7
0.500	0.020	347.8
0.736	0.029	250.1

Table 4.3 (cont'd)

For a=0.350 in, b=0.140 in:

Length of Blade in	Blade Thickness in	Natural Frequency Hz
0.100	0.004	814.5
0.125	0.005	793.1
0.150	0.006	769.1
0.200	0.008	716.7
0.250	0.009	689.6
0.250	0.010	662.7
0.500	0.020	446.1
0.667	0.026	356.1

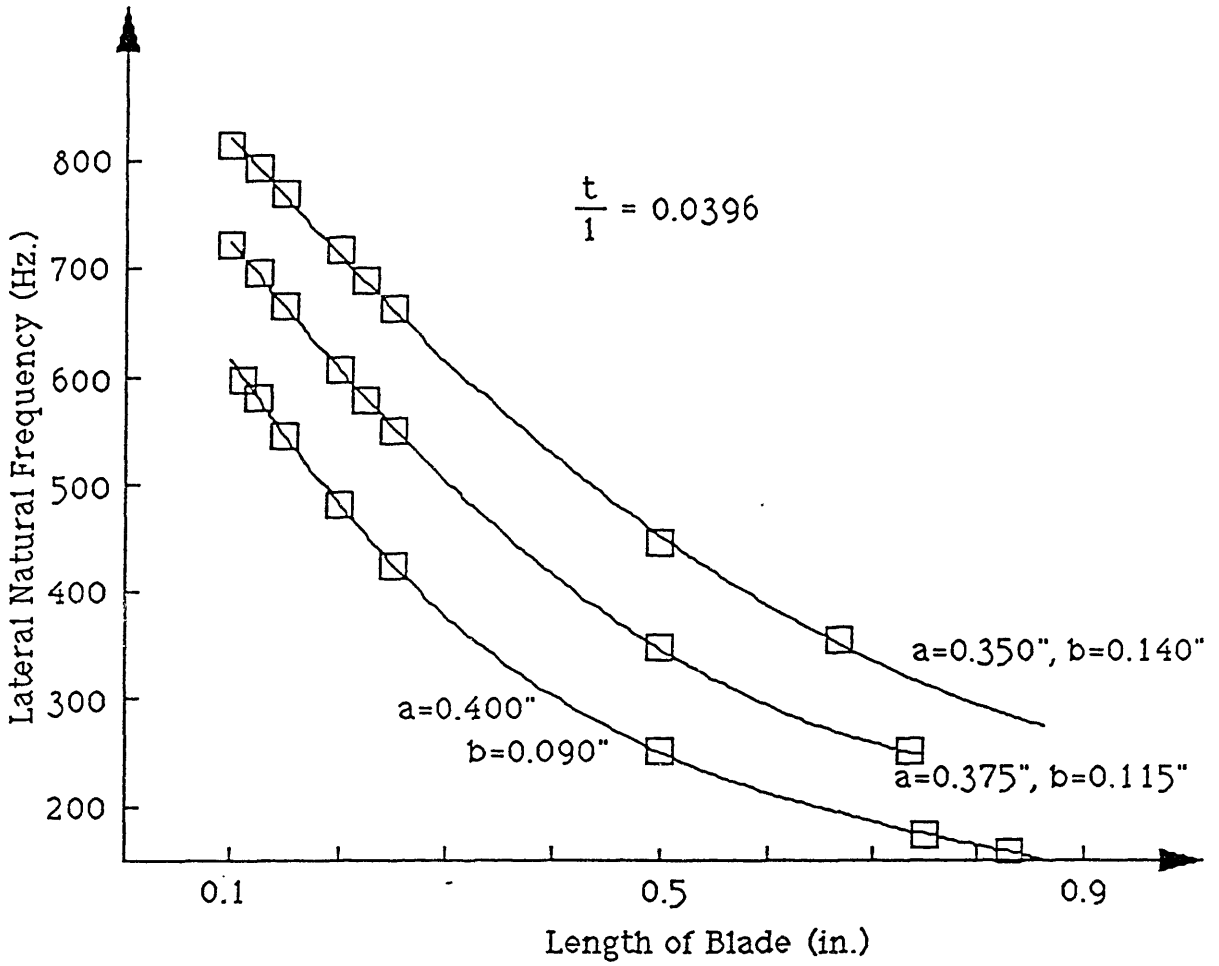

Figure 4.1 - Lateral Natural Frequency vs. Length of Blades

Another limitation to the values of *a* and *b* was the curvature of the outer diameter of the frame pieces. It was imperative that the entire working length of the blade (the portion of the blade that would undergo bending during operation) be within the boundary of the outer diameter of the frames to prevent accidental machining of the blade when the protruding portions of the tubes were machined off. If possible, it was also desirable not to have any portion of the blade be machined when the protruding portions of the tubes were removed.

A small study was done to determine the maximum distance from the center that the outer edge of the outermost blade could be. This was mainly dependent upon the outer diameter of the tubes. This dimension in turn was dependent upon the size of the frame pieces. Here, the diameter of the tubes was limited by the length of the bridge between the opposite ends of the bottom and middle frames (Fig. 4.2). If the tube radius was too large, then the tubes would intersect each other and not fit. It was found that a gap of 0.500" between two pairs of leaves on the same axis would be able to accommodate 0.375" diameter tubes comfortably.

It was also desirable to have at least 0.100" on each side of the length of the blades brazed into the tube. Thus, for a 0.375" diameter tube, the maximum working length of the blade would be 0.175". A schematic of this set-up was performed using GEODRAW, a computer drafting software package distributed by the Structural Dynamics Research Corporation (SDRC). As shown in Figure 4.2, it was found that if a 0.375" long blade were used, and a 0.005" clearance between the corner of the blade and the outer diameter of the frame implemented to prevent any machining of the blade, the maximum distance between

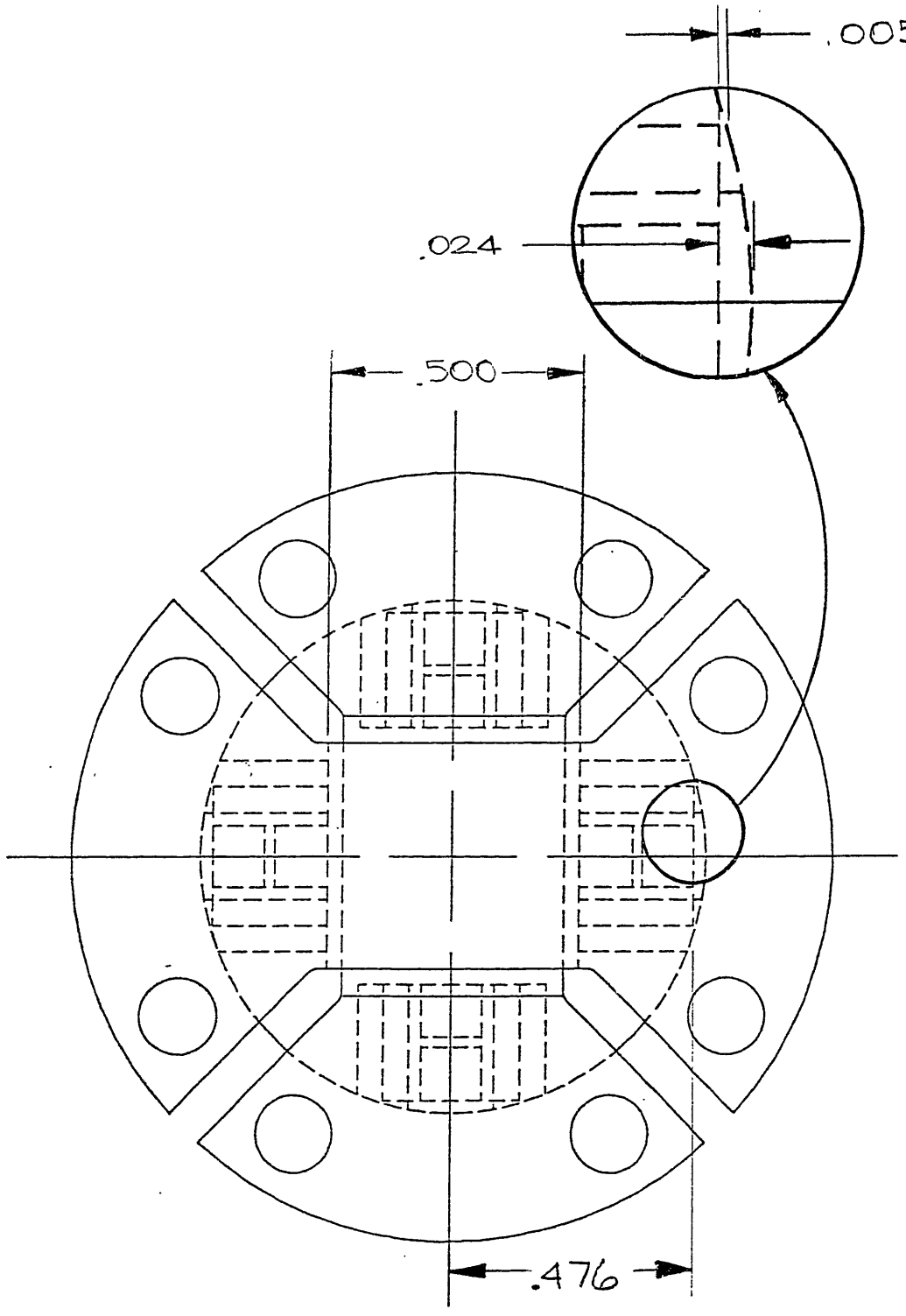

Figure 4.2 - Bottom View of Assembly Showing Bridge Length and Clearance Between Blade and Outer Diameter

the center of the flexure and the outermost part of the blade would be 0.476". Therefore, Eqn. 4.1 becomes:

$$a + b + .010" < .476" \tag{4.2}$$

The 0.500" gap between pairs of blades gave the following constraint:

$$a - b - .010" = .250" \tag{4.3}$$

By solving these two equations simultaneously, the distance from the center of the flexure to the center of the blades, a = 0.363" and the width of the blades b = 0.103" for a .375" long blade with a working length of .175".

Several programs were written in Pascal and 'C' to analyze the data using these equations and to determine the optimal blade thickness. It was decided that 0.005" would be the lower bound for the thickness because it would be very difficult to machine or surface grind any material thinner than 0.005". A graph of these results is shown in Figure 4.3. All of the curves shown are lower bounds. The curve for the natural rocking frequency about x and y, which is an upper bound is not shown because it is off the range of the graph. The shaded portion of the graph is the area where b and t may fall.

The first design of the blade is shown in Figure. 4.4. The chosen thickness was 0.007". This thickness was chosen because it was the lowest thickness that would meet all of the specifications. The smallest thickness was desirable because it would minimize the stress experienced by the blade. The radii of the fillet were positioned so that

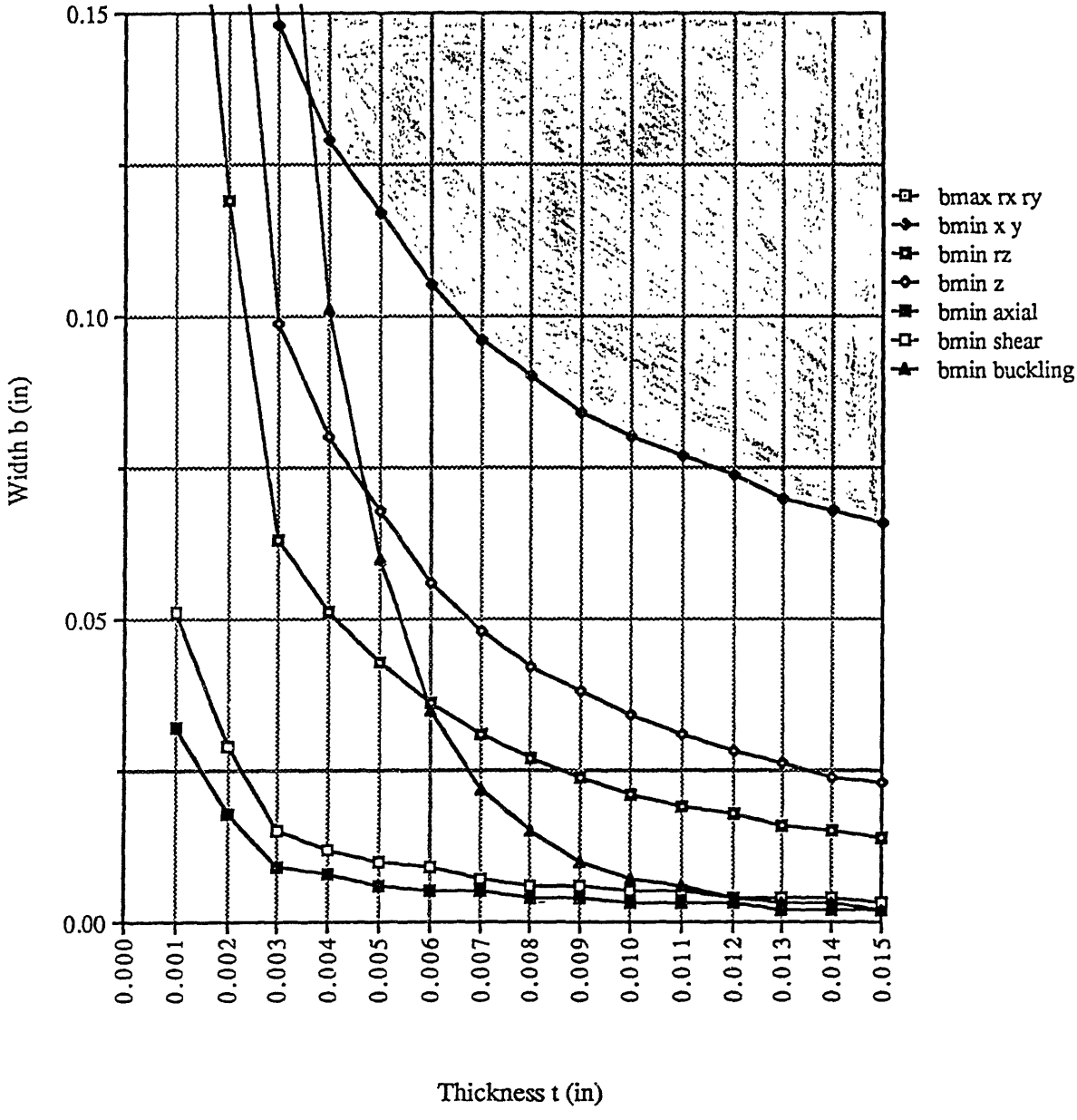

Figure 4.3 - Width vs. Thickness for a = 0.363

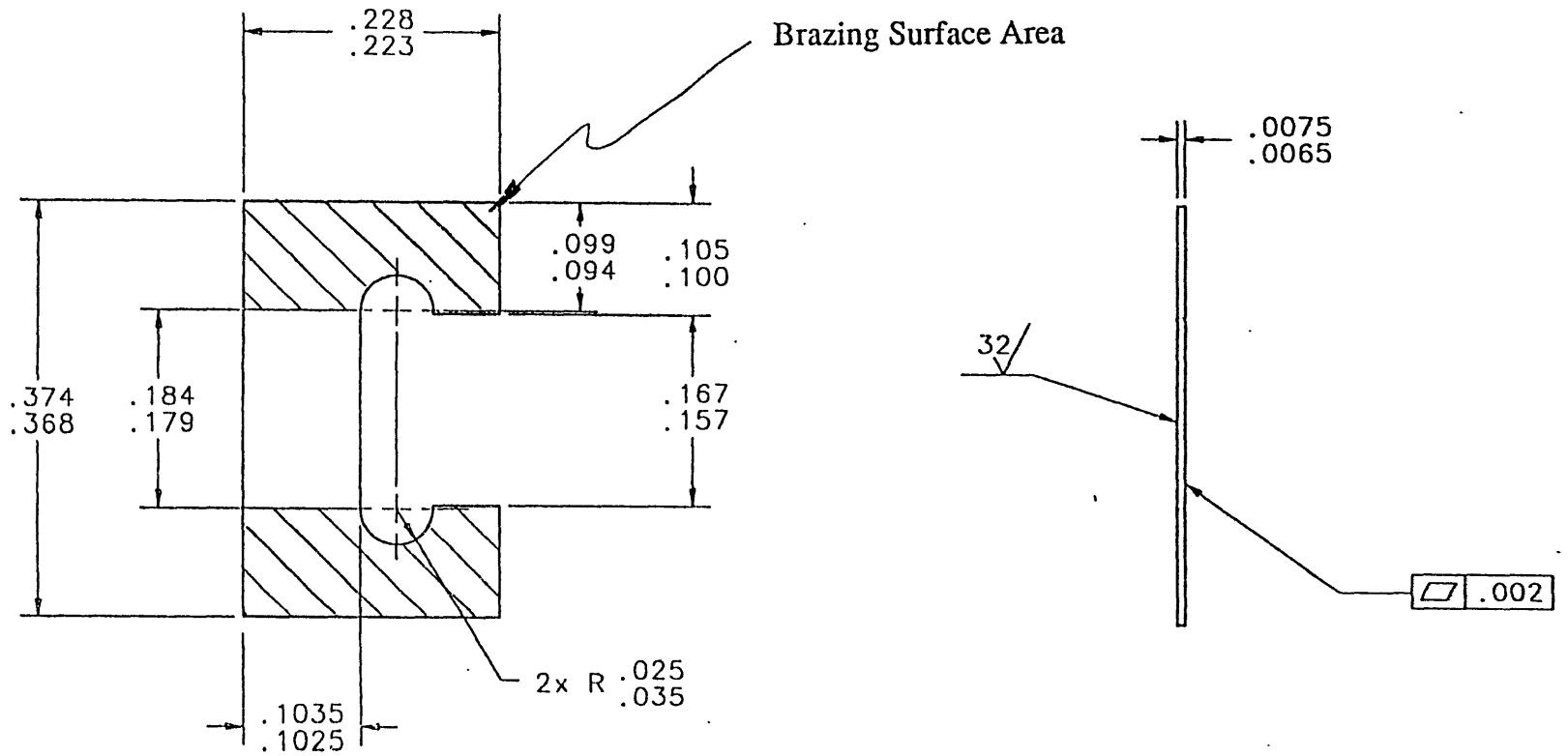

Figure 4.4 - Initial Blade Design

they would not be exposed outside the inner radius of the tube. This was done to prevent any stress concentrations at the interfaces and to make the performance more closely match the predictions. If the fillet radii were positioned so that they were exposed, the radii would not have been taken into account in the calculations. Thus, the performance predictions would have been inaccurate. The blade was also designed to maximize the brazing surface area.

When the slots in the jig tubes for these blades were being machined, however, a slitting saw blade to meet the initial 0.008" slot in the jig was not available. A decision was made to increase the slot to accomodate a 0.010" slitting saw. This meant that the thickness of the blade would have to increase to 0.009". More analysis was done to study the effects of this change. It was found that increasing the thickness of the blade by 0.002" increased the stiffness of the flexures, the natural frequencies, as well as the critical loads quite a bit. The stiffnesses about the x and y axes were more than doubled. However, the requirements and specifications for the flexure were still satisfied with the thicker blades. The maximum stress experienced by the blades also increased significantly. This maximum stress was 68 ksi, which was still under the fatigue limit of PH 13-8 Mo.

A comparison of the predicted performance characteristics for a 0.009" thick blade with the flexure requirements as well as the predicted flexure stiffnesses is shown in Table 4.4.

Table 4.4 - Performance Predictions for a 0.009" Thick Blade

Parameter	Requirement	Predicted Performance
Angular Travel	±87 mrad	±87 mrad
Natural Rocking Freq.	0-10 Hz	1.7 Hz
Natural Freq. about z	40 Hz	84 Hz
Lateral Natural Freq.	550 Hz	678 Hz
Axial Natural Freq.	550 Hz	918 Hz
Critical Lateral Load	-	185 lbs
Critical Axial Load	-	670 lbs
Stiffness About x and y	-	4.205 in-lb/rad
Stiffness About z	-	20520 in-lb/rad
Stiffness along x and y	-	84910 lb/in
Stiffness Along z	-	155700 lb/in

4.4 Fabrication Considerations

Two main processes were involved in the fabrication of this flexure assembly. These were the brazing process and the heat treating process. Since both of these processes required very high temperatures, care needed to be taken so as to not have either process hamper the other. It was important that the brazing process and temperatures required did not make the metal unable to be heat treated or deteriorate its mechanical properties. It was also important that the heat treatment did not deteriorate the braze joints. There were other factors that were important in each process, and these factors will be discussed in the following sections.

4.4.1 The Brazing Process

Brazing is a joining process used in a large variety of applications. The pieces joined in this process are bonded by a filler metal which has a lower melting temperature than that of the base metals. The filler metal comes in various forms, such as foil, wire, and powder, and is either placed in between the metals to be joined or alongside the joint. Since the joint clearances are small, as the parts are heated, the filler metal melts and flows through the entire joint by capillary action. When the assembly is brought back down to room temperature, the filler metal solidifies and bonds the parts together.

Many factors go into the brazing process that can determine the quality of the braze joint. They include the type of brazing method used, the atmosphere in which the brazing is performed, the base metals to be joined, the filler metal used to braze the two pieces, the type of joint used, the joint clearance, and the temperatures and times.

These must be chosen carefully in order to obtain an optimum braze joint. Since the solution treatment temperature of the PH 13-8 Mo was at 1700° F, it was important that the filler metals used have a melting point higher than that so that during the solution treatment, the filler would not remelt. It was also important that the filler material for the first braze require a minimal joint clearance. This was important because a large joint clearance would allow the blades to shift off their bending axis. Thus, by bending off of its intended bending axis, the higher stress experienced by the blade could cause failure. It was also important that the filler metal would not react with the base metals. Such an occurance could cause the blades to become more brittle, a characteristic undesirable in a flexure blade.

Because of these considerations, a filler material consisting of 35% gold and 65% copper was selected for the first braze, which bonded the blades into the tubes (Fig. 2.3). This was chosen because it only required a 0.0005" clearance between parts. This alloy has a brazing temperature of about 1900° F, which is 200° above the solution treatment temperature. For the second braze, which would braze the blade and tube assemblies into the frames (Fig. 2.4), a 82% gold and 18% nickel alloy (AWS Classification BAu-4, also known as Nioro) was chosen. Nioro requires a gap of about 0.002" and has a brazing temperature of 1800° F. This would allow the assembly to be brazed at 1800° F and then brought down to 1700° F for solution treatment without affecting either braze joint.

Both braze cycles were to be furnace brazed. There were basically two different furnace atmospheres in which these could have been brazed. The first was in dry hydrogen, and the second was in a

vacuum. One concern was the possibility of the aluminum within the PH 13-8 Mo rising to the surfaces during the heating, forming an oxide, and eventually impeding the brazing process by not allowing the surfaces to wet properly. One way to avoid this is by nickel plating the parts to be brazed. Most of the parts in the flexure assembly could have been easily nickel plated except for the jig tubes. Since only an electrolytic nickel plating was acceptable, it would have been nearly impossible to plate the 0.010" gaps in the tubes. However, if the brazing was done in a very tight vacuum with a pressure of 1×10^{-5} Torr, the possibility of the aluminum forming an oxide would be very small. Therefore, it was decided not to nickel plate the parts. The flexure would be brazed in a vacuum furnace at a pressure of 1×10^{-5} Torr. It also could have been performed in a dry hydrogen atmosphere, however, the brazing house used to perform the brazing process only had vacuum furnaces.

4.4.2 The Heat Treating Process

Once the assembly was brazed, it was to undergo a heat treatment in order to attain the highest strength possible. PH 13-8 Mo requires two treatments in order to get its high strength properties. The first treatment is a solution treatment, which brings the material to Condition A. The material is usually sent from the mill in Condition A, solution treated at 170C° F. In this condition, it can be machined, welded, brazed, and re-solution treated just as long as it is cooled to below 60° F before age hardening. This must be done due to the martensite transformation temperatures which are characteristic of this material. After the solution treatment, it is then age hardened.

There are several different specified age hardening temperatures for this material, and each temperature gives different properties and strengths. Table 4.5 shows some of the different types of age hardened conditions and the typical mechanical properties of each. It is interesting to note that these properties are not dependent upon grain orientation.

Table 4.5 - Mechanical Properties for Various Age Hardened Conditions (Taken from Armco Product Data Bulletin No. S-24)

Property	Condition A		RH950		H950		H1000		H1050	
	Long.	Trans.	Long.	Trans.	Long.	Trans.	Long.	Trans.	Long.	Trans.
UTS, (ksi)	160	160	235	235	225	225	215	215	190	190
0.2% YS, (ksi)	120	120	215	215	210	210	205	205	180	180
e (2 in) %	17	17	12	12	12	12	13	13	15	15
Hardness (R_C)	33	33	48	48	47	47	45	45	43	43

After the brazing, it was intended that the flexures undergo a re-solution treatment to bring the entire assembly back to Condition A. This was going to be done after the second braze cycle, which had a brazing temperature of 1800° F. Once the brazing was complete, the entire assembly was to be cooled to 1700° F for the solution treatment. It was found, however, that this process would not really be the same as Condition A. This type of process would be similar to solution treating the entire assembly at 1800° F, the highest temperature attained during the heat cycle. In order to attain the Condition A, the entire assembly would have to be cooled to below 60° and then

brought back up to 1700° F. From the literature published by Armco, the manufacturer of PH 13-8 Mo, this 100° F difference in solution treatment temperature does not result in a drastic reduction in strength (Fig. 4.5). The ultimate tensile strength does not change noticeably, and the 2% yield strength decreases by roughly 5 ksi. Despite these small changes, it was decided to go with the initial plan and not cool the assembly to 60° F. The main reason for this decision was the cost of performing another furnace run.

There were three age hardening treatment candidates that were considered for the two-axis flexure. These were H950, RH950, and H1000. The H950 and H1000 conditions would be obtained by merely heating the entire assembly to either 950° F or 1000° F, holding it there for 4 hours, and then air cooling it to room temperature. The RH950 required an additional step before the age hardening. This step was to bring the entire assembly to below -100° F for 2 hours, and then heat it up to 950° F for the age hardening. The refrigeration cycle basically would improve the ductility of the metal by getting rid of any retained austenite, which is not desirable because it makes the material more brittle. Neither of these treatments were chosen, however. A modified treatment which combined the RH950 and the H1000 was used. After the solution treatment, the assembly was to be cooled and refrigerated at -100° F for 2 hours and then brought up to 1000° F for 4 hours for the age hardening. The refrigeration cycle was introduced to hopefully regain any of the loss in mechancial properties caused by solution treatment at 1800° F. The 1000° F age hardening temperature was chosen because it would make the material slightly more ductile than if it was hardened at 950° F. Also, according to a metallurgist at Armco,

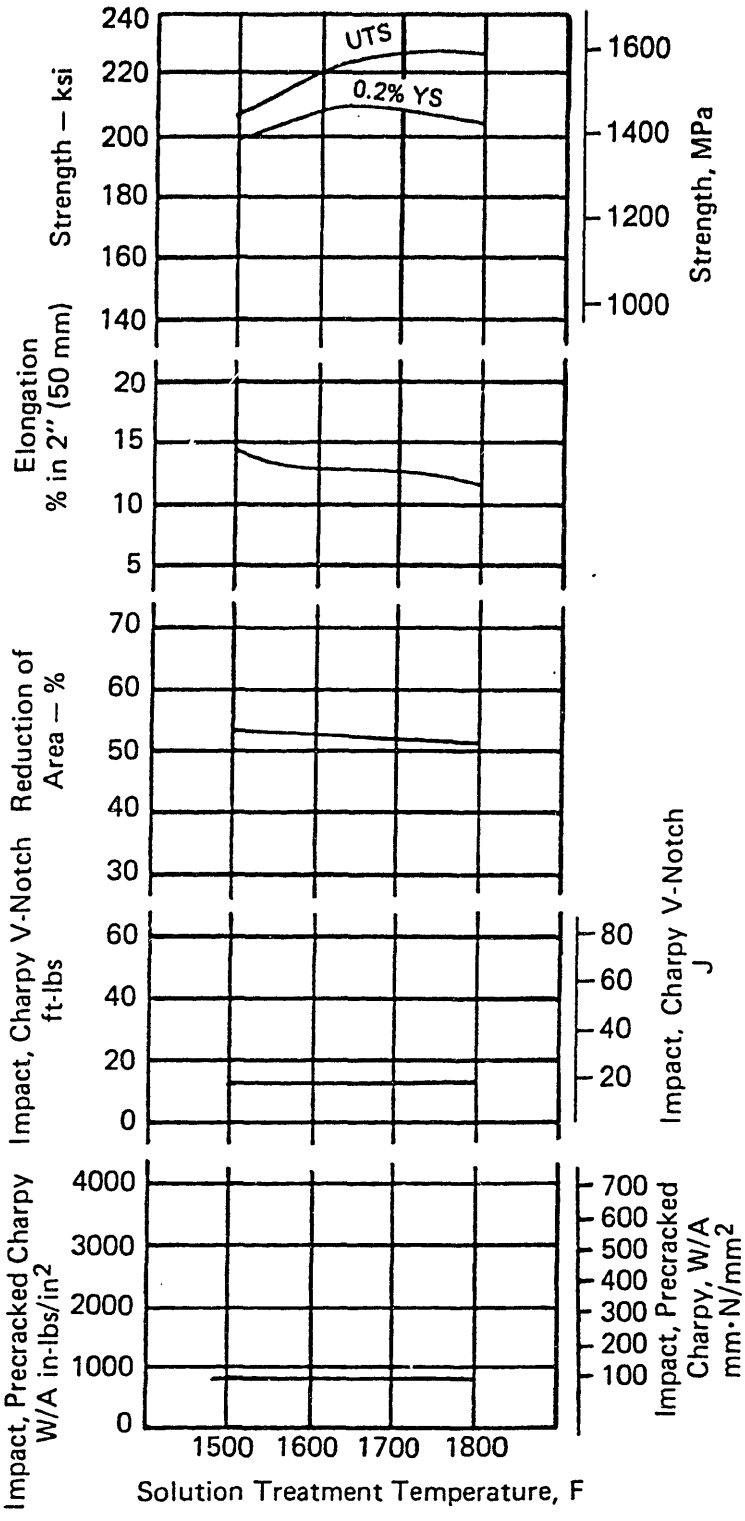

Figure 4.5 - Effect of Variation in Solution Treatment Temperature
(Reprinted from Armco Product Data Bulletin No. S-24)

the H1000 Condition would have slightly better fatigue properties than the H950.

One major concern about the brazing and heat treating of this flexure was the final condition of the blades. The reason for the concern was their thinness. These blades were to be brazed to comparably heavier masses, and since they were so thin, they would cool much more rapidly than the heavier masses in contact with their ends. Hence, the possibility existed that there would be a large difference in microstructure in the blade where it met the tube due to the potentially large thermal gradients that it would experience.

It was uncertain how large this difference in microstructure would be, how much this would affect the mechanical properties of the metal, or how large an impact this difference in microstructure would have on the performance of the blade, especially the fatigue life. Therefore, to get a better idea of the effect of the heating and cooling cycles on the blade, several witness coupons were machined. These coupons had roughly the same thickness as the blades, but were square instead of 'C' shaped. To simulate the effect of having the ends sandwiched in the slots, small blocks were also machined to place the witness coupons between. These blocks represented roughly one-eighth of the total weight of all three frame pieces and jig tubes. Thus, for each furnace run, one witness coupon would be placed between these blocks and go through the furnace cycle with the parts, and then accompany those parts throughout the heat treating and age hardening. Once the assemblies were finished, these coupons would be hardness tested in several places along their entire length to quantify the difference in properties along the blade.

4.5 Design Summary

The detail drawings for the parts for the two-axis flexure assembly are shown in Appendix B. It was designed to be able to travel the required ±87 mrad plus an extra 17 mrad before the top frame would come in contact with the bottom frame.

The blades were 0.009" thick, and were to be brazed into 0.010" slots in the jigging tubes, giving a 0.0005" clearance on each side of the blade for the brazing filler metal, which for the first braze cycle was 65%-35% Copper-Gold. These would be brazed at 1900° F and held at this temperature between 8-9 minutes. These tubes and jigs were then to be brazed into the frame pieces using BAu-4 Nickel-Gold (Nioro) alloy. The clearances for this braze was appoximately 0.002", and the brazing would be done at 1800° F. Once completely brazed, the assembly would be cooled, refrigerated at -100° F for 2 hours, and then age hardened for 4 hours at 1000° F.

Chapter 5
The Fabrication of the Prototypes

The fabrication process of the two-axis flexure consisted of three main parts: machining the parts, brazing the assembly, and heat treating the assembly. This chapter will describe these processes in more detail and discuss how the processes were actually performed and any problems that were encountered.

5.1 Machining the Parts

Since the only available form of PH 13-8 was in round bar, all of the parts, including the blades, were machined out of either 2.0", 1.0", or 0.5" round bar. The first parts to be machined were the top frames. There were relatively few problems associated with the machining of this part, although several minor errors were made by the machinist. On two of the top frames, the small 0.105" diameter counterbores were accidentally countersunk. In other words, instead of a squared surface, they were angled. The main reason for these holes was to keep any part of the working length of the blade from accidentally being brazed to the back wall of the hole cut for the tube. Thus, as the tube would register against the flat surface of the 0.190 diameter counterbore, the blades would not come in contact with any part of the top frame because of the small 0.105" diameter counterbore. Although the holes were countersunk, there was enough material for the tubes to register against. Therefore, the tube was not able to go deeper into the frame than intended, and the mistake was not disastrous.

Some problems were also encountered with machining the tubes slots. As mentioned previously, a 0.008" thick slitting saw was not available, so a 0.010" thick saw was used instead. However, as the machinist used these saws to cut the slots, they would easily wear down and break, causing the slots to be misaligned. Because of this, the slots were wire Electrical Discharge Machined (EDM), and there were no further problems encountered in the cutting of these slots.

The bottom and middle frame pieces were also machined with few problems. However, there was some mismatching in terms of the tolerances. In other words, the hole positions of the bottom frame were coming in at the high end or above the tolerance zone, while those of the middle frame were coming in at the low end or below the zone. The difference came out to be about 0.0025-0.007", which was enough to cause some wobbling of the top frame when the whole assembly was pieced together with the tubes. The impact of this problem would not be determined until the whole assembly was assembled and tested. However, the frame pieces were all matched and clocked so that the wobbling was minimized.

The machining of the blades was a rather slow process because these 0.009" thick blades had to be machined out of round bar stock. It would have been more ideal to make these out of plate or sheet, but the material did not come in those forms. Therefore, the shapes of the blades had to be milled out of the round bar using a Numerical Controlled Milling Machine, then cut off in 0.030 thick slices, and then surface ground, one at a time, down to 0.009". The blades had to be flipped periodically to prevent curling. To insure the longest fatigue life, the direction of grinding was along the length of the blade.

Once all of the parts were machined, they were fit together to get an idea of how the flexure would look and to see if there were going to be any problems in brazing or jigging. It was found that many of the slots were slightly shorter than called out. Some were up to 0.005" too short. Since it would have been difficult to redo the slots, the edges away from the working length of the blade were filed down on those blades which protruded out over the flat face of the jig tube. Because of this, each blade was matched to a slot. Therefore, since the blades and tube slots were now matched, care had to be taken in order to keep them together until they were brazed.

Due to some burrs that were on the corners of the slots in the tubes, some of the blades had some surface scratches on them. To reduce any risk of these scratches causing a crack propagation, these blades with scratches on them were hand lapped using a very fine diamond paper. They were held onto a flat block using an adhesive and then lapped in a figure eight, using an oil as a lubricant, until the surfaces were flat and the surface scratches disappeared.

For identification purposes, all of the jig tubes as well as the frame pieces were stamped with a number. Some of the blades had a somewhat snug fit in the slots, while some had a very loose fit. Some of the jigs had slots which had a misalignment which was visibly noticeable. All of these characteristics were noted and recorded.

5.2 Brazing the Assembly

All of the brazing of this flexure assembly was performed at the Scarrott Metallurgical Company in Los Angeles, California in a vacuum

furnace. The parts were delivered as machined, with all the jigs and blades paired.

As previously mentioned, the first braze step, which brazed the blades into the tubes, was to be done using a 65%-35% copper gold filler material at 1900° F. The jigs numbered 1, 3, 4, and 5 were used for the first furnace run. These were chosen for several reasons. Jigs 1 and 3 each had one blade which had a snug fit and one with a loose fit. Therefore, these two would give a good indication of how the alloy flowed through each type of fit. Jigs 4 and 5 were chosen because they had slots which were out of alignment, which made them unusable unless they were needed as a last resort. All of the parts were immersed in acetone for degreasing. The blades were then placed in the slots and the filler material applied. The filler material came in the form of powder, was mixed with Nicrobraz, a type of cement or paste, and then applied using a syringe on the outside of Jigs 1, 4, and 5 over the slot and the end of the blade (Fig. 5.1a). On Jig 3, the filler material was applied on the inner radius of the tube using a paint brush (Fig. 5.1b). This type of application was rather difficult and time consuming compared to using the syringe. However, this type of application of filler material would insure that there would be a fillet radius where the blade met the tube. The intent of the outer diameter application was to have the filler material wick into the joint clearance by capillary action and flow all the way through to the inner diameter and form a small fillet. The presence of this fillet would indicate whether or not the filler material flowed through the entire joint. For the inner diameter application, the presence of filler material on the outer surface of the blade around the slot would indicate a successful braze.

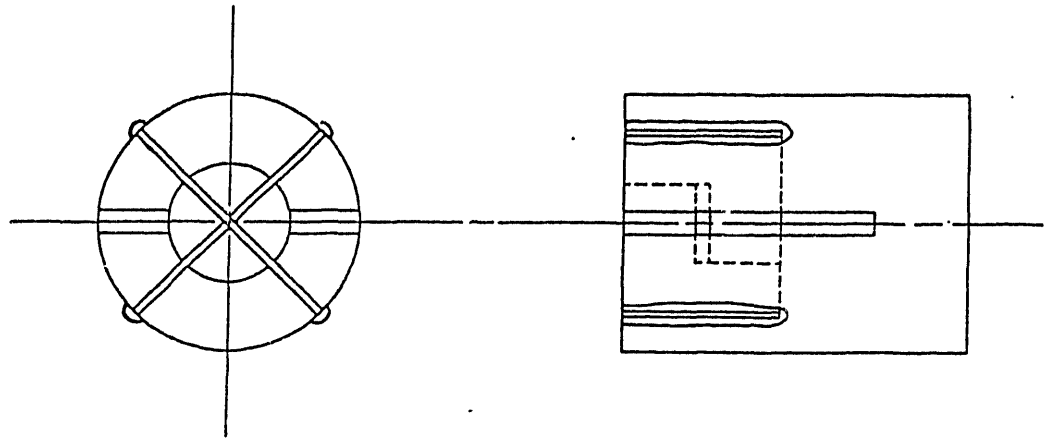

a) Jigs # 1, 4, and 5

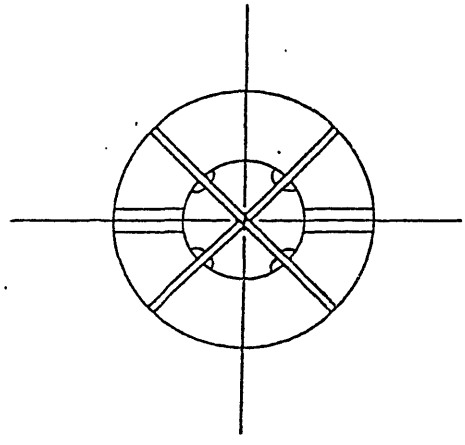

b) Jig #3

Figure 5.1 - Application of Powdered Filler Material for Jigs #1, 3, 4, and 5

Once all of the filler material was applied, all four assemblies, plus one witness coupon in between the blocks and another held in place by a wire, were placed in the furnace, preheated to 1750° F, and held there for 15 minutes to assure uniform temperature of all the parts. The assemblies were then brought up to 1900° F and held between 8 and 9 minutes for the brazing, and then air cooled.

The results from this first furnace run were very unsatisfactory. There were absolutely no fillets on the assemblies which had the filler material applied on the outer diameter, and there was no presence of filler material on the outer diameter of Jig 3. There were, however, large fillets at the corner of the blade and tube on Jig 3. For Jigs 1, 4, and 5, there was a lot of filler material which ran down the outside surface of the tube and solidified on the outside surface, but it did not appear that any of the filler wicked into the clearance gap. Jig 4 was brought through another furnace run, this time upsidedown. It was hoped that the excess filler material which had run down the sides would flow back down to where the slot was located and then flow into the gap. The temperature was also raised to 1950° F to increase the flow capability of the filler. However, when the assembly was brought out of the furnace, the filler still did not flow through. It did flow down to the slot, but no fillets appeared on the inner diameter. It seemed as if the filler was unable to wet the blade. A radiographic inspection confirmed this. Figure 5.2 shows a picture from this inspection of Blade and Jig Assembly 3, which was the assembly in which the filler material was applied on the inside diameter of the jig. The dark areas indicated the presence of filler material. This could be seen on the inner diameter where the blades met the tubes, which was where the

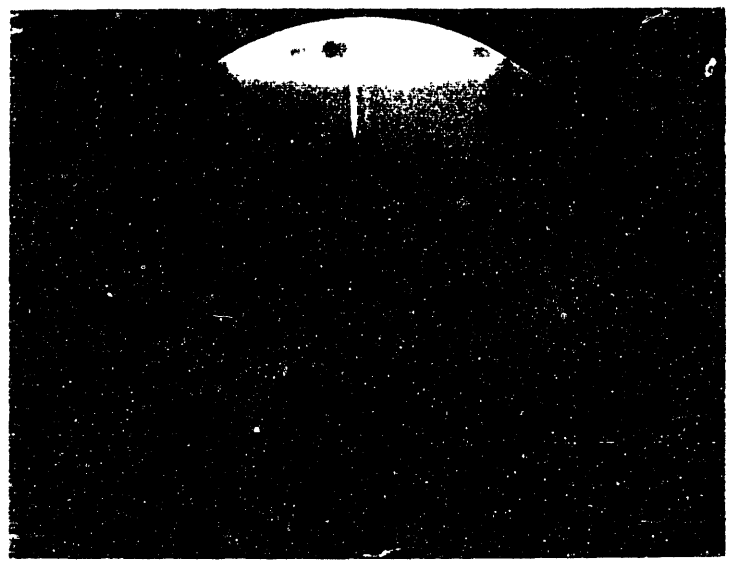

Figure 5.2 - Radiographic Photo of Blade and Jig Assembly #3

fillet radii could be seen by visual inspection. There also appeared to be some filler material which flowed into the half circles present on the outline of the blade. These half circles seemed to have served as reservoirs for the filler material. A metallographic inspection also showed that the blades were not wetting properly. Blade and Jig Assembly 3 was inspected, and it showed that there was wetting of the slots, but no wetting of the blade.

There are several causes that will impede the wetting of the metal. As mentioned earlier in Section 4.4.1, one of these causes is the presence of aluminum oxide on the surfaces of the parts to be brazed. Since the filler seemed to flow and wet the jigs without any problems, it did not seem that an aluminum oxide layer came from the aluminum within the PH 13-8 Mo. However, it was discovered that the blades were surface ground using a grinding wheel that was made out of white aluminum oxide. Therefore, there was probably an aluminum oxide layer on the surface of the blade which would not allow the blade to wet properly. Thus, the filler would not flow through the tight gap and no fillet would form.

Because of this possible aluminum oxide layer, an experiment was performed to test the effect of this layer on the wetting. Three of the witness coupons, which were originally milled, were ground using the same surface grinding wheel material. One of these was left as is, another was hand lapped using silicon-carbide, a substance which does not affect the wetting process, and the third was chemically cleaned. These were placed in the furnace with a block covering part of it. Some of the 65-35 copper gold powder was applied on the joint between the block and the blade as well as near the middle of the surface of the

blade (Fig. 5.3). The powder was placed in the joint to see how well the filler would flow through a line-to-line fit between mating parts. If it was able to flow through this type of fit without any problems, then it would be more certain that the problems with brazing were due to the wetting of the blade. If it was unable to flow through this type of fit, then there was a chance that the problem was due to the filler material not being able to flow through a tight fit.

The powder was applied in the middle of the surface of the blade to get a better idea of the wetting characteristics of the filler on the different types of surfaces. If the problem was due to the aluminum oxide layer left on by the grinding wheel, then the witness coupon that was left as is should have shown very poor wetting. The witness coupon that was chemically cleaned should have exhibited very good wetting, since this type of cleaning removes any oxides and does not leave any on the surface. The witness coupon that was hand lapped using silicon carbide should have also exhibited better wetting than the coupon that was only surface ground. How much better the silicon carbide lapped coupon would wet would show how effectively the lapping removed the aluminum oxide layer. Two small plates of Type 305 Stainless were also placed in the furnace. These were placed so that they overlapped each other about one inch. A drop of filler material was placed on one of the plates, and some was placed at one of the joints. This was done to get an idea of how the 65-35 copper gold alloy acted with other types of base metals.

After the furnace cycle, the witness coupons and blocks were examined. The Type 305 Stainless plates showed excellent wetting and pull through. It appeared that the filler material flowed through the

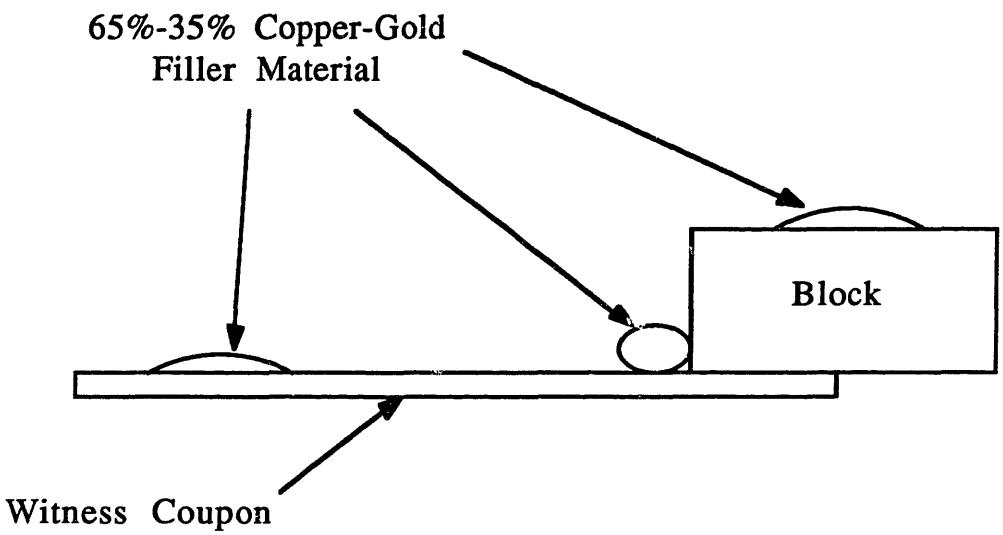

Figure 5.3 - Filler Material Placement for Wetting and Pull-Through Experiment

entire joint because there was a very nice fillet on the side opposite of where the filler material was initially placed. The coupon that was left as is did not exhibit very good wetting. There was a bead roughly the same size as the drop which was applied before brazing. This indicated that the filler material stayed still and did not flow. At the braze joint, there was very little pull through, and no fillet radius appeared on the side opposite of where the filler material was applied. The coupon that was chemically cleaned showed better wetting than the coupon that was only ground. However, it still exhibited poor pull through. No fillet radius was present on the side opposite of where the filler material was applied. Instead, there was some evidence of filler material in the form of small dots along the edge of the joint. This indicated that the filler material flowed through the joint somewhat, but it did not wet the coupon properly. The coupon which was hand lapped using silicon carbide exhibited the best wetting of the three coupons. The filler material covered almost the entire exposed surface of the coupon. However, there was probably some movement of the block or the blade because they came out of the furnace in a position different than the position in which it was originally placed. This sample was rerun in the furnace to get a better idea of the pull-through characteristics. During this run, the bottom of the blade was accidentally brazed to the tantalum foil upon which it rested. However, there was no presence of a fillet on the side of the coupon opposite of where the filler material was placed. In order to see how well the filler material did pull through, the block and coupon assembly was metallographically inspected. This inspection showed that the filler material was wetting the coupon material properly, but it was not

flowing through the joint gap at all. Therefore, it was concluded that the joint gap was too small for this application.

Since the brazing process using 65%-35% copper gold powder was not working, a new plan was implemented. Since it appeared that the joint gap was too small, the slots were widened to 0.011" using 240 and 320 grit silicon carbide grinding paper. The blades were also hand lapped using 400 grit silicon carbide grinding paper. The filler material was placed in the form of foil on each side of the blade to insure that the filler was in the gap. Since 65%-35% copper gold foil was unavailable, a 35% gold-3% nickel-62% copper alloy (AWS classification BAu-3, also known as Nicoro) was used. It was in the form of 0.002" foil and was hand lapped to 0.001" in order to fit into the slots. Blade and Jig Assembly 2 was placed into the furnace using this method. A sketch illustrating how this piece looked before brazing is shown in Figure 5.4.

The results from this run were very satisfactory. All of the joints formed fillets on the inner diameter of the jig. One fillet, however, was exceptionally large. An oversize fillet, though, should be able to be prevented by controlling the amount of foil that protrudes into the inner diameter of the jig. Since this run was successful, Blade and Jig Assemblies 6-11 were all prepared in a similar fashion to that of jig assembly 2 and run through the furnace. These all showed adequate braze joints, although not all of the joints were consistent. Some showed small fillets in the inner diameter, while others did not show a fillet at all. It did appear, however, that the joints would be sufficient to hold the blades in place for this application.

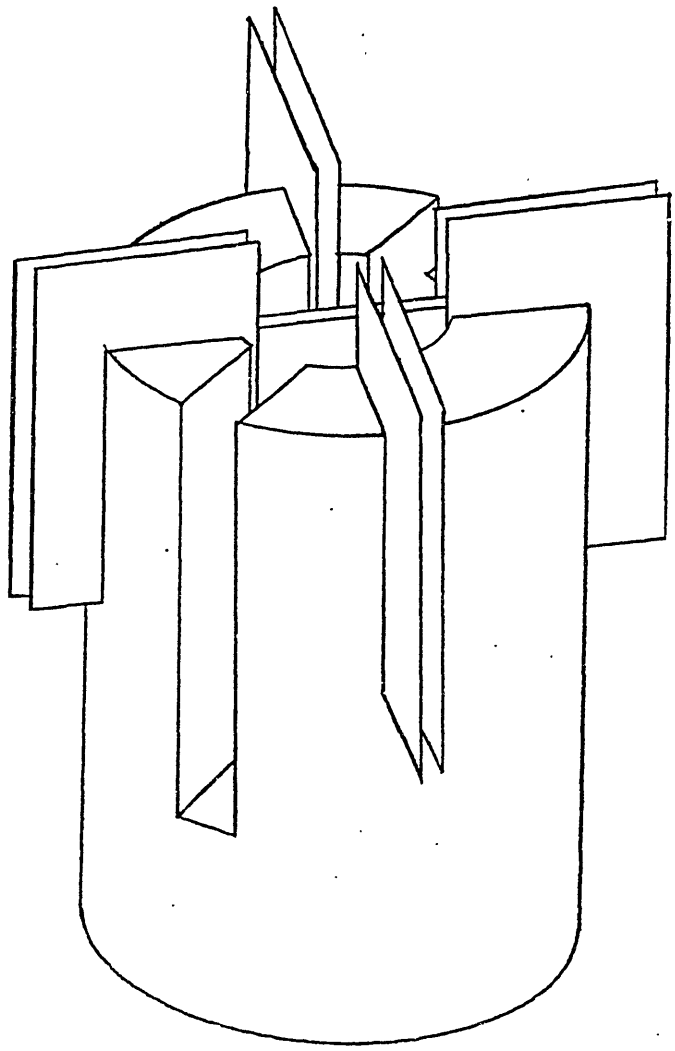

Figure 5.4 - Placement of Nicoro Foil for Jig Assembly #2

Four of these blade and tube assemblies were used in the final braze of the first prototype. The frame pieces which were stamped with a number 3 were used for the first run of the second braze step. All of the excess braze filler material was sanded off of the outer surfaces using a silicon carbide grit paper. Then the frame pieces as well as the blade and tube assemblies were all ultrasonically cleaned with acetone. To prevent any filler material from brazing the flexing elements to each other, Stop-Off, a substance which prevents wetting of a surface, was applied to any surface upon which filler material might flow. This included all of the surfaces on the frame pieces which were facing another frame piece as well as the larger gaps in the tubes. After the Stop-Off was allowed to dry, the Nioro filler material, which was in the form of 0.001" foil, was tack welded onto the tubes. Care was taken to insure that the tack welds were not located on the part of the tube which was to be brazed into the frame pieces. Once all of the Nioro foils were tack welded into place, the assembly was pieced together and clamped. The height of the tops of the tubes were all measured with respect to the other tops to insure that the flexure would pivot about the same plane. The tolerancing of the drawing called out for the axes of the pairs of blades to be within 0.0025" of each other. If the axes were unable to meet this tolerance, then it was important that the pair of blades along one axis be as closely aligned as possible. When this assembly was measured, the tops came within 0.005" of each other. Since one axis (the middle frame axis) seemed about 0.003" lower than the other, 0.003" shims were placed underneath the middle frame in order to raise the height of its axis.

Once this was done, all of the tops of the tubes were within 0.002" of each other.

Nickel-Chrome strapping was used to keep the assembly stationary during the brazing cycle. One strap was wrapped around the outer flange of the bottom and middle frame pieces to center them with respect to each other. Another strap was wrapped around the protruding ends of the tubes to keep them registered against the counterbores in the top frame piece. Four more straps were attached to the top frame piece and to the plate upon which the whole assembly rested. This was done to keep the top frame piece in place. All of these straps were held in place by tack welds. A diagram illustrating this set up is shown in Figure 5.5.

The assembly was placed in the furnace with a 300 gram weight placed on top of it to aid in keeping any of the parts from moving. Also placed in the furnace were two of the witness coupons which went through the first furnace run. The witness coupon that was placed in between the blocks for the first braze run was also placed in between blocks for this braze run. The other coupon was placed in the furnace held upright by a wire. The assembly and coupons were brazed at 1800° F for 7-9 minutes and then air cooled to below 60° F. The results from this furnace run were also satisfactory. Two of the joints had good fillets visible on the outside of the joint. The other two joints had some small, visible gaps, but they did appear to be adequate joints.

5.3 Heat Treating the Assembly

Once completely brazed, the assembly was heat treated in order to obtain the highest strength. The assembly and witness coupons were

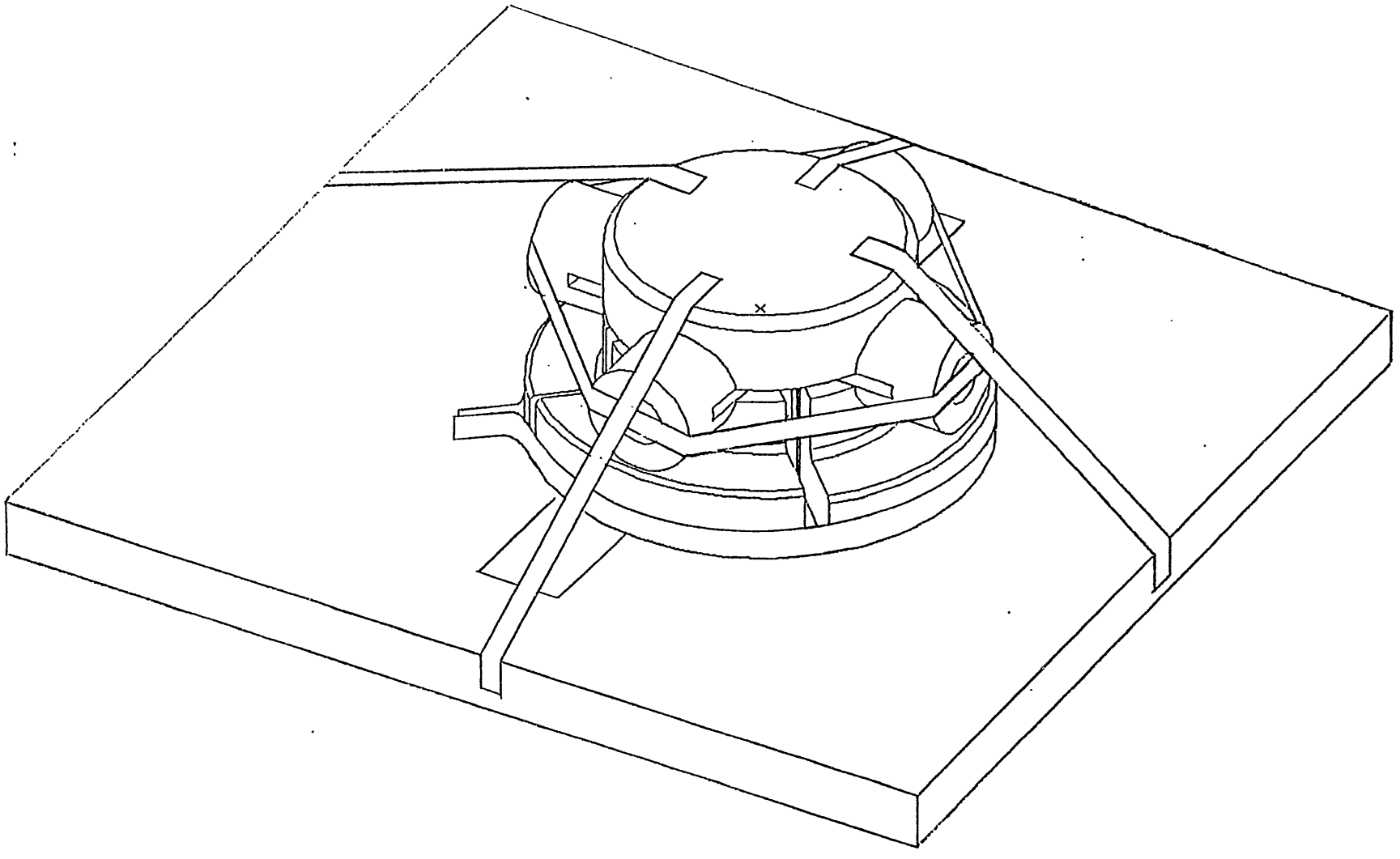

Figure 5.5 - Setup for the Second Braze Step

first placed in a cold box and refrigerated at -100° F for two hours. After the cold treatment, the parts were placed in the furnace and age hardened at 1000° F for four hours, and then air cooled.

Hardness tests were conducted at various points on the frame pieces to determine the heat treat condition. The results from the readings taken from the frame pieces averaged a hardness of about 43 on the Rockwell C scale.

Because the witness coupons were so thin, it was not possible to get accurate readings for their hardness using the normal method of hardness testing. Therefore, a microhardness test was performed on the witness coupons to determine their hardness. The coupons were mounted and polished, and then the readings taken from three different locations on the blade. As mentioned earlier, this was done to give an indication of whether or not there were large differences in the properties along the length of the blade. The readings from one end of the coupon which was in between the blocks indicated a Rockwell C hardness of 46.5, the middle indicated 47.5, and the other end indicated 48. The readings from the coupon which was standing in the furnace all averaged 48.3 Rockwell C. From this information, it did not appear that there were drastic differences in microstructure along the length of the blades.

5.4 Machining Off the Protruding Ends of the Tubes

The final process of completing the flexure was to remove the protruding ends of the tubes. Once these were removed, the middle frame would be free to flex. This process, however, was not as trivial as it may have seemed. First of all, the material was in the age

hardened condition. Therefore, if the ends were to be sawed off, a carbide tool would have to be used. Also, extreme care had to be taken to insure that the assembly did not experience critical loads or torques which might cause the blade material to yield or even fail. Therefore, all of the frame pieces had to be secure so that they would not move with respect to each other. Any clamping along the z axis, however, would probably damage the assembly because once the protruding ends of the tubes were removed, all of the clamping force would be transmitted throught the 0.009" thick blades.

The process which was used was Electrical Discharge Machining (EDM). This process was ideal because it would be able to cut through tough materials yet it would not exert any significant loads on any of the parts. The flexure would experience only very localized heating during the process, and it would require minimal clamping. For the first prototype, the ends were Electrical Discharge Machined off using a flat blade. Therefore, the tube was not flush with the 1" frame diameter. A curved tube edge flush with the frame diameter could have been achieved using a curved blade during the EDM. Square edges were acceptable, however, since the small protruding corners of the tubes would not interfere with the operation of the flexure. Once these ends of the tubes were removed, the flexure assembly was ready to be tested. A photograph of the finished prototype is shown in Figure 5.6.

Figure 5.6 - Finished Prototype

Chapter 6
Performance Testing

6.1 Test Objectives

The characteristics that were the most important in this flexure were the stiffnesses, hysteresis, natural frequencies, and fatigue life. A test plan was created to determine these quantities so that these values could be compared to the performance predictions.

To be more specific, the following quantities were to be obtained:

-Rotational stiffnesses about the x, y, and z axes and 45° between x and y.

-Hysteresis about the x and y axes and 45° between x and y.

-Translational stiffnesses along the x, y, and z axes

-Natural frequencies about the x, y, and z axes

-Natural frequencies along the x, y, and z axes

-Damping characteristics

-Fatigue life

6.2 Test Setup and Procedure

An inertial mass was machined out of aluminum such that its physical properties would closely match those of the driven mass of the selected application. This mass was 10.0" in diameter, 0.25" thick with a 0.520" hole in the center for the flexure. Mounting holes were also machined so that this mass could be bolted onto the flexure. Table 6.1 shows a comparison of the properties and performance predictions of the driven mass of the chosen application to those of the test inertial mass. The stiffness measurements about the x and y axes were

Table 6.1 - Comparison of the Application Driven Mass and the Experimental Inertial Mass

	Application Driven Mass	Experimental Inertial Mass
Weight	1.81 lbs	1.93 lbs
$I_{xx} = I_{yy}$	0.038 in-lbs-s^2	0.031 in-lbs-s^2
I_{zz}	0.074 in-lbs-s^2	0.063 in-lbs-s^2
* $F_{qx} = F_{qy}$	1.7 Hz	1.9 Hz
*F_{qz}	84 Hz	90 Hz
* $F_x = F_y$	678 Hz	656 Hz
*F_z	918 Hz	888 Hz

*These are the predicted values of the flexure assembly when attached to the indicated mass

obtained statically using force and angular deflection measurements. The instrumentation needed to obtain the dynamic measurements was not available at the time of testing, so no dynamic analysis will be included in this thesis.

6.2.1 Static Stiffness and Hysteresis Measurements

For the static stiffness and hysteresis measurements, the flexure assembly was mounted on a small circular plate and bolted to a horizontal mounting surface. Small cylindrical spacers were inserted between the flexure bottom frame and the small plate to allow the middle frame to pivot. The inertial mass was mounted to the middle frame and raised up with spacers so that the center of gravity of the inertial mass was approximately at the intersection of the two bending axes of the flexure. A mirror was mounted on top of the inertial mass so that it would not come in contact with the top frame during operation. A diagram of this setup is shown in Figure 6.1.

The static stiffness measurements were obtained using nickels as weights to apply the force and a laser beam setup to measure the angular deflection. The nickels, which were each approximately 5 grams in weight, were used to deflect the inertial mass by placing them four inches from the z axis of the flexure. A laser beam was reflected off of the mirror onto a wall, and by measuring the deflection of this beam on the wall and knowing the distance from the wall to the mirror, angular deflection measurements could be obtained using the following equation:

$$\theta = \frac{1}{2} \sin^{-1}\left[\frac{\delta a}{\sqrt{a^2 + (x^2 + \delta^2)^2}\sqrt{a^2 + x^2}}\right] \tag{6.1}$$

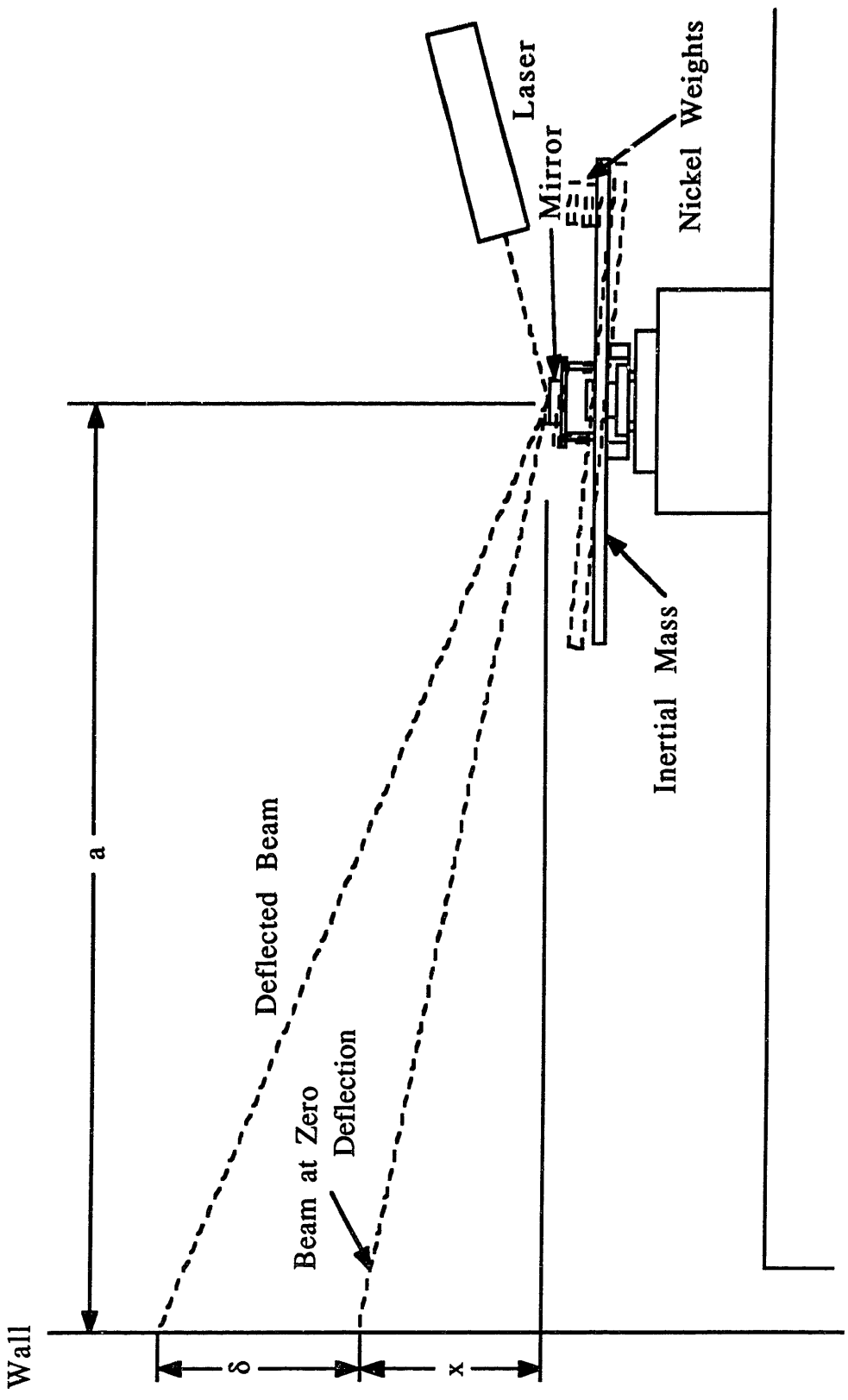

Figure 6.1 - Setup for Static Stiffness Measurements

where θ is the angular deflection, a is the distance from the center of the mirror to the wall, δ is the measured linear deflection on the wall, and x is the initial height of the beam above the mirror with no weights on the inertial mass (Fig. 6.1). Using this setup, data was obtained in the following manner. First, the null position of the beam on the wall was recorded. Once this was done, the nickels were added, one by one, onto the inertial mass. After each nickel was placed on the inertial mass and all of the oscillations damped out, the position of the beam was recorded on a piece of paper which was taped to the wall. Once the inertial mass was deflected over 87 mrad (which took nine nickels), the nickels were removed, one at a time, and each position recorded again. This was done to see how repeatable the system was and if there was any noticeable hysteresis. The angular deflection was measured again with no weights on the inertial mass to see how far the null point had shifted, and then the nickels were applied and then removed on the opposite side of the axis. Using this method, the flexure was pivoted ± 87 mrad about one axis. Two sets of readings were taken about each of four axes; x, y, and the two axes that were 45° between x and y. The forces were converted to torque, and torque vs. angular deflection graphs were plotted. The resulting angular deflections were also compared to the theoretical values, and the resulting error vs. applied torque was also plotted. From the slope of the torque vs. angular deflection plot, the rotational stiffness about the x and y axes as well as 45° between the x and y axes were obtained, and from the error vs. torque graphs, a hysteresis loop was obtained. The error vs. torque graphs were also normalized to the resulting

stiffness curve about that particular axis. Therefore, the two error vs. torque graphs that were obtained for each axis compared the measured angular deflections to the theoretical flexure stiffness (4.205 in-lbs/rad) and the stiffness calculated from the data.

6.2.1.1 Experimental Error

There were several possible sources of error in the static measurements. Some of them dealt with the measurements of the values from Equation 6.1. Most of these measurement errors, however, were quite small and would only affect the angular deflection measurements by roughly 0.1 mrad. The biggest source of error was the measurement of the linear deflection on the wall, δ. Since the beam was roughly 0.10" in diameter, it is conceivable that the measurements were off by one-third the diameter, or 0.03". This would result in a measurement error of 0.3 mrad. Another probable source of error was differences in the applied torque. These differences could have been caused by inconsistent placement of the nickels on the inertial mass. In other words, they probably were not all placed 4" from the center of the flexure. Also, the center of gravity of the weights, which were nickels taped together, probably was not consistently along the axis of the nickels, thus causing a different applied torque than desired. A third source of error was that the actual torques should have been multiplied by a $\cos\theta$ term due to the tilt of the inertial mass. This would result in the actual torques applied being 0.0013 in-lbs less than recorded when eight nickels were applied. This results in a error of 0.3 mrad.

6.2.2 Fatigue Testing

The fatigue life of the flexure was to be determined by flexing the assembly ±87 mrad about the axes. If the flexure showed no signs of failure after ten million cycles, then the infinite life requirement of the flexure would be satisfied.

A diagram illustrating the setup of the fatigue test is shown in Figure 6.2. The flexure was mounted on a coupling which, in turn, was mounted onto a shaft of a motor. The middle frame of the flexure was attached to a shaft which was held by a bearing on the opposite end. The bearing was grounded by a clamp such that the flexure was pivoted 87 mrad. When the motor was turned on, the bottom frame would spin with the shaft, and as this happened, the middle frame would be pivoted 87 mrad about all of the axes in the x-y plane. A strobe was used to determine the rotational speed of the assembly.

For the fatigue test, the assembly was spun at 1666 rpm. This rate would cause the flexure to undergo 100,000 cycles each hour. The rotation was stopped every hour for inspection to see if there was any cracks or failure of the blades.

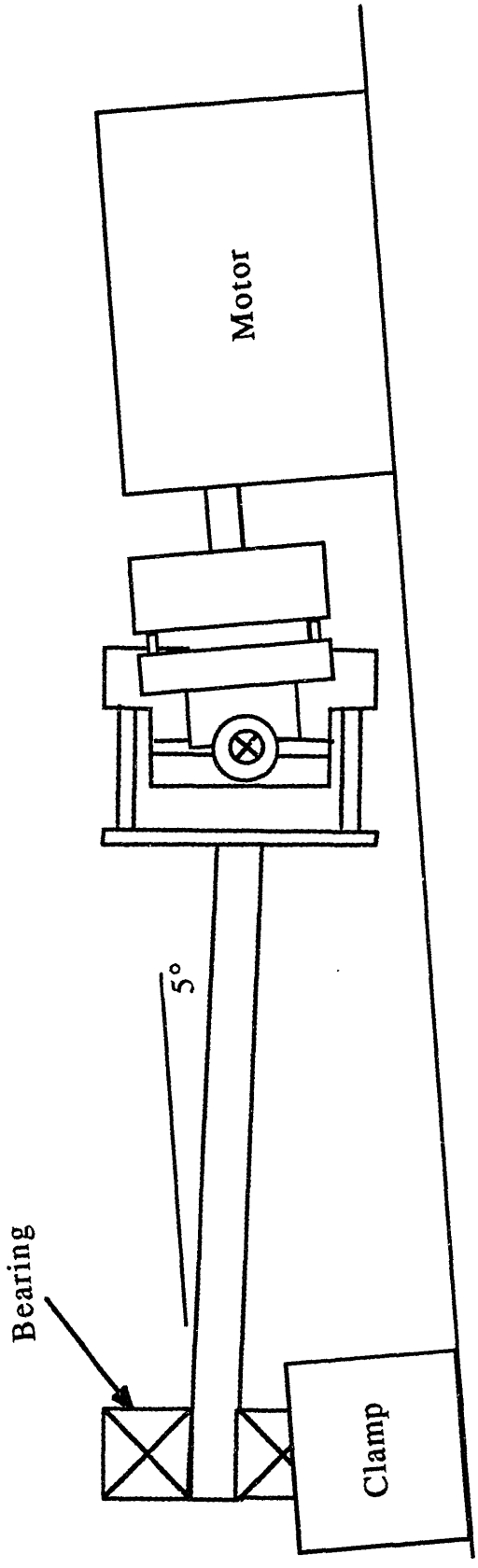

Figure 6.2 - Fatigue Test Setup

Chapter 7

Test Results and Analysis

7.1 General Characteristics

With the inertial mass mounted on it, the flexure was very stiff about the z axis as well as in translation along all of the axes, but very soft in rotation about the x and y axes. There was very little damping about the x and y axes as well. When deflected and allowed to freely pivot, the inertial mass would rock back and forth for over a minute. When the inertial mass was deflected about the pure x or y axis, it would usually continue to rock along that same axes. However, when the inertial mass was deflected about the 45° offset axes between the x and y axes, it would begin to nutate.

7.2 Static Measurements

7.2.1 Stiffness

Data taken from a set of measurements about the x axis of Flexure Assembly 2 is shown in Table 7.1. The resulting Torque vs. Angular Deflection curve is shown in Figure 7.1. Data from two complete runs of weights (one run consisting of placing one through nine nickels on one side, taking them off, placing them on the other side, and taking them off) about this axis are included in this plot. The resulting equation of the line using an average of the slopes from a least squares fit of each line is at the top of the graph. The slope of this line (4.161) is the resulting stiffness of the flexure about this axis. A typical plot showing the error with respect to the theoretical flexure stiffness for this same axis is shown in Figure 7.2. This graph shows measurements

Table 7.1 - Data from the X Axis of Flexure 2

# of Nickels	Applied Torque (in-lbs)	Theoretical Deflection (radians)	Measured Stiffness Deflection (radians)	Deflection Run 1 - Down (radians)	Error from Theoretical Run 1 - Down (radians)	Error from Measured Stiffness Run 1 - Down (radians)	Deflection Run 1 - Up (radians)	Error from Theoretical Run 1 - Up (radians)	Error from Measured Stiffness Run 1 - Up (radians)
1	-0.0442	-0.0105	-0.0106	-0.0106	-0.0001	0.0000	-0.0113	-0.0008	-0.0007
2	-0.0893	-0.0212	-0.0214	-0.0214	-0.0002	0.0000	-0.0221	-0.0009	-0.0007
3	-0.1331	-0.0317	-0.0319	-0.0320	-0.0003	-0.0001	-0.0326	-0.0009	-0.0007
4	-0.1779	-0.0423	-0.0427	-0.0430	-0.0007	-0.0003	-0.0432	-0.0009	-0.0005
5	-0.2223	-0.0529	-0.0534	-0.0533	-0.0004	0.0001	-0.0538	-0.0009	-0.0004
6	-0.2651	-0.0630	-0.0636	-0.0642	-0.0012	-0.0006	-0.0640	-0.0010	-0.0004
7	-0.3092	-0.0735	-0.0742	-0.0750	-0.0015	-0.0008	-0.0747	-0.0012	-0.0005
8	-0.3530	-0.0839	-0.0848	-0.0854	-0.0015	-0.0006	-0.0844	-0.0005	0.0004
9	-0.3970	-0.0944	-0.0953	-0.0945	-0.0001	0.0008	-0.0945	-0.0001	0.0008
0	0.0000	0.0000	0.0001	0.0000	0.0000	-0.0001	-0.0009	-0.0009	-0.0010
1	0.0442	0.0105	0.0107	0.0108	0.0003	0.0001	0.0098	-0.0007	-0.0009
2	0.0893	0.0212	0.0215	0.0216	0.0004	0.0001	0.0207	-0.0005	-0.0008
3	0.1331	0.0317	0.0321	0.0320	0.0003	-0.0001	0.0315	-0.0002	-0.0006
4	0.1779	0.0423	0.0428	0.0428	0.0005	0.0000	0.0421	-0.0002	-0.0007
5	0.2223	0.0529	0.0535	0.0534	0.0005	-0.0001	0.0529	0.0000	-0.0006
6	0.2651	0.0630	0.0638	0.0637	0.0007	-0.0001	0.0631	0.0001	-0.0007
7	0.3092	0.0735	0.0744	0.0743	0.0008	-0.0001	0.0738	0.0003	-0.0006
8	0.3530	0.0839	0.0849	0.0848	0.0009	-0.0001	0.0845	0.0006	-0.0004
9	0.3970	0.0944	0.0955	0.0954	0.0010	-0.0001	0.0954	0.0010	-0.0001

Table 7.1 (cont'd) - Data from the X Axis of Flexure 2

# of Nickels	Applied Torque (in-lbs)	Theoretical Deflection (radians)	Measured Stiffness Deflection (radians)	Deflection Run 2 - Down (radians)	Error from Theoretical Run 2 - Down (radians)	Error from Measured Stiffness Run 2 - Down (radians)	Deflection Run 2 - Up (radians)	Error from Theoretical Run 2 - Up (radians)	Error from Measured Stiffness Run 2 - Up (radians)
1	-0.0440	-0.0105	-0.0105	-0.0106	-0.0001	-0.0001	-0.0107	-0.0002	-0.0002
2	-0.0886	-0.0211	-0.0212	-0.0210	0.0001	0.0002	-0.0212	-0.0001	0.0000
3	-0.1325	-0.0315	-0.0318	-0.0315	0.0000	0.0003	-0.0316	-0.0001	0.0002
4	-0.1785	-0.0424	-0.0428	-0.0426	-0.0002	0.0002	-0.0426	-0.0002	0.0002
5	-0.2175	-0.0517	-0.0522	-0.0517	0.0000	0.0005	-0.0518	-0.0001	0.0004
6	-0.2656	-0.0632	-0.0638	-0.0634	-0.0002	0.0004	-0.0635	-0.0003	0.0003
7	-0.3112	-0.0740	-0.0747	-0.0741	-0.0001	0.0006	-0.0742	-0.0002	0.0005
8	-0.3540	-0.0842	-0.0850	-0.0846	-0.0004	0.0004	-0.0846	-0.0004	0.0004
9	-0.3963	-0.0943	-0.0952						
0	0.0000	0.0000	0.0001	0.0000	0.0000	-0.0001	-0.0002	-0.0002	-0.0003
1	0.0440	0.0105	0.0106	0.0113	0.0008	0.0007	0.0106	0.0001	0.0000
2	0.0886	0.0211	0.0214	0.0220	0.0009	0.0006	0.0214	0.0003	0.0000
3	0.1325	0.0315	0.0319	0.0324	0.0009	0.0005	0.0320	0.0005	0.0001
4	0.1785	0.0424	0.0430	0.0433	0.0009	0.0003	0.0432	0.0008	0.0002
5	0.2175	0.0517	0.0523	0.0529	0.0012	0.0006	0.0526	0.0009	0.0003
6	0.2656	0.0632	0.0639	0.0647	0.0015	0.0008	0.0642	0.0010	0.0003
7	0.3112	0.0740	0.0749	0.0757	0.0017	0.0008	0.0754	0.0014	0.0005
8	0.3540	0.0842	0.0851	0.0859	0.0017	0.0008	0.0859	0.0017	0.0008
9	0.3963	0.0943	0.0953	0.0960	0.0017	0.0007	0.0960	0.0017	0.0007

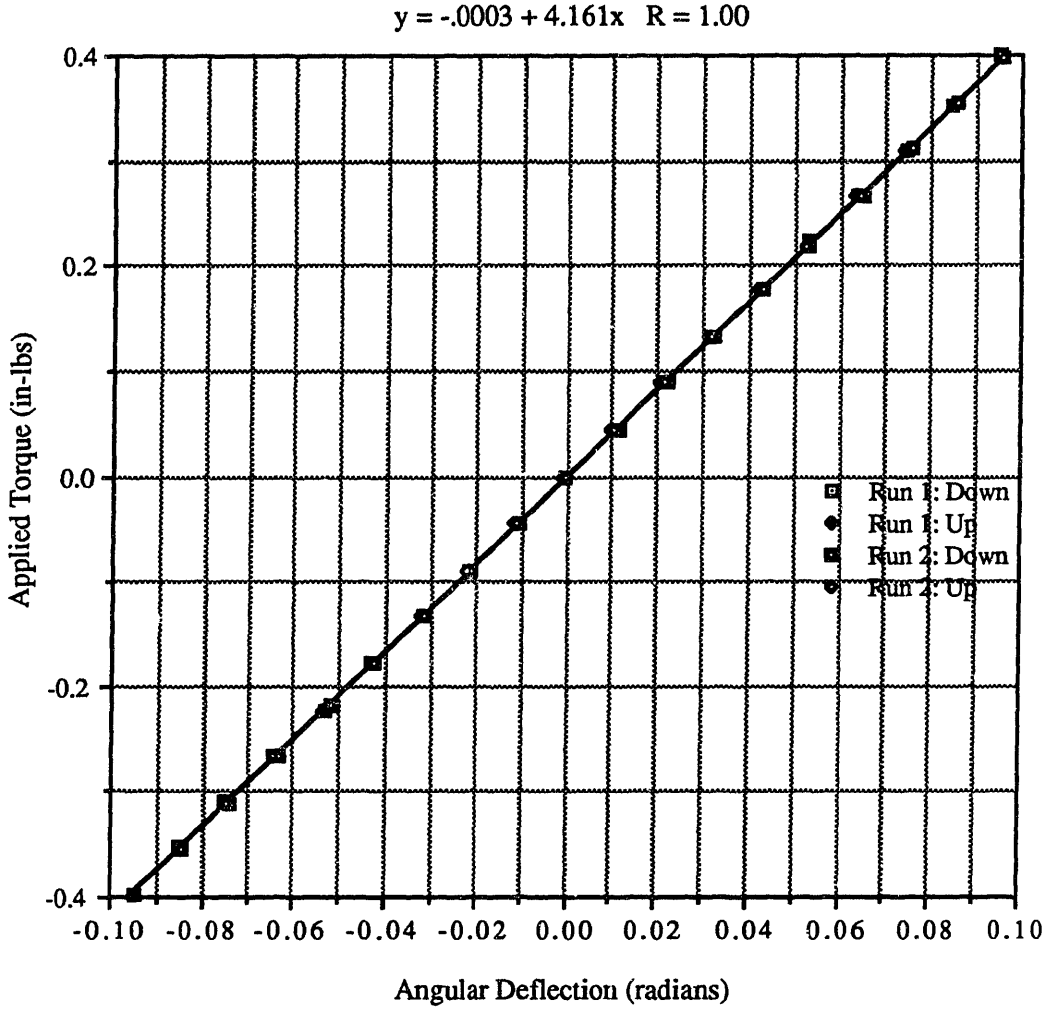

Figure 7.1 - Torque vs. Angular Deflection for the X Axis of Flexure 2

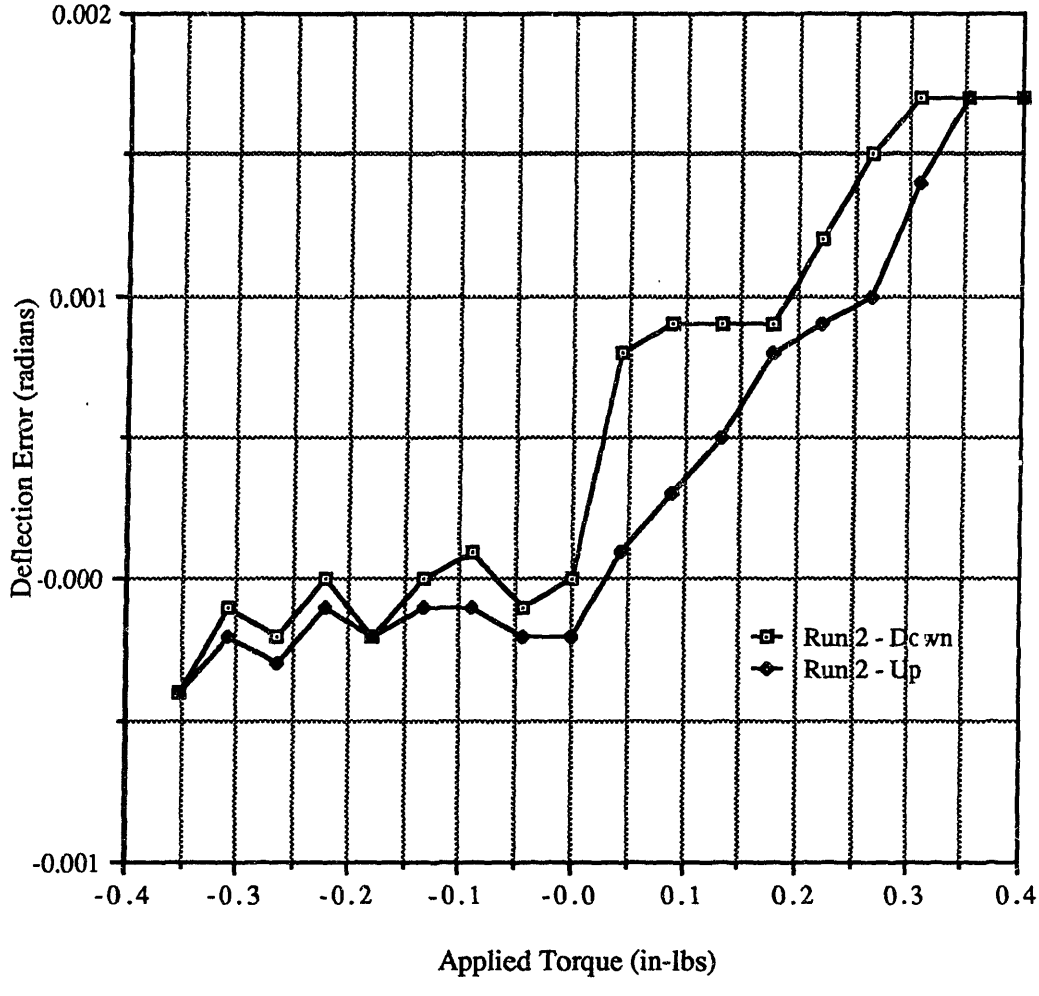

Figure 7.2 - Deflection Error vs. Torque for the X Axis of Flexure 2

from one run only. The direction of travel (down being the negative direction and up being the positive) is indicated on the legend. Shown in Figure 7.3 is a graph showing the error with respect to the stiffness obtained from the averaging of the slopes from the least squares fit of each line. All of the other data and plots are shown in Appendix A. A summary of the data from these plots is shown in Table 7.2.

Table 7.2 - Summary of the Results from the Static Stiffness Measurements

Property	Flexure 1	Flexure 2	Flexure 3
Stiffness:			
x axis	4.667	4.161	3.693
45° Offset Axis	4.327	4.141	3.920
y axis	4.024	4.094	4.094
45° Offset Axis	4.359	4.124	3.880

Varying stiffnesses were obtained from the three flexures. These stiffnesses ranged between 3.693 in-lbs/rad for the x axis of Flexure 3 to 4.667 in-lbs/rad for the x axis of Flexure 1. Not only did the stiffnesses vary between the flexures, but they also varied within flexures. Flexure 1 had the widest range of stiffnesses between its axes, having a range of over 0.6 in-lbs/rad. Flexure 2 appeared to be the most consistent, having a range of only 0.075 in-lbs/rad. This flexure also had the stiffnesses closest to the theoretical values calculated previously. As was expected, the stiffnesses measured about the 45° offset axes were consistent for each flexure. Flexure 3 had the

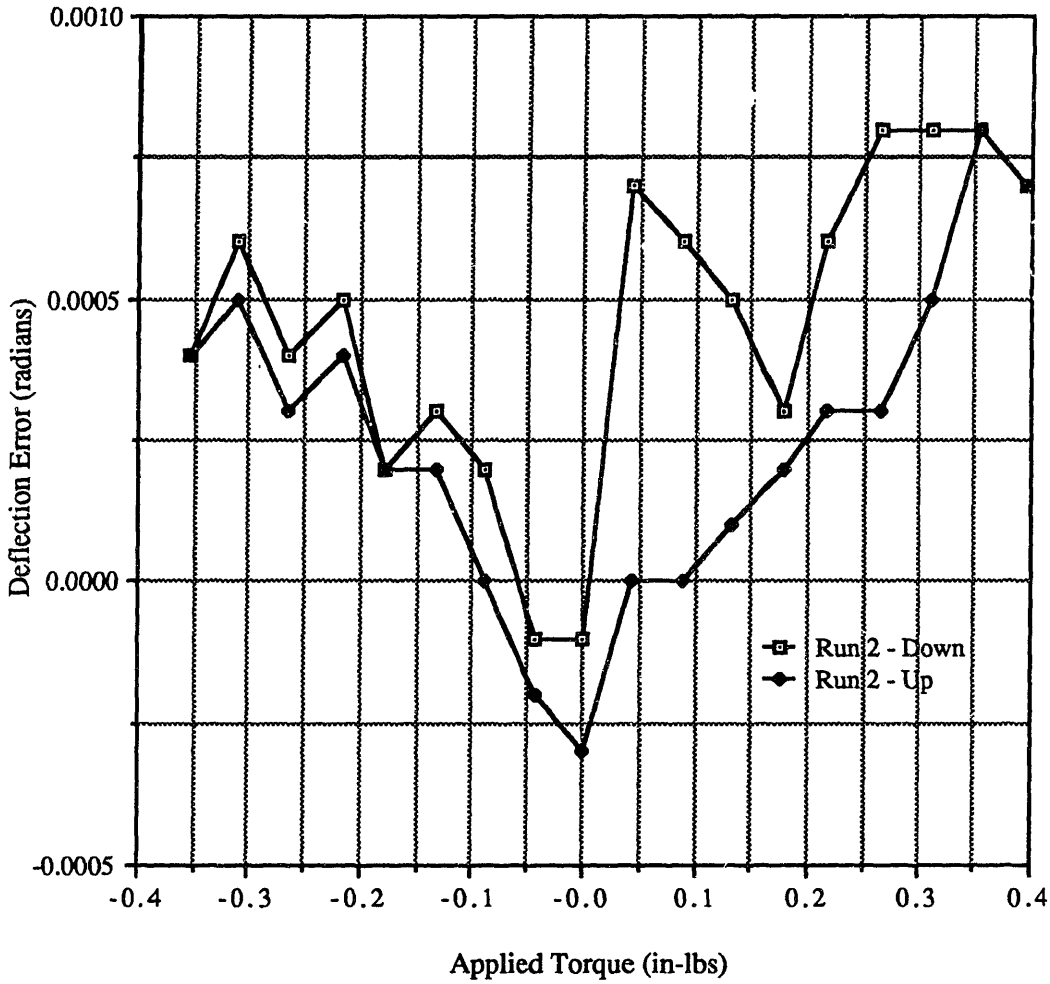

Figure 7.3 - Normalized Error Curve for the X-Axis of Flexure 2

widest range of stiffnesses about the 45° offset axes, which was only 0.042 in-lbs/rad. In all three cases, the stiffnesses about the two 45° offset axes were very close to the average of the stiffnesses about the x and y axes.

There are several probable causes for the varying stiffnesses. The main reason is the differences in the fillet radii of the braze joints between the tubes and the blades. Since the fillet radii of these joints were inconsistent, the actual working length of the blades could have varied as much as 0.030". This would result in a difference of 0.769 in-lbs/rad in stiffness. Another factor contributing to the differences in stiffness is the difference in the dimensions of the blades. There was 0.001" tolerance on the width of the blades, a 0.001" tolerance on the thickness, and a 0.002" tolerance on the hole in the tube. Not taking the fillet radii of the braze joints into account, these differences in tolerances could result in a stiffness as low as 4.184 in-lbs/rad and as high as 5.863 in-lbs/rad. In actuality, the blade thickness came out to be between 0.009" and 0.0093", thus resulting in an upper limit of 4.640 in-lbs/rad for the stiffness from the dimensional tolerances.

7.2.2 Hysteresis

The error curves indicate that there is some hysteresis in the flexure when flexed the full range. This hysteresis usually resulted in a shift of the null point of less than 1 mrad, although it did reach as high as 2 mrad in Flexure 1. Further testing was performed on Flexure 3 to determine the limits of the hysteresis. In these tests, a set of nickels was placed on one side, a measurement taken, then the nickels removed and the null shift measured. After this was done, the set of

nickels was placed on the other side and a measurement taken, and then another measurement taken with the nickels removed. This was done for each axis starting with a set of eight nickels, and then decreasing the set by one or two nickels until no measureable hysteresis was found. Table 7.3 shows the measured null point shift of all of the axes of Flexure 3 as well as the applied torque and the angular deflections. None of the axes would exhibit hysteresis when four nickels were applied. One axis did not exhibit hysteresis even when six nickels were applied. From the data, it appeared that all of the axes would exhibit hysteresis when pivoted over 60 mrad.

Table 7.3 - Hysteresis Measurements

Flexure Axis	# of Nickels Applied	Torque Applied (+/- in-lbs)	Null Point Shift (radians)	Negative Deflection (radians)	Positive Deflection (radians)
X Axis	4	0.1785	0.0000	0.0465	0.0479
	5	0.2175	0.0002	0.0590	0.0580
	6	0.2656	0.0004	0.0724	0.0727
	7	0.3112	0.0005	0.0842	0.0839
	8	0.3540	0.0008	0.0965	0.0951
45° Offset Axis	5	0.2175	0.0001	0.0553	0.0555
	6	0.2656	0.0003	0.0678	0.0675
	7	0.3112	0.0004	0.0794	0.0797
	8	0.3540	0.0007	0.0910	0.0898
Y Axis	4	0.1785	0.0000	0.0438	0.0439
	5	0.2175	0.0000	0.0532	0.0534
	6	0.2656	0.0003	0.0655	0.0651
	8	0.3540	0.0007	0.0876	0.0870
45 ° Offset Axis	6	0.2656	0.0000	0.0682	0.0686
	7	0.3112	0.0001	0.0797	0.0806
	8	0.3540	0.0004	0.0916	0.0907

From this information, it was concluded that the flexure blades are not completely elastic in the full working range. It appears that there is some plastic deformation when the assembly is pivoted over 55-60 mrad. Possible causes for this hysteresis are the following:

1. Some deterioration of the mechanical properties due to the heating and cooling cycles, heat treatment, and differences in microstructure near the blade and tube interface.

2. Plastic deformation of the braze filler material between the blade and tube slots.

3. Different fillet radii on the opposite sides of a blade, or the presence of a large fillet on one side and the absence of a fillet on the other.

The fillet radii of the joint between the blade and the tube is a possible cause for both the differences in the stiffnesses of the flexures as well as the presence of hysteresis. Because of these possibilities, the fillet radii need to be carefully controlled when the blade and tube assemblies are brazed together.

7.3 Fatigue Test Results

Between four and five hours of operation (400,000-500,000 cycles), some chattering was heard in the flexure. Upon closer inspection, it was found that one of the blades had failed completely and had broken into two pieces. The break was located about 0.015-0.020" from the blade and tube interface on an innermost blade along

the y axis of the flexure. It was also very close to the edge of the fillet formed by the braze material. This is the area where the highest stresses occur in the flexure blade. There are several possible causes to the premature failure.

Probably the main cause was the fact that at a deflection of 87 mrad, the material was not within the elastic region. From the static measurement results, hysteresis was present at 55 mrad. Therefore, if the flexure was being deflected into the plastic region, then the fatigue life would be reduced drastically.

Another possible cause might have been a difference in microstructure in the blade around the braze joint. As mentioned previously, due to the heating and cooling cycles and the large difference between the mass of the blades and the rest of the flexure, a difference in microstructure could have resulted along the blade and tube interface. Even though the hardness appeared to be consistent along the length of the blade from the hardness tests, there could have been some microstructural differences that would not be detected from the hardness tests.

Another major cause could have been the inaccuracy of the setup. There was a 0.004" runout of the shaft which was connected to the plate connecting the shaft to the mirror, which meant that there was some eccentricity when the assembly was rotated. Since the rotational speed was quite high, this could have put some extra loads on the flexure blades, thus contributing to a premature failure.

Therefore, the failure of the flexure could have been due to the test setup or the properties of the material. Because of the uncertainty of the causes of the premature failure, it is very difficult to draw any

conclusions without running more tests. Such tests would have to eliminate or reduce all of the potential problems associated with the test setup in order to be conclusive. This could be done by carefully aligning the shaft on the plate such that the runout was reduced, lowering the speed of the test so that any other loads caused by the angular momentum of the shaft were minimized, and carefully aligning the flexure to the axis of rotation of the motor. Although an attempt to minimize these factors was made for the first test, it is possible tha. the imperfections were still large enough to cause premature failure at the high speed that was used. If these imperfections were minimized to such a level that there would be a high level of confidence that they would not affect the fatigue life significantly, yet the flexure still failed, then the root of the problem would be in the strength and properties of the PH 13-8 Mo.

Chapter 8
Conclusions and Recommendations

After several modifications were made, the assembly and brazing of the flexure was successfully completed using PH 13-8 Mo as the base metal. Nicoro foil was the filler material used for the first braze, which brazed the blades into the tubes, and Nioro foil was used for the second braze, which brazed the blade and tube assemblies into the frame pieces. With the exception of the fatigue results and high hysteresis, the flexure performed as expected. It was rotationally soft about the x and y axes and very stiff about the z axis as well as in translation along all three axes.

The hysteresis indicated that either the blade material, the filler material, or both underwent some plastic deformation when the flexure was deflected over 55 mrad. This presented problems because it could have meant that either the strength of the material had deteriorated from the brazing and heat treatment or the loads experienced by the blades at this deflection were much higher than predicted.

The low fatigue life tends to support the idea that the material properties might deteriorate due to the heating and cooling cycles during the brazing and heat treating. If the flexure blades were undergoing plastic deformation at a deflection of 87 mrad, this would bring about a premature failure. The results from the fatigue tests, however, were inconclusive due to the presence of eccentricities in the test setup which could have also contributed to the premature failure.

More research and experimentation needs to be done to determine the actual effects of the brazing and heat treating on the mechanical properties of the PH 13-8 Mo flexure blades. By doing so, the possible causes of the problems due to hysteresis and fatigue could be narrowed down. If the problems are due to the heating and cooling cycles of these processes and a method is found to eliminate these negative effects on the blades, then this two-axis flexure design would be able to meet all of its intended purposes and would eliminate all of the shortcomings that are present in the existing two-axis flexures.

When designing a two-axis flexure using the crossed-leaf approach, the following recommendations should be followed:

1. Tolerances for the critical dimensions, such as the height of the radii in the frame pieces holding the tubes, should be tight so that the axes of the blade will be collinear.

2. The slots should be 0.002" wider than the thickness of the blade and the EDM surface of the slot lapped with silicon carbide. A silicon carbide grinding wheel should be used if the blades are surface ground. A wheel made out of aluminum oxide should not be used, as this will impede the wetting of the blades.

3. Filler material in the form of 0.001" foil should be used for the brazing of the blades into the tubes to insure that the filler material wets both the surface of the blade and the surface of the slot in the tube.

4. The placement of the foil between the blades and the tubes must be carefully controlled to insure that the desired fillet radii result. If not carefully controlled, the stiffnesses between the axes can vary significantly.

5. Before brazing the entire assembly, the tops of the tubes in the frame pieces should be measured. If the differences between these measurements are out of the tolerance range, shims can be placed underneath to even them out.

6. If the fatigue failure was indeed due to the change in the mechanical properties from the heating and cooling cycles causing plastic deformation in the blades, then the infinite life angular range of the flexure may only be ±55 mrad. Therefore, the elastic range of the flexure should be found before the infinite life angular range is determined.

Bibliography

American Welding Society Committee on Brazing and Soldering, *Brazing Manual*, Third Edition, Revised, American Welding Society, Miami, 1975.

Armco, Inc., *Armco PH 13-8 Mo Stainless Steel*, Product Data Bulletin No. S-24, (October, 1986), Armco Inc.

Hickey, C. F. Jr., "PH 13-8 Mo," *Aerospace Structural Metals Handbook*,

Kohl, W. H., *Materials and Techniques for Electron Tubes*, Reinhold Publishing Corporation, New York, 1960.

Shanley, F. R., *Strength of Materials*, McGraw-Hill Book Company, Inc., New York, 1957.

Troeger, H., "Considerations in the Applications of Flexural Pivots," *Automatic Control*, pp. 41-46, November, 1962

Young, W. E., "An Investigation of the Cross-Spring Pivot," *Journal of Applied Mechanics*, pp. A113-A120, June, 1944.

Appendix A
Data and Graphs

Table A.1 - Data from the X Axis of Flexure 1

# of Nickels	Applied Torque (in-lbs)	Theoretical Deflection (radians)	Measured Stiffness Deflection (radians)	Deflection Run 1 - Down (radians)	Error from Theoretical Run 1 - Down (radians)	Error from Measured Stiffness Run 1 - Down (radians)	Deflection Run 1 - Up (radians)	Error from Theoretical Run 1 - Up (radians)	Error from Measured Stiffness Run 1 - Up (radians)
1	-0.0440	-0.0105	-0.0116	-0.0094	0.0011	0.0022	-0.0125	-0.0020	-0.0009
2	-0.0886	-0.0211	-0.0211	-0.0190	0.0021	0.0021	-0.0220	-0.0009	-0.0009
3	-0.1325	-0.0315	-0.0306	-0.0287	0.0028	0.0019	-0.0331	-0.0016	-0.0025
4	-0.1785	-0.0424	-0.0404	-0.0385	0.0039	0.0019	-0.0409	0.0015	-0.0005
5	-0.2175	-0.0517	-0.0488	-0.0472	0.0045	0.0016	-0.0494	0.0023	-0.0006
6	-0.2656	-0.0632	-0.0591	-0.0585	0.0047	0.0006			
7	-0.3112	-0.0740	-0.0688	-0.0678	0.0062	0.0010	-0.0691	0.0049	-0.0003
8	-0.3540	-0.0842	-0.0780	-0.0787	0.0055	-0.0007	-0.0788	0.0054	-0.0008
9	-0.3963	-0.0943	-0.0871	-0.0878	0.0065	-0.0007	-0.0878	0.0065	-0.0007
0	0.0000	0.0000	-0.0022	-0.0011	-0.0011	0.0011	-0.0034	-0.0034	-0.0012
1	0.0440	0.0105	0.0073	0.0083	-0.0022	0.0010	0.0059	-0.0046	-0.0014
2	0.0886	0.0211	0.0168	0.0178	-0.0033	0.0010	0.0157	-0.0054	-0.0011
3	0.1325	0.0315	0.0262	0.0271	-0.0044	0.0009	0.0251	-0.0064	-0.0011
4	0.1785	0.0424	0.0361	0.0366	-0.0058	0.0005	0.0350	-0.0074	-0.0011
5	0.2175	0.0517	0.0444	0.0488	-0.0029	0.0044	0.0432	-0.0085	-0.0012
6	0.2656	0.0632	0.0547	0.0549	-0.0083	0.0002	0.0542	-0.0090	-0.0005
7	0.3112	0.0740	0.0645	0.0647	-0.0093	0.0002	0.0638	-0.0100	-0.0007
8	0.3540	0.0842	0.0737	0.0734	-0.011	-0.0003	0.0728	-0.0110	-0.0009
9	0.0396	0.0943	0.0828	0.0823	-0.012	-0.0005	0.0823	-0.0120	-0.0005

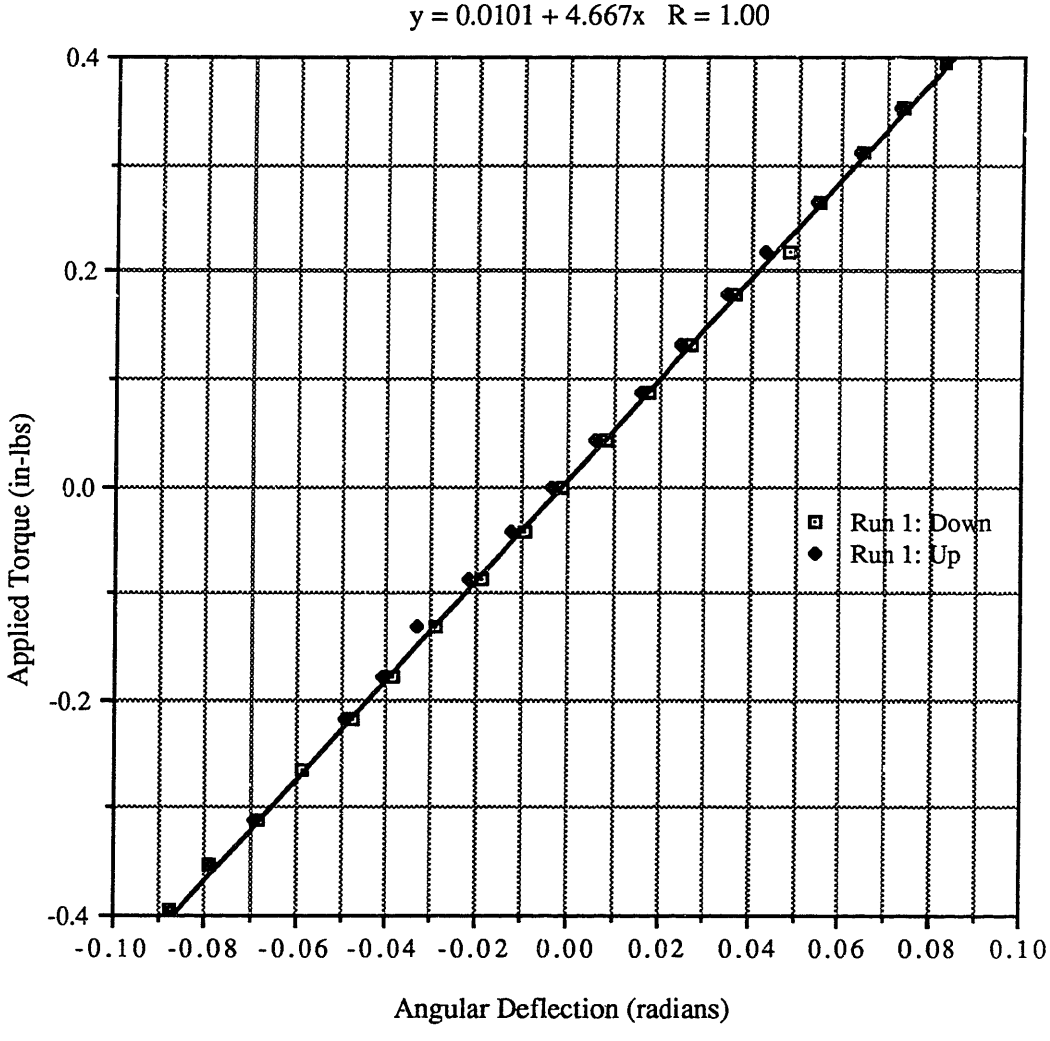

Figure A.1 - Torque vs. Angular Deflection for the X Axis of Flexure 1

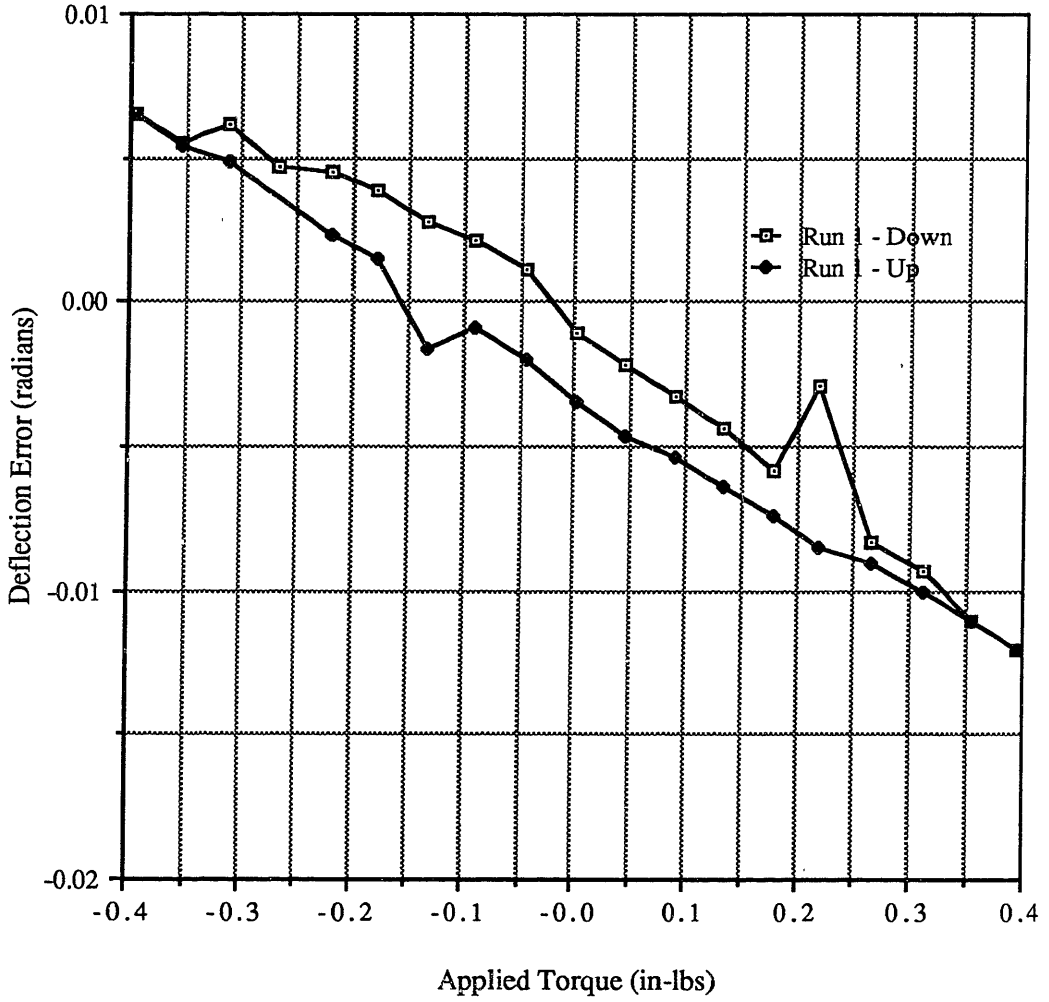

Figure A.2 - Deflection Error vs. Torque for the X Axis of Flexure 1

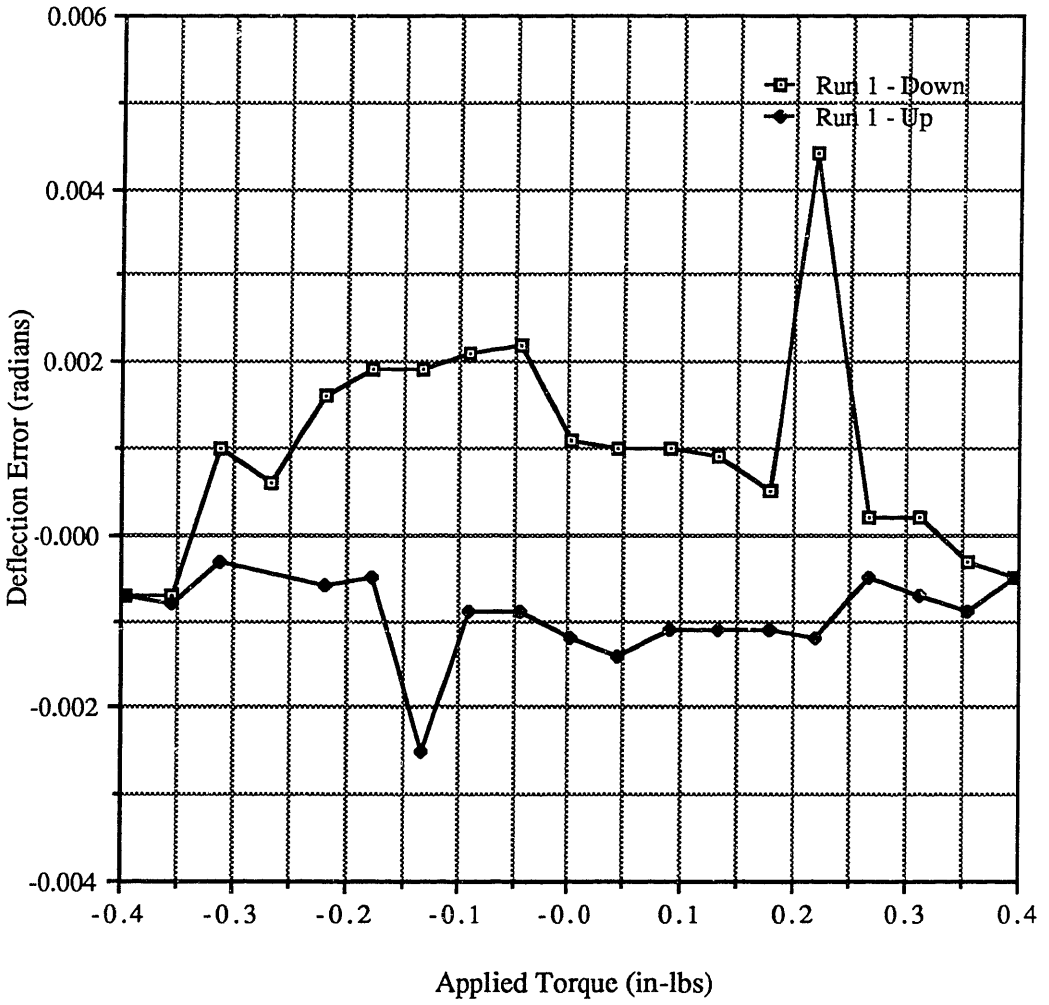

Figure A.3 - Normalized Error Curve for the X Axis of Flexure 1

Table A.2 - Data from a 45° Offset Axis of Flexure 1

# of Nickels	Applied Torque (in-lbs)	Theoretical Deflection (radians)	Measured Stiffness Deflection (radians)	Deflection Run 1 - Down (radians)	Error from Theoretical Run 1 - Down (radians)	Error from Measured Stiffness Run 1 - Down (radians)	Deflection Run 1 - Up (radians)	Error from Theoretical Run 1 - Up (radians)	Error from Measured Stiffness Run 1 - Up (radians)
1	-0.0440	-0.0105	-0.0112	-0.0098	0.0007	0.0014	-0.0112	-0.0007	0.0000
2	-0.0886	-0.0211	-0.0215	-0.0202	0.0009	0.0013	-0.0221	-0.0010	-0.0006
3	-0.1325	-0.0315	-0.0316	-0.0303	0.0012	0.0013	-0.0322	-0.0007	-0.0006
4	-0.1785	-0.0424	-0.0422	-0.0409	0.0015	0.0013	-0.0427	-0.0003	-0.0005
5	-0.2175	-0.0517	-0.0513	-0.0504	0.0013	0.0009	-0.0517	0.0000	-0.0004
6	-0.2656	-0.0632	-0.0624	-0.0617	0.0015	0.0007	-0.0628	0.0004	-0.0004
7	-0.3112	-0.0740	-0.0729	-0.0725	0.0015	0.0004	-0.0732	0.0008	-0.0003
8	-0.3540	-0.0842	-0.0828	-0.0830	0.0012	-0.0002	-0.0833	0.0009	-0.0005
9	-0.3963	-0.0943	-0.0926	-0.0933	0.0010	-0.0007	-0.0933	0.0010	-0.0007
0	0.0000	0.0000	-0.0010	-0.0007	-0.0007	0.0003	-0.0018	-0.0018	-0.0008
1	0.0440	0.0105	0.0092	0.0097	-0.0008	0.0005	0.0082	-0.0023	-0.0010
2	0.0886	0.0211	0.0195	0.0200	-0.0011	0.0005	0.0187	-0.0024	-0.0008
3	0.1325	0.0315	0.0296	0.0303	-0.0012	0.0007	0.0289	-0.0026	-0.0007
4	0.1785	0.0424	0.0403	0.0408	-0.0016	0.0005	0.0395	-0.0029	-0.0008
5	0.2175	0.0517	0.0493	0.0498	-0.0019	0.0005	0.0487	-0.0030	-0.0006
6	0.2656	0.0632	0.0604	0.0607	-0.0025	0.0003	0.0602	-0.0030	-0.0002
7	0.3112	0.0740	0.0709	0.0712	-0.0028	0.0003	0.0710	-0.0030	0.0001
8	0.3540	0.0842	0.0808	0.0808	-0.0034	0.0000	0.0804	-0.0038	-0.0004
9	0.0396	0.0943	0.0906	0.0904	-0.0039	-0.0002	0.0904	-0.0039	-0.0002

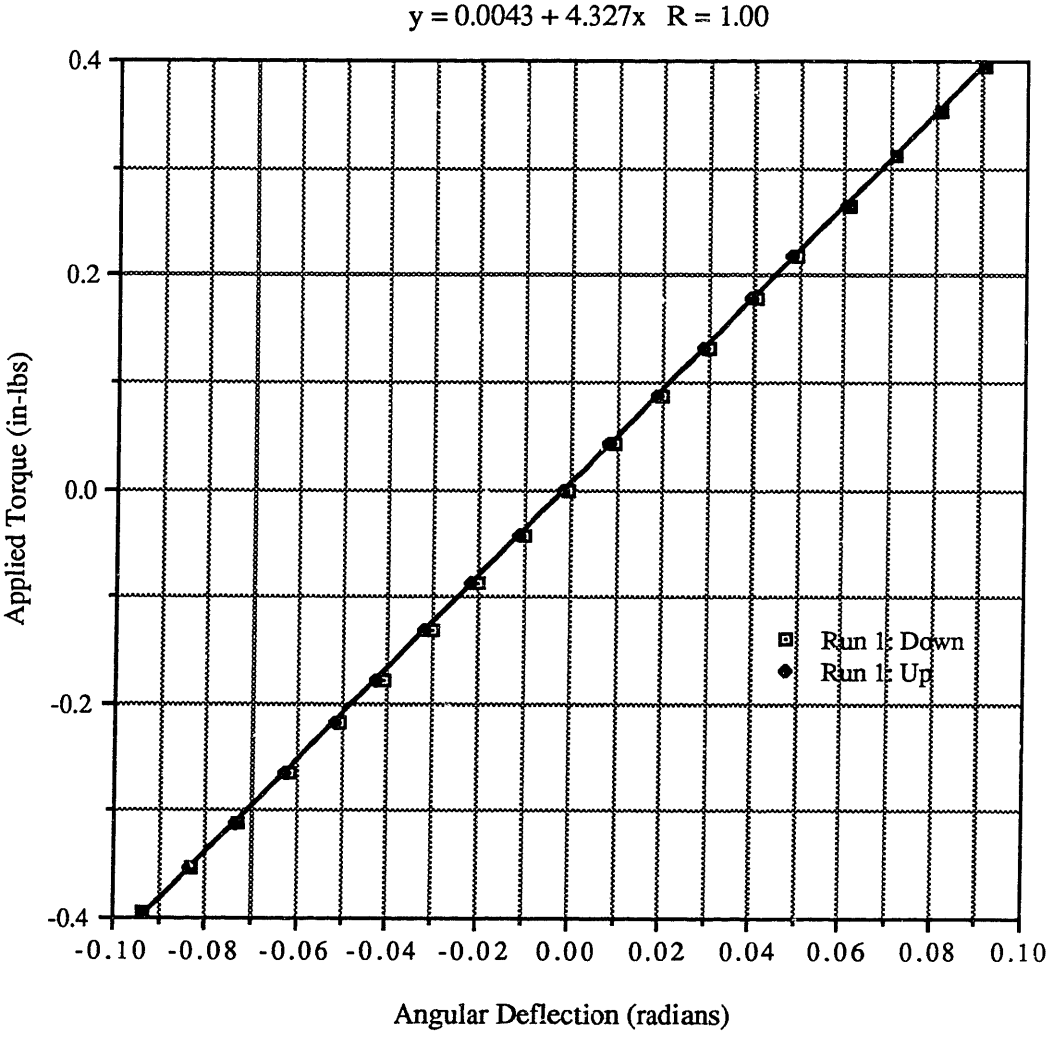

Figure A.4 - Torque vs. Angular Deflection for a 45° Offset Axis of Flexure 1

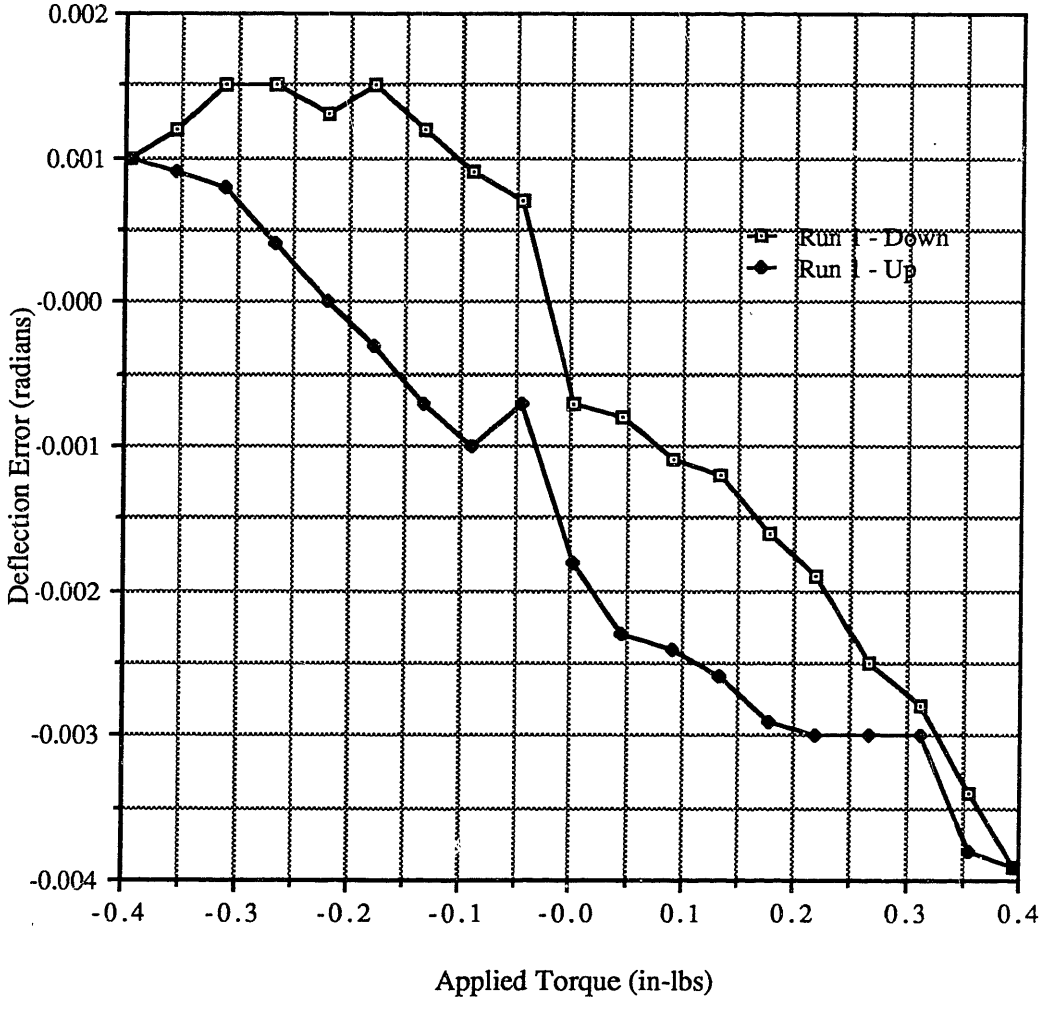

Figure A.5 - Deflection Error vs. Torque for a 45° Offset Axis of Flexure 1

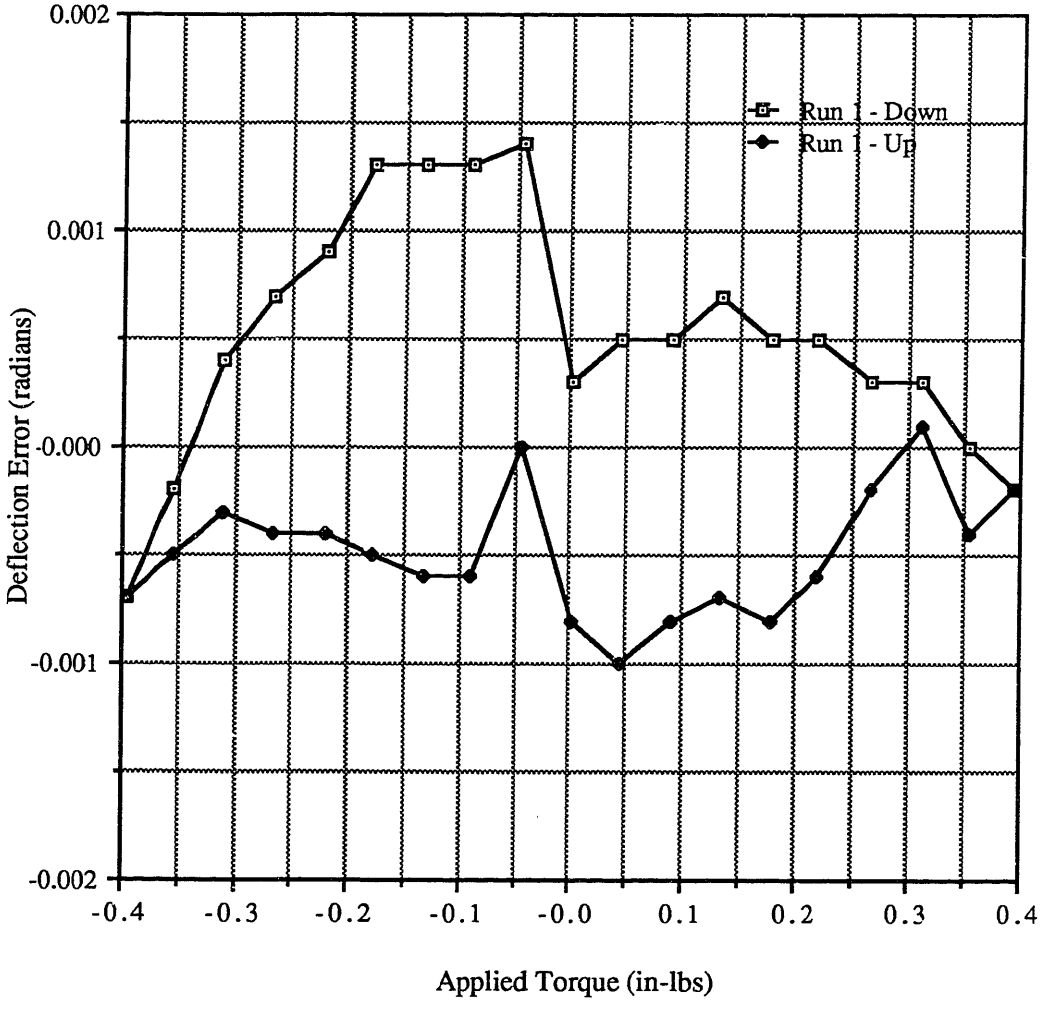

Figure A.6 - Normalized Error Curve for a 45° Offset Axis of Flexure 1

Table A.3 - Data from the Y Axis of Flexure 1

# of Nickels	Applied Torque (in-lbs)	Theoretical Deflection (radians)	Measured Stiffness Deflection (radians)	Deflection Run 1 - Down (radians)	Error from Theoretical Run 1 - Down (radians)	Error from Measured Stiffness Run 1 - Down (radians)	Deflection Run 1 - Up (radians)	Error from Theoretical Run 1 - Up (radians)	Error from Measured Stiffness Run 1 - Up (radians)
1	-0.0440	-0.0105	-0.0112	-0.0109	-0.0004	0.0003	-0.0115	-0.0010	-0.0003
2	-0.0886	-0.0211	-0.0223	-0.0219	-0.0008	0.0004	-0.0225	-0.0014	-0.0002
3	-0.1325	-0.0315	-0.0332	-0.0327	-0.0012	0.0005	-0.0341	-0.0026	-0.0009
4	-0.1785	-0.0424	-0.0447	-0.0433	-0.0009	0.0014	-0.0446	-0.0022	0.0001
5	-0.2175	-0.0517	-0.0543	-0.0539	-0.0022	0.0004	-0.0544	-0.0027	-0.0001
6	-0.2656	-0.0632	-0.0663	-0.0661	-0.0029	0.0002	-0.0664	-0.0032	-0.0001
7	-0.3112	-0.0740	-0.0776	-0.0774	-0.0034	0.0002	-0.0775	-0.0035	0.0001
8	-0.3540	-0.0842	-0.0883	-0.0885	-0.0043	-0.0002	-0.0884	-0.0042	-0.0001
9	-0.3963	-0.0943	-0.0988	-0.0992	-0.0049	-0.0004	-0.0992	-0.0049	-0.0004
0	0.0000	0.0000	-0.0003	0.0000	0.0000	0.0003	-0.0007	-0.0007	-0.0004
1	0.0440	0.0105	0.0106	0.0109	0.0004	0.0003	0.0101	-0.0004	-0.0005
2	0.0886	0.0211	0.0217	0.0219	0.0008	0.0002	0.0213	0.0002	-0.0004
3	0.1325	0.0315	0.0326	0.0328	0.0013	0.0002	0.0323	0.0008	-0.0003
4	0.1785	0.0424	0.0441	0.0443	0.0019	0.0002	0.0438	0.0014	-0.0003
5	0.2175	0.0517	0.0538	0.0541	0.0024	0.0003	0.0536	0.0019	-0.0002
6	0.2656	0.0632	0.0657	0.0658	0.0026	0.0001	0.0656	0.0024	-0.0001
7	0.3112	0.0740	0.0770	0.0770	0.0030	0.0000	0.0770	0.0030	0.0000
8	0.3540	0.0842	0.0877						
9	0.0396	0.0943	0.0982						

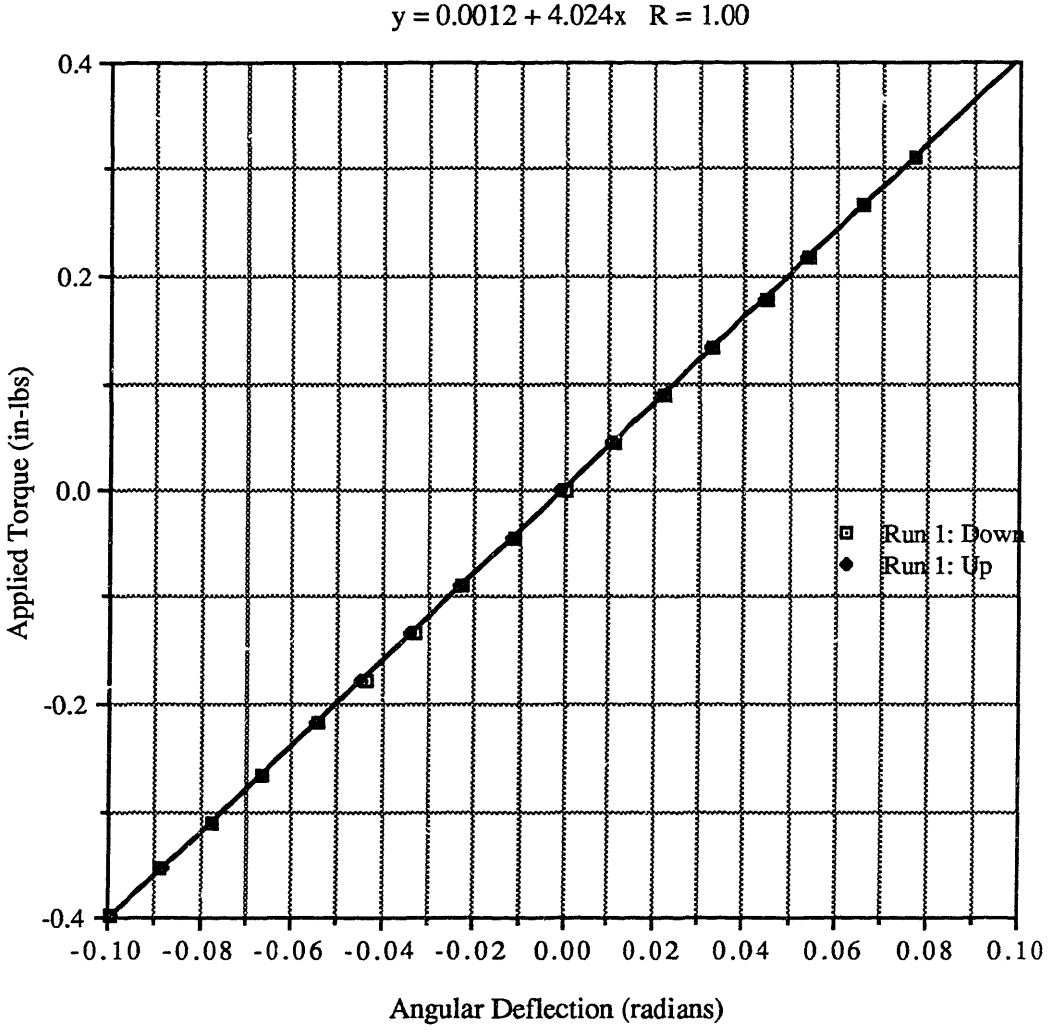

Figure A.7 - Torque vs. Angular Deflection for the Y Axis of Flexure 1

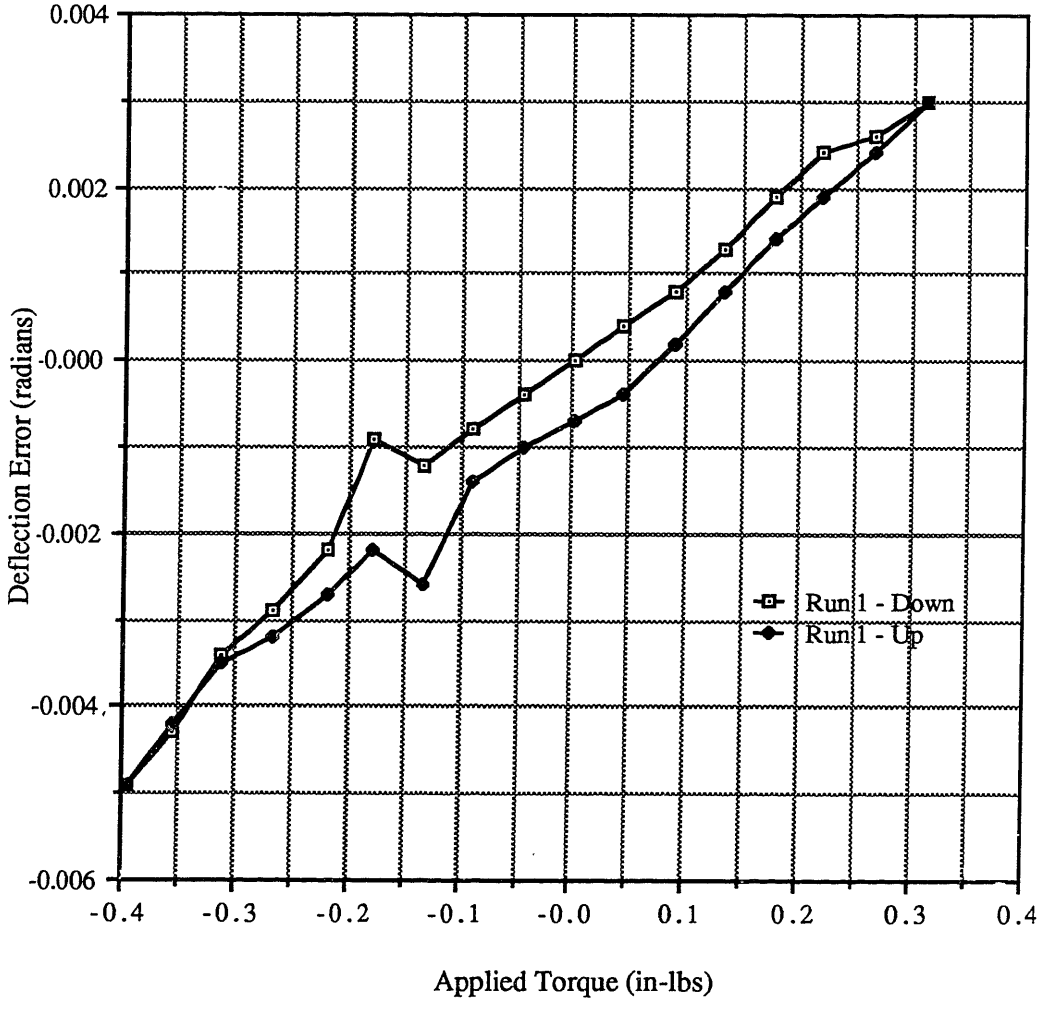

Figure A.8 - Deflection Error vs. Torque for the Y Axis of Flexure 1

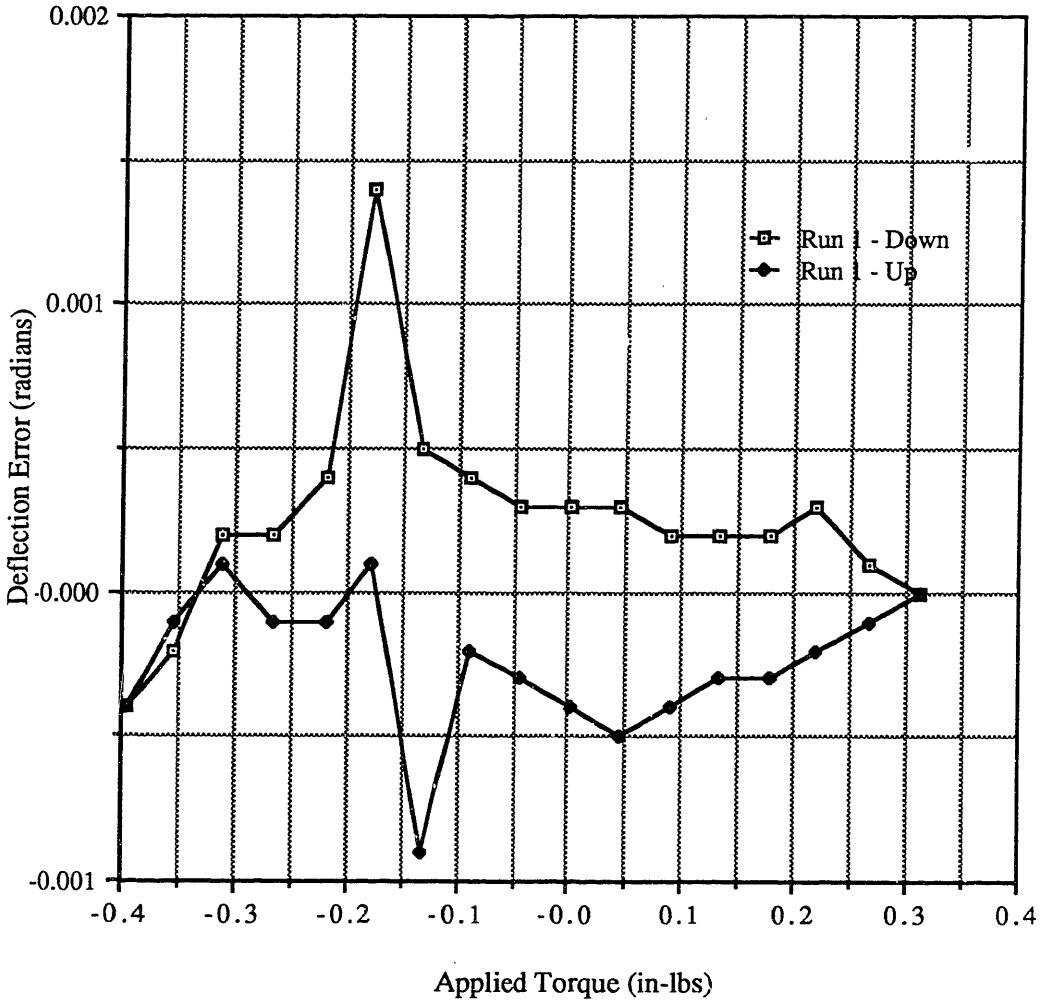

Figure A.9 - Normalized Error Curve for the Y Axis of Flexure 1

Table A.4 - Data from a 45° Offset Axis of Flexure 1

# of Nickels	Applied Torque (in-lbs)	Theoretical Deflection (radians)	Measured Stiffness Deflection (radians)	Deflection Run 1 - Down (radians)	Error from Theoretical Run 1 - Down (radians)	Error from Measured Stiffness Run 1 - Down (radians)	Deflection Run 1 - Up (radians)	Error from Theoretical Run 1 - Up (radians)	Error from Measured Stiffness Run 1 - Up (radians)
1	-0.0440	-0.0105	-0.0107	-0.0101	0.0004	0.0006	-0.0111	-0.0006	-0.0004
2	-0.0886	-0.0211	-0.0210	-0.0205	0.0006	0.0005	-0.0213	-0.0002	-0.0003
3	-0.1325	-0.0315	-0.0310	-0.0307	0.0008	0.0003	-0.0312	0.0003	-0.0002
4	-0.1785	-0.0424	-0.0416	-0.0411	0.0013	0.0005	-0.0418	0.0006	-0.0002
5	-0.2175	-0.0517	-0.0505	-0.0501	0.0016	0.0004	-0.0507	0.0010	-0.0002
6	-0.2656	-0.0632	-0.0616	-0.0613	0.0019	0.0003	-0.0618	0.0014	-0.0002
7	-0.3112	-0.0740	-0.0720	-0.0718	0.0022	0.0002	-0.0719	0.0021	0.0001
8	-0.3540	-0.0842	-0.0819	-0.0821	0.0021	-0.0002	-0.0821	0.0021	-0.0002
9	-0.3963	-0.0943	-0.0916	-0.0913	0.003	0.0003	-0.0913	0.0030	0.0003
0	0.0000	0.0000	-0.0006	-0.0008	-0.0008	-0.0002	-0.0011	-0.0011	-0.0005
1	0.0440	0.0105	0.0095	0.0094	-0.0011	-0.0001	0.0089	-0.0016	-0.0006
2	0.0886	0.0211	0.0197	0.0197	-0.0014	0.0000	0.0192	-0.0019	-0.0005
3	0.1325	0.0315	0.0298	0.0297	-0.0018	-0.0001	0.0293	-0.0022	-0.0005
4	0.1785	0.0424	0.0403	0.0405	-0.0019	0.0002	0.0402	-0.0022	-0.0001
5	0.2175	0.0517	0.0493	0.0495	-0.0022	0.0002	0.0490	-0.0027	-0.0003
6	0.2656	0.0632	0.0603	0.0606	-0.0026	0.0003	0 0599	-0.0033	-0.0004
7	0.3112	0.0740	0.0708	0.0712	-0.0028	0.0004	0.0705	-0.0035	-0.0003
8	0.3540	0.0842	0.0806	0.0805	-0.0037	-0.0001	0.0801	-0.0041	-0.0005
9	0.0396	0.0943	0.0903	0.0910	-0.0033	0.0007	0.0910	-0.0033	0.0007

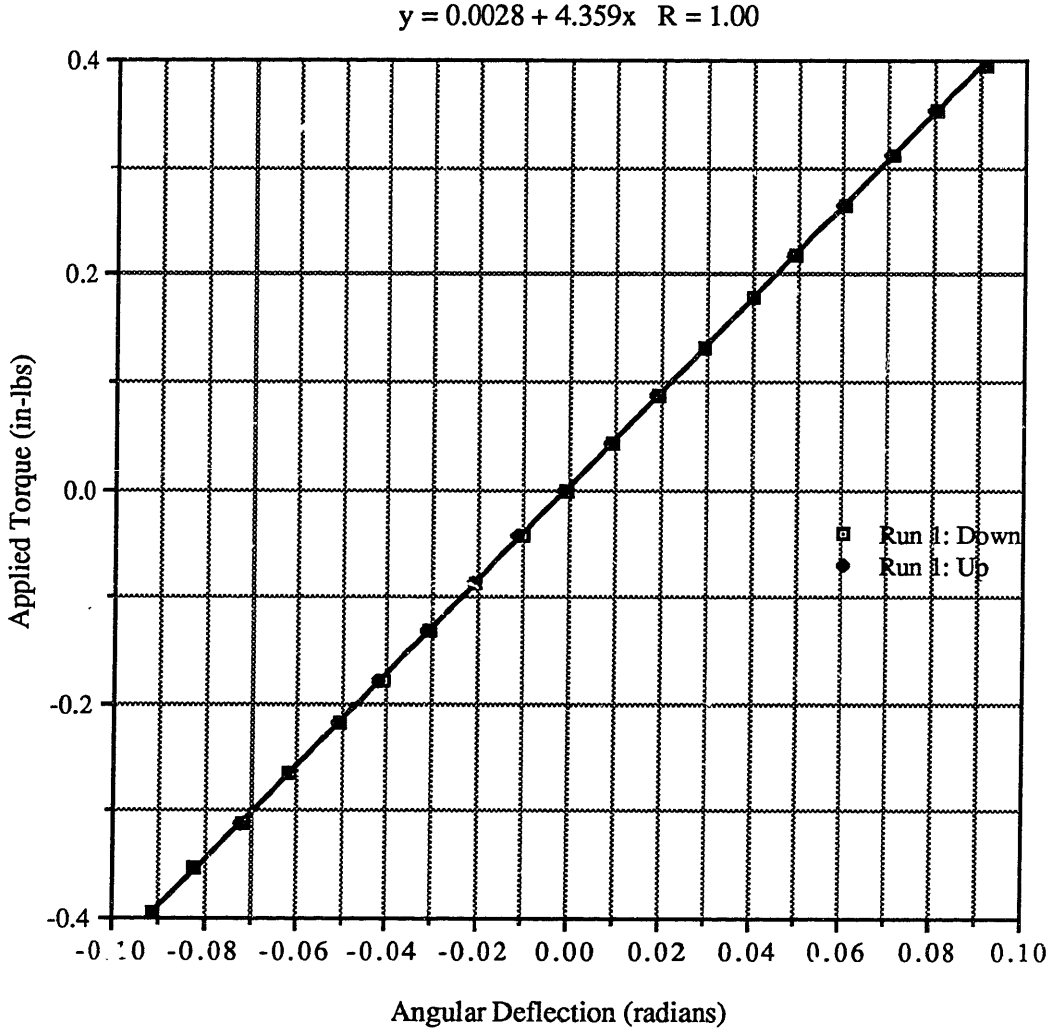

Figure A.10 - Torque vs. Angular Deflection for a 45° Offset Axis of Flexure 1

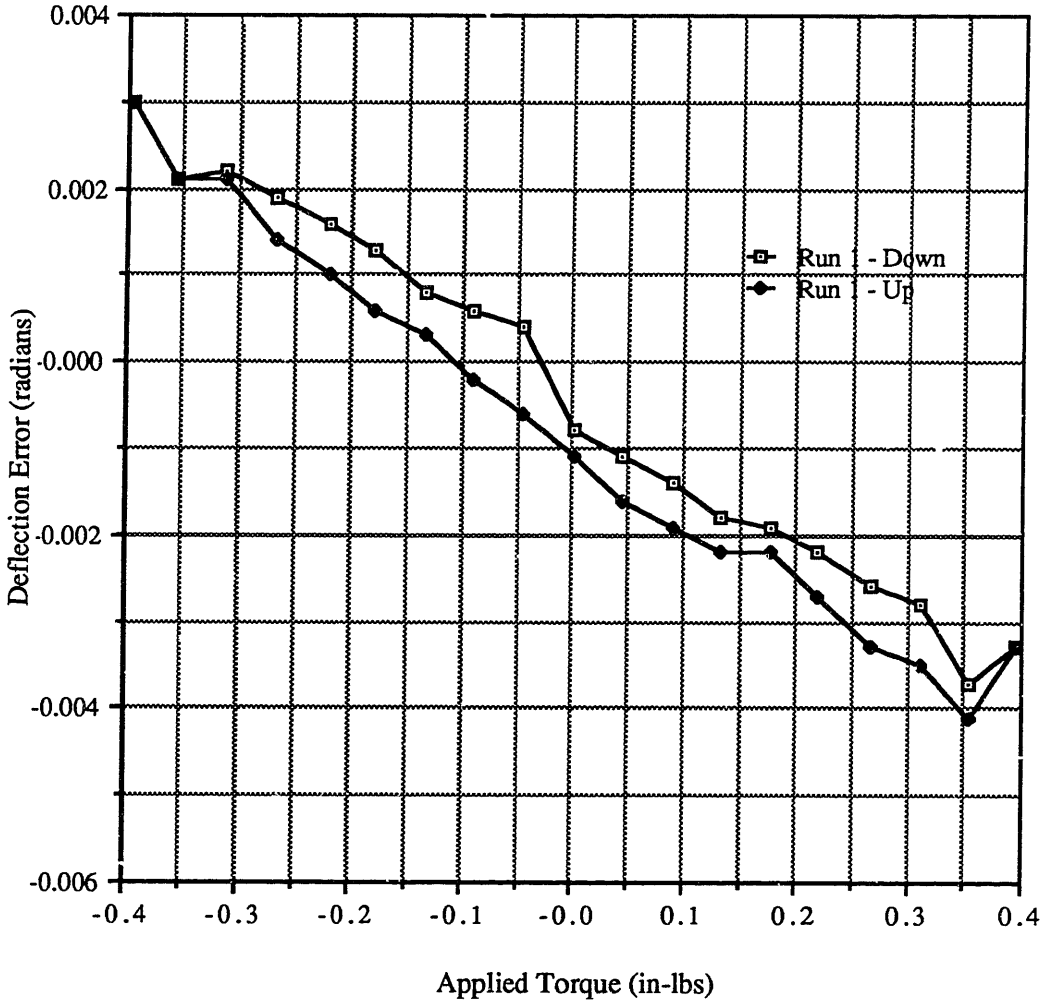

Figure A.11 - Deflection Error vs. Torque for a 45° Offset Axis of Flexure 1

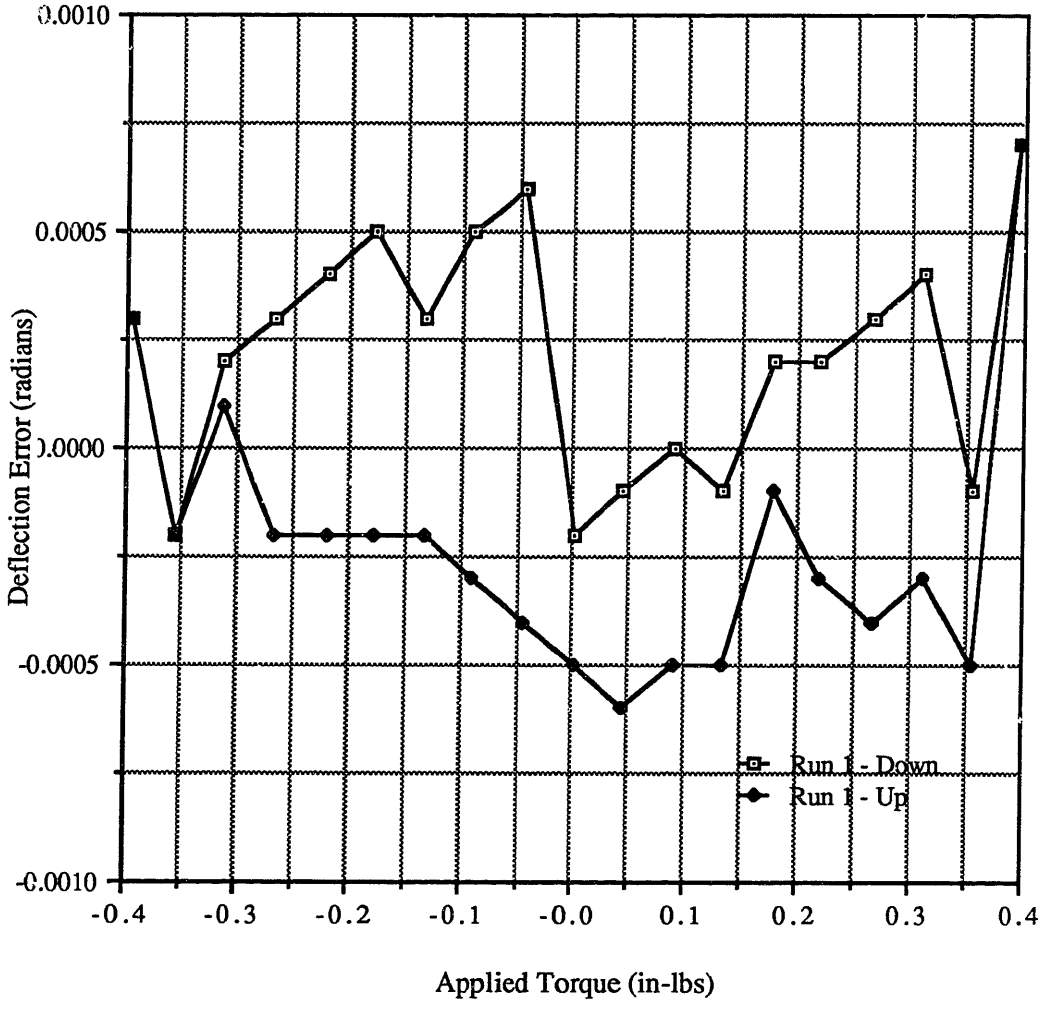

Figure A.12 - Normalized Error Curve for a 45° Offset Axis of Flexure 1

Table A.5 - Data from the X Axis of Flexure 2

# of Nickels	Applied Torque (in-lbs)	Theoretical Deflection (radians)	Measured Stiffness Deflection (radians)	Deflection Run 1 - Down (radians)	Error from Theoretical Run 1 - Down (radians)	Error from Measured Stiffness Run 1 - Down (radians)	Deflection Run 1 - Up (radians)	Error from Theoretical Run 1 - Up (radians)	Error from Measured Stiffness Run 1 - Up (radians)
1	-0.0442	-0.0105	-0.0106	-0.0106	-0.0001	0.0000	-0.0113	-0.0008	-0.0007
2	-0.0893	-0.0212	-0.0214	-0.0214	-0.0002	0.0000	-0.0221	-0.0009	-0.0007
3	-0.1331	-0.0317	-0.0319	-0.0320	-0.0003	-0.0001	-0.0326	-0.0009	-0.0007
4	-0.1779	-0.0423	-0.0427	-0.0430	-0.0007	-0.0003	-0.0432	-0.0009	-0.0005
5	-0.2223	-0.0529	-0.0534	-0.0533	-0.0004	0.0001	-0.0538	-0.0009	-0.0004
6	-0.2651	-0.0630	-0.0636	-0.0642	-0.0012	-0.0006	-0.0640	-0.0010	-0.0004
7	-0.3092	-0.0735	-0.0742	-0.0750	-0.0015	-0.0008	-0.0747	-0.0012	-0.0005
8	-0.3530	-0.0839	-0.0848	-0.0854	-0.0015	-0.0006	-0.0844	-0.0005	0.0004
9	-0.3970	-0.0944	-0.0953	-0.0945	-0.0001	0.0008	-0.0945	-0.0001	0.0008
0	0.0000	0.0000	0.0001	0.0000	0.0000	-0.0001	-0.0009	-0.0009	-0.0010
1	0.0442	0.0105	0.0107	0.0108	0.0003	0.0001	0.0098	-0.0007	-0.0009
2	0.0893	0.0212	0.0215	0.0216	0.0004	0.0001	0.0207	-0.0005	-0.0008
3	0.1331	0.0317	0.0321	0.0320	0.0003	-0.0001	0.0315	-0.0002	-0.0006
4	0.1779	0.0423	0.0428	0.0428	0.0005	0.0000	0.0421	-0.0002	-0.0007
5	0.2223	0.0529	0.0535	0.0534	0.0005	-0.0001	0.0529	0.0000	-0.0006
6	0.2651	0.0630	0.0638	0.0637	0.0007	-0.0001	0.0631	0.0001	-0.0007
7	0.3092	0.0735	0.0744	0.0743	0.0008	-0.0001	0.0738	0.0003	-0.0006
8	0.3530	0.0839	0.0849	0.0848	0.0009	-0.0001	0.0845	0.0006	-0.0004
9	0.3970	0.0944	0.0955	0.0954	0.0010	-0.0001	0.0954	0.0010	-0.0001

Table A.5 (cont'd) - Data from the X Axis of Flexure 2

# of Nickels	Applied Torque (in-lbs)	Theoretical Deflection (radians)	Measured Stiffness Deflection (radians)	Deflection Run 2 - Down (radians)	Error from Theoretical Run 2 - Down (radians)	Error from Measured Stiffness Run 2 - Down (radians)	Deflection Run 2 - Up (radians)	Error from Theoretical Run 2 - Up (radians)	Error from Measured Stiffness Run 2 - Up (radians)
1	-0.0440	-0.0105	-0.0105	-0.0106	-0.0001	-0.0001	-0.0107	-0.0002	-0.0002
2	-0.0886	-0.0211	-0.0212	-0.0210	0.0001	0.0002	-0.0212	-0.0001	0.0000
3	-0.1325	-0.0315	-0.0318	-0.0315	0.0000	0.0003	-0.0316	-0.0001	0.0002
4	-0.1785	-0.0424	-0.0428	-0.0426	-0.0002	0.0002	-0.0426	-0.0002	0.0002
5	-0.2175	-0.0517	-0.0522	-0.0517	0.0000	0.0005	-0.0518	-0.0001	0.0004
6	-0.2656	-0.0632	-0.0638	-0.0634	-0.0002	0.0004	-0.0635	-0.0003	0.0003
7	-0.3112	-0.0740	-0.0747	-0.0741	-0.0001	0.0006	-0.0742	-0.0002	0.0005
8	-0.3540	-0.0842	-0.0850	-0.0846	-0.0004	0.0004	-0.0846	-0.0004	0.0004
9	-0.3963	-0.0943	-0.0952						
0	0.0000	0.0000	0.0001	0.0000	0.0000	-0.0001	-0.0002	-0.0002	-0.0003
1	0.0440	0.0105	0.0106	0.0113	0.0008	0.0007	0.0106	0.0001	0.0000
2	0.0886	0.0211	0.0214	0.0220	0.0009	0.0006	0.0214	0.0003	0.0000
3	0.1325	0.0315	0.0319	0.0324	0.0009	0.0005	0.0320	0.0005	0.0001
4	0.1785	0.0424	0.0430	0.0433	0.0009	0.0003	0.0432	0.0008	0.0002
5	0.2175	0.0517	0.0523	0.0529	0.0012	0.0006	0.0526	0.0009	0.0003
6	0.2656	0.0632	0.0639	0.0647	0.0015	0.0008	0.0642	0.0010	0.0003
7	0.3112	0.0740	0.0749	0.0757	0.0017	0.0008	0.0754	0.0014	0.0005
8	0.3540	0.0842	0.0851	0.0859	0.0017	0.0008	0.0859	0.0017	0.0008
9	0.3963	0.0943	0.0953	0.0960	0.0017	0.0007	0.0960	0.0017	0.0007

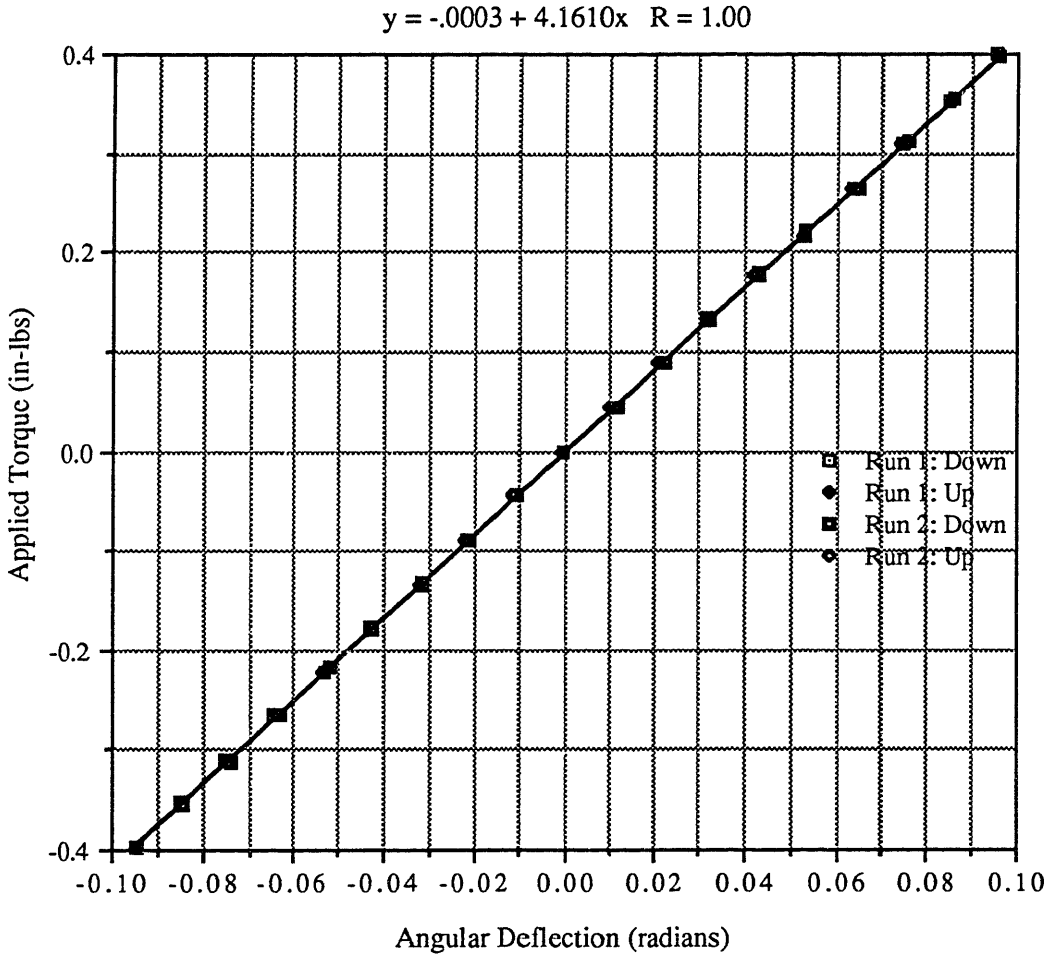

Figure A.13 - Torque vs. Angular Deflection for the X Axis of Flexure 2

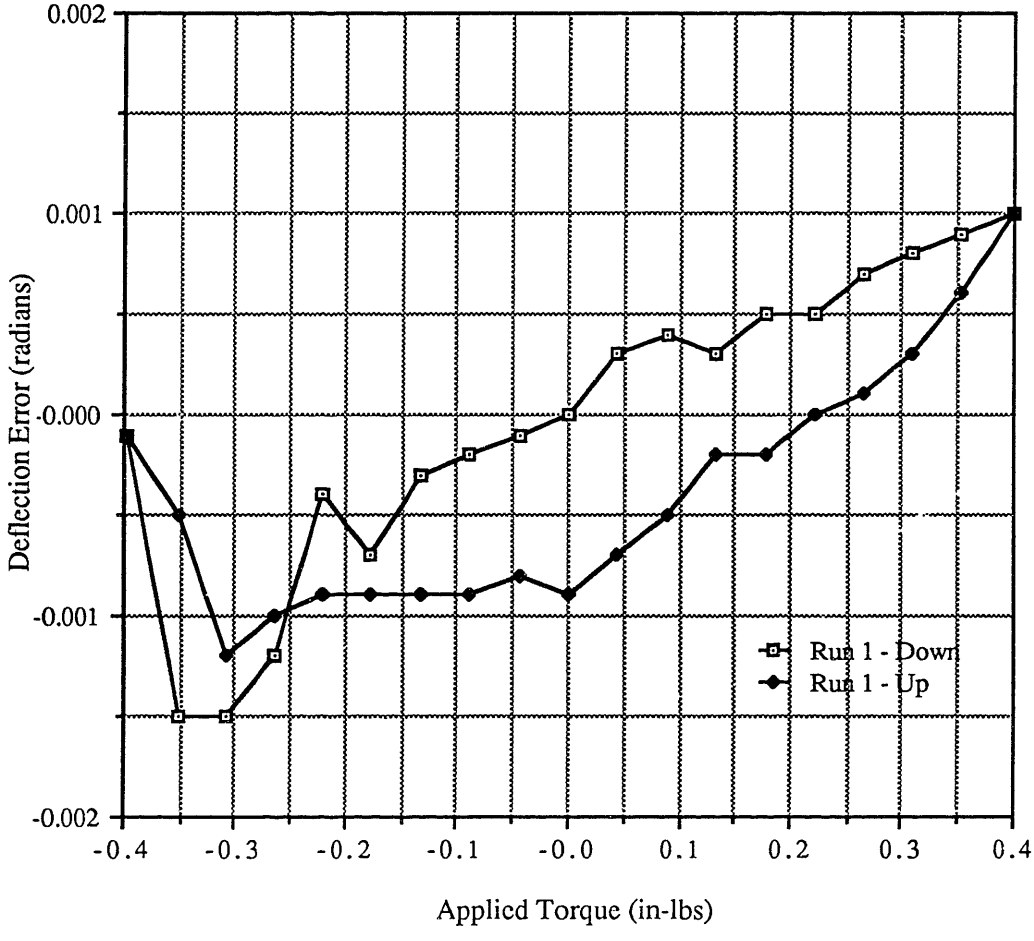

Figure A.14 - Deflection Error vs. Torque for the X Axis of Flexure 2

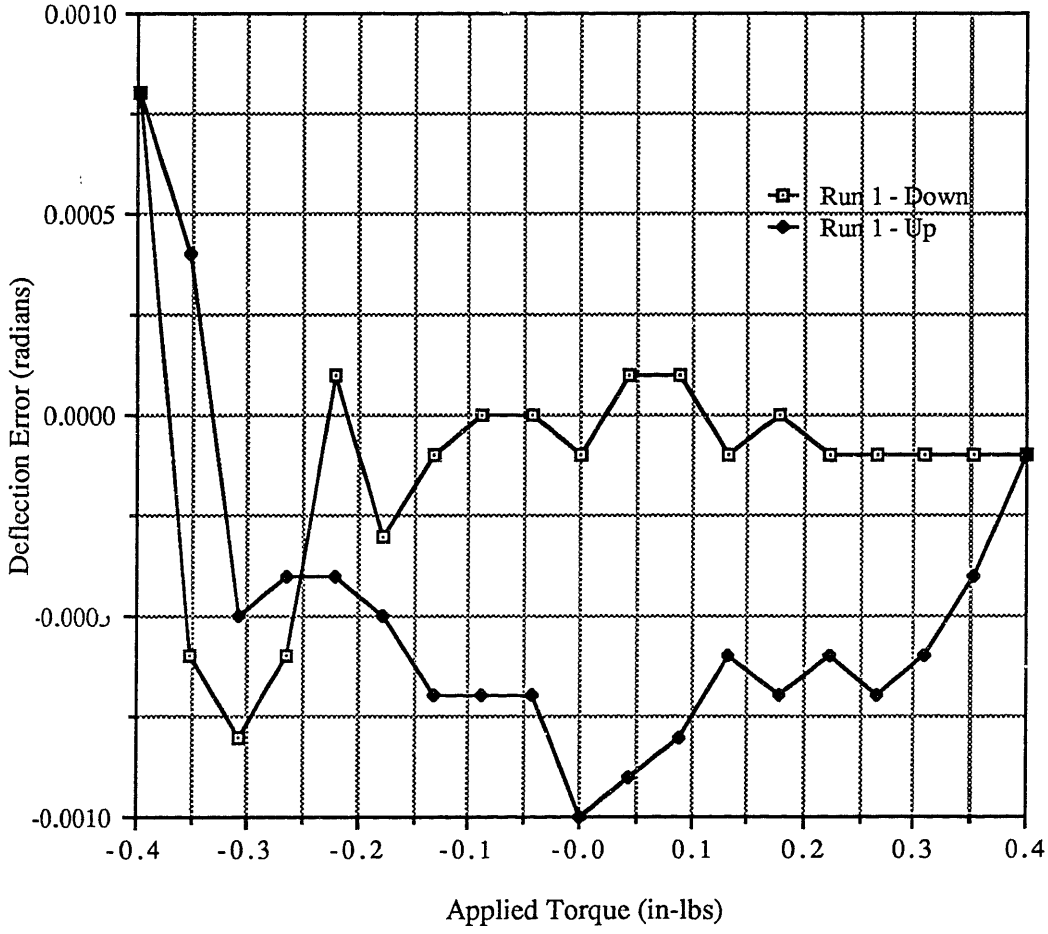

Figure A.15 - Normalized Error Curve for the X Axis of Flexure 2

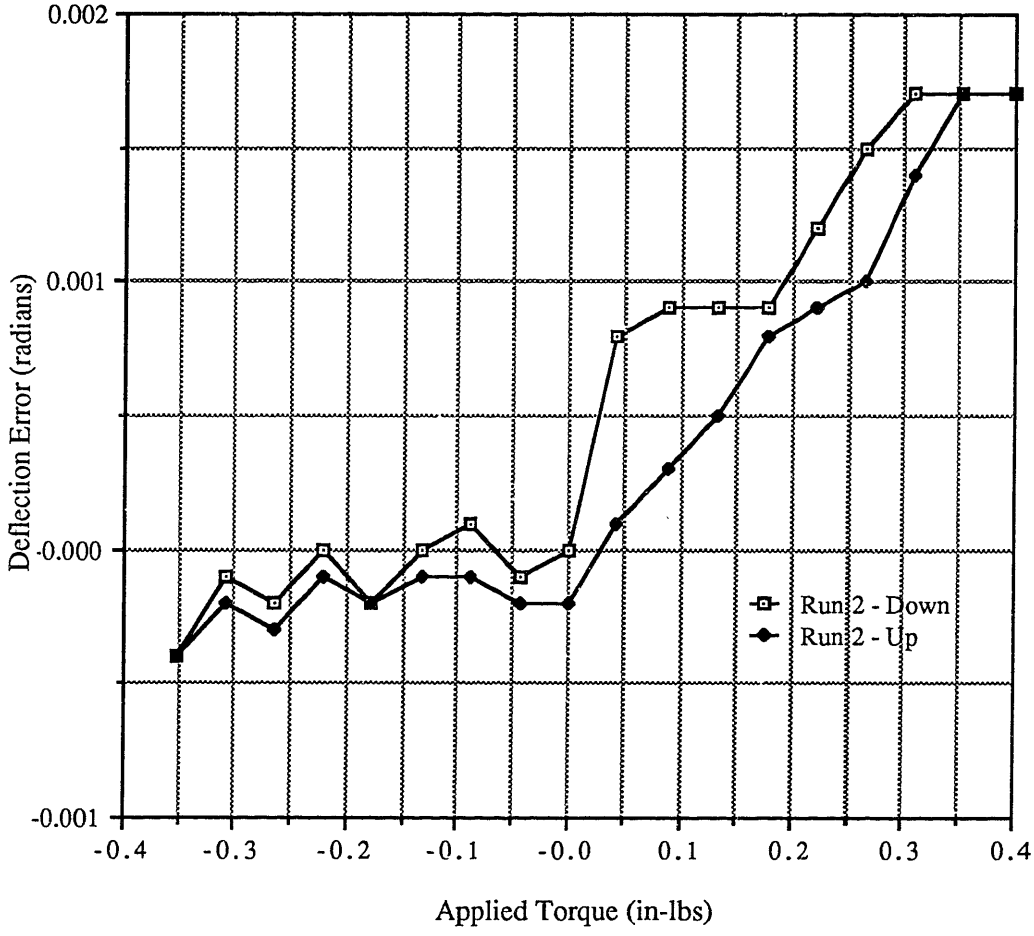

Figure A.16 - Deflection Error vs. Torque for the X Axis of Flexure 2

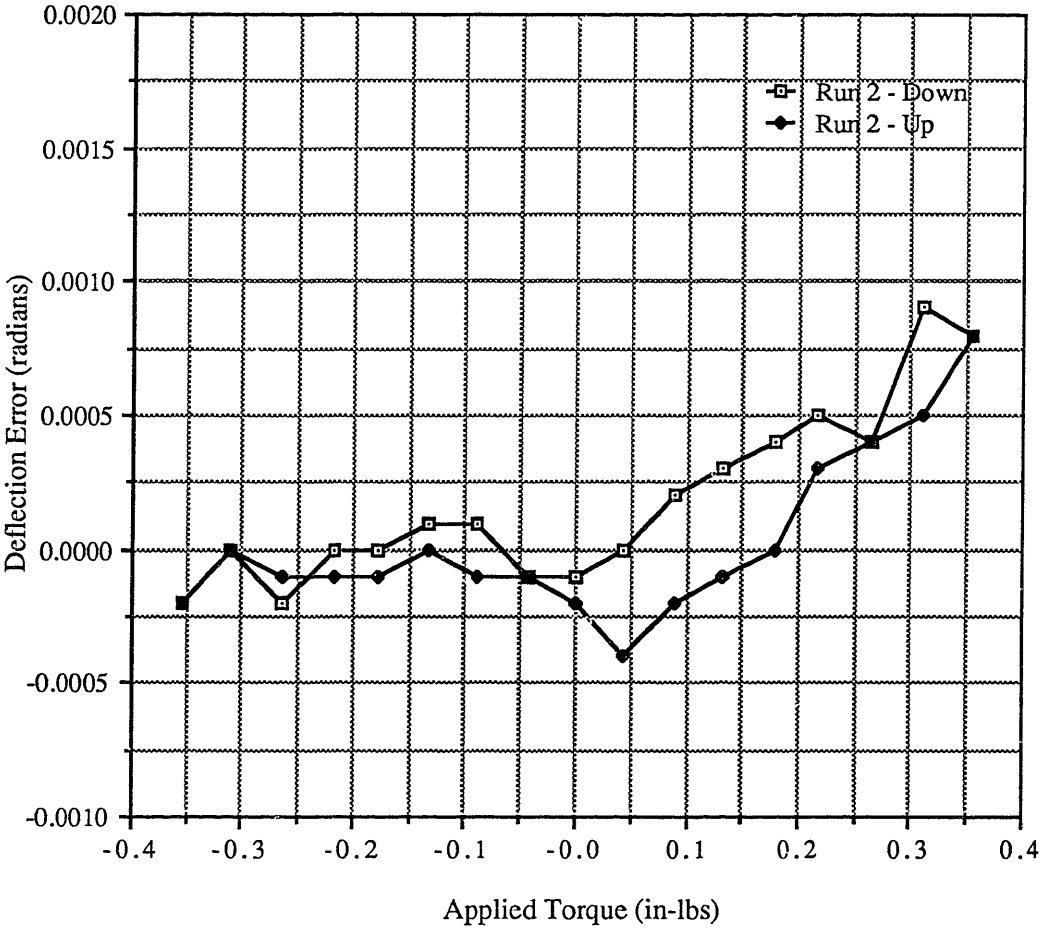

Figure A.17 - Normalized Error Curve for the X-Axis of Flexure 2

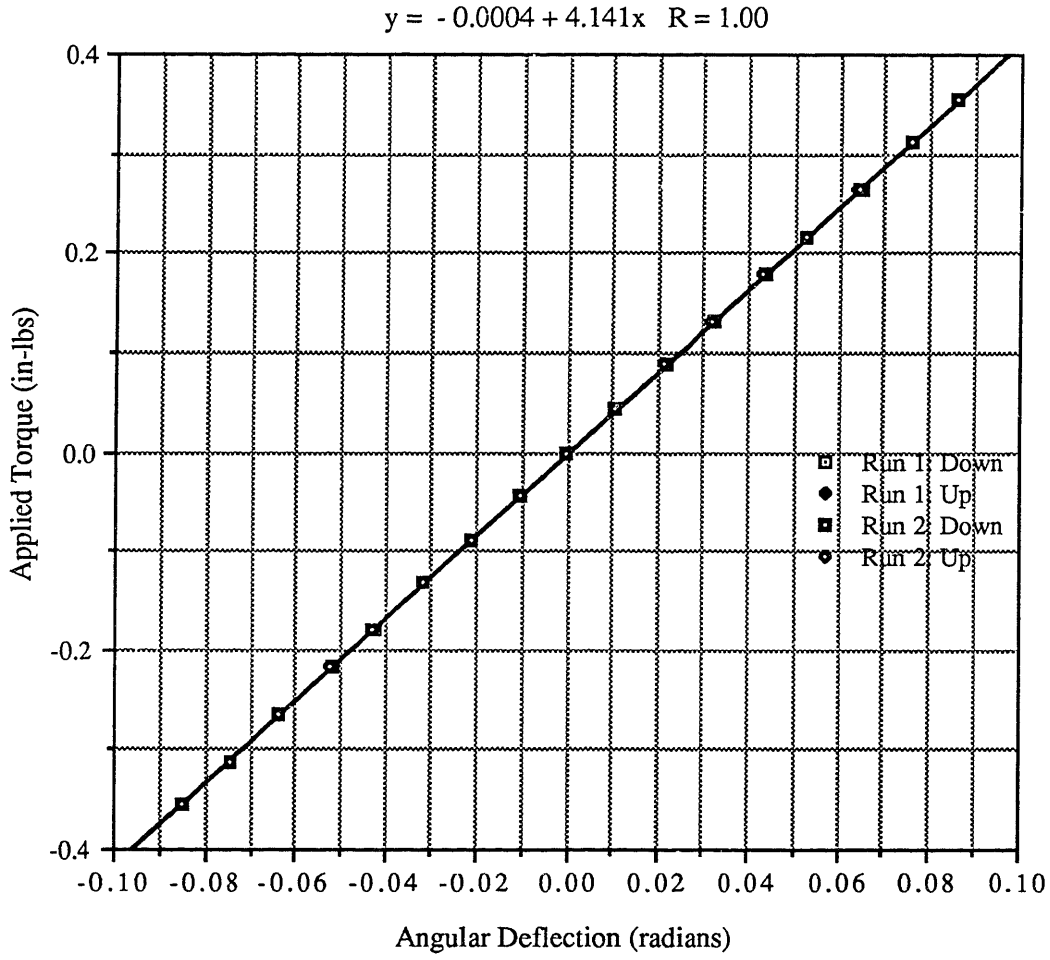

Figure A.18 - Torque vs. Angular Deflection for a 45° Offset Axis of Flexure 2

Table A.6 (cont'd) - Data from a 45° Offset Axis of Flexure 2

# of Nickels	Applied Torque (in-lbs)	Theoretical Deflection (radians)	Measured Stiffness Deflection (radians)	Deflection Run 2 - Down (radians)	Error from Theoretical Run 2 - Down (radians)	Error from Measured Stiffness Run 2 - Down (radians)	Deflection Run 2 - Up (radians)	Error from Theoretical Run 2 - Up (radians)	Error from Measured Stiffness Run 2 - Up (radians)
1	-0.0440	-0.0105	-0.0105	-0.0106	-0.0001	-0.0001	-0.0106	-0.0001	-0.0001
2	-0.0886	-0.0211	-0.0213	-0.0211	0.0000	0.0002	-0.0213	-0.0002	0.0000
3	-0.1325	-0.0315	-0.0319	-0.0317	-0.0002	0.0002	-0.0318	-0.0003	0.0001
4	-0.1785	-0.0424	-0.0430	-0.0428	-0.0004	0.0002	-0.0429	-0.0005	0.0001
5	-0.2175	-0.0517	-0.0524	-0.0522	-0.0005	0.0002	-0.0523	-0.0006	0.0001
6	-0.2656	-0.0632	-0.0640	-0.0640	-0.0008	0.0000	-0.0639	-0.0007	0.0001
7	-0.3112	-0.0740	-0.0751	-0.0747	-0.0007	0.0004	-0.0747	-0.0007	0.0004
8	-0.3540	-0.0842	-0.0854	-0.0852	-0.0010	0.0002	-0.0852	-0.0010	0.0002
9	-0.3963	-0.0943	-0.0956						
0	0.0000	0.0000	0.0001	0.0000	0.0000	-0.0001	-0.0001	-0.0001	-0.0002
1	0.0440	0.0105	0.0107	0.0106	0.0001	-0.0001	0.0102	-0.0003	-0.0005
2	0.0886	0.0211	0.0215	0.0216	0.0005	0.0001	0.0212	0.0001	-0.0003
3	0.1325	0.0315	0.0321	0.0322	0.0007	0.0001	0.0318	0.0003	-0.0003
4	0.1785	0.0424	0.0432	0.0434	0.0010	0.0002	0.0430	0.0006	-0.0002
5	0.2175	0.0517	0.0526	0.0528	0.0011	0.0002	0.0526	0.0009	0.0000
6	0.2656	0.0632	0.0642	0.0643	0.0011	0.0001	0.0643	0.0011	0.0001
7	0.3112	0.0740	0.0752	0.0758	0.0018	0.0006	0.0754	0.0014	0.0002
8	0.3540	0.0842	0.0855	0.0859	0.0017	0.0004	0.0859	0.0017	0.0004
9	0.3963	0.0943	0.0958						

Table A.6 - Data from a 45° Offset Axis of Flexure 2

# of Nickels	Applied Torque (in-lbs)	Theoretical Deflection (radians)	Measured Stiffness Deflection (radians)	Deflection Run 1 - Down (radians)	Error from Theoretical Run 1 - Down (radians)	Error from Measured Stiffness Run 1 - Down (radians)	Deflection Run 1 - Up (radians)	Error from Theoretical Run 1 - Up (radians)	Error from Measured Stiffness Run 1 - Up (radians)
1	-0.0440	-0.0105	-0.0105	-0.0106	-0.0001	-0.0001	-0.0106	-0.0001	-0.0001
2	-0.0886	-0.0211	-0.0213	-0.0210	0.0001	0.0003	-0.0213	-0.0002	0.0000
3	-0.1325	-0.0315	-0.0319	-0.0315	0.0000	0.0004	-0.0317	-0.0002	0.0002
4	-0.1785	-0.0424	-0.0430	-0.0427	-0.0003	0.0003	-0.0427	-0.0003	0.0003
5	-0.2175	-0.0517	-0.0524	-0.0522	-0.0005	0.0002	-0.0521	-0.0004	0.0003
6	-0.2656	-0.0632	-0.0640	-0.0640	-0.0008	0.0000	-0.0639	-0.0007	0.0001
7	-0.3112	-0.0740	-0.0751	-0.0747	-0.0007	0.0004	-0.0747	-0.0007	0.0004
8	-0.3540	-0.0842	-0.0854	-0.0852	-0.0010	0.0002	-0.0850	-0.0008	0.0004
9	-0.3963	-0.0943	-0.0956						
0	0.0000	0.0000	0.0001	0.0000	0.0000	-0.0001	-0.0001	-0.0001	-0.0002
1	0.0440	0.0105	0.0107	0.0106	0.0001	-0.0001	0.0102	-0.0003	-0.0005
2	0.0886	0.0211	0.0215	0.0216	0.0005	0.0001	0.0212	0.0001	-0.0003
3	0.1325	0.0315	0.0321	0.0322	0.0007	0.0001	0.0320	0.0005	-0.0001
4	0.1785	0.0424	0.0432	0.0434	0.0010	0.0002	0.0430	0.0006	-0.0002
5	0.2175	0.0517	0.0526	0.0528	0.0011	0.0002	0.0527	0.0010	0.0001
6	0.2656	0.0632	0.0642	0.0647	0.0015	0.0005	0.0640	0.0008	-0.0002
7	0.3112	0.0740	0.0752	0.0758	0.0018	0.0006	0.0754	0.0014	0.0002
8	0.3540	0.0842	0.0855	0.0860	0.0018	0.0005	0.0859	0.0017	0.0004
9	0.0396	0.0943	0.0958						

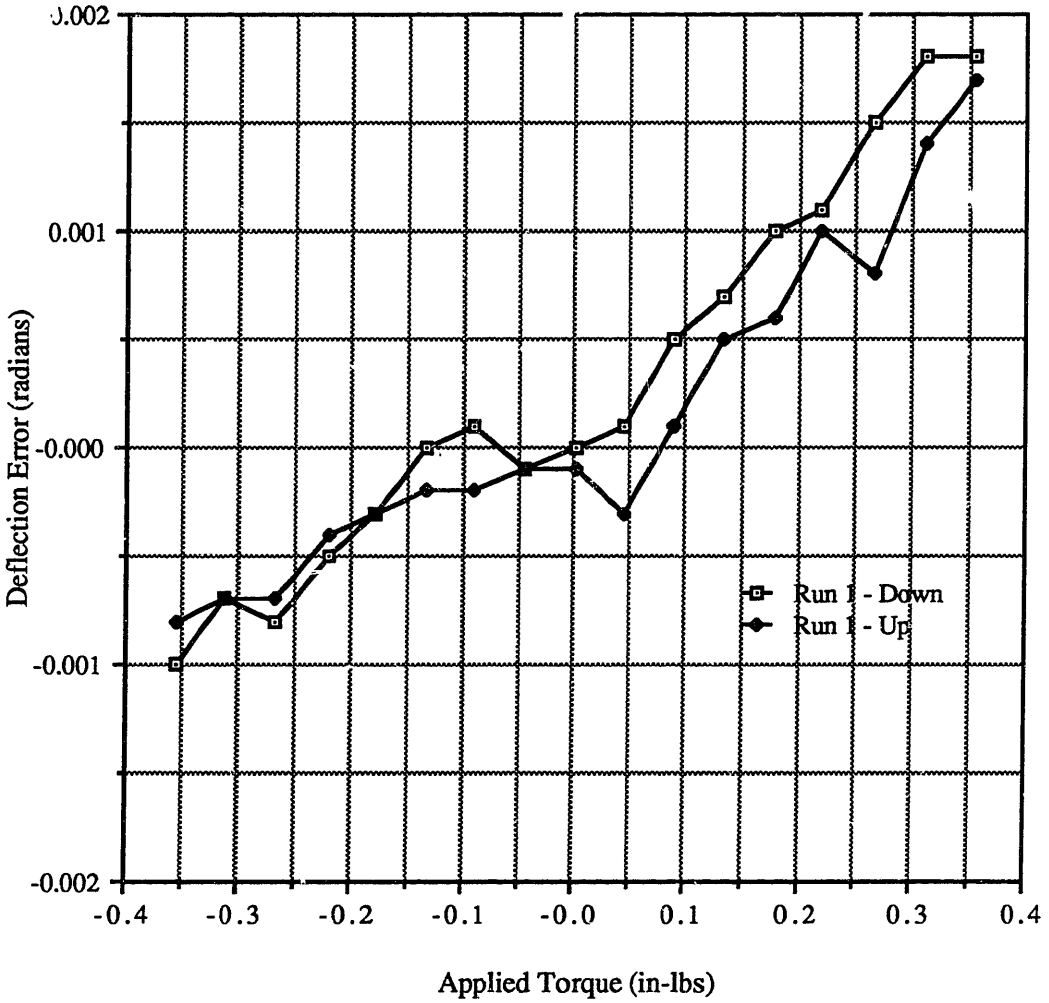

Figure A.19 - Deflection Error vs. Torque for a 45° Offset Axis of Flexure 2

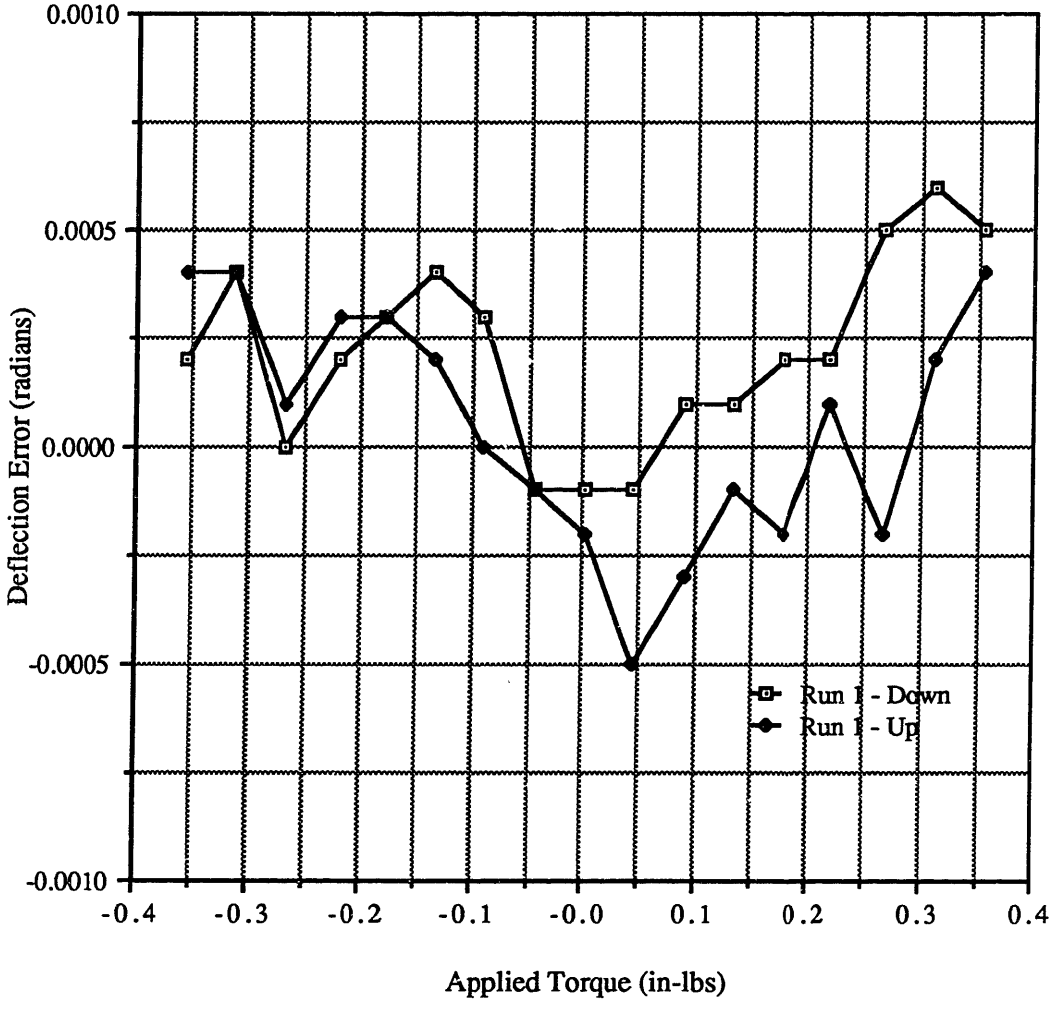

Figure A.20 - Normalized Error Curve for a 45° Offset Axis of Flexure 2

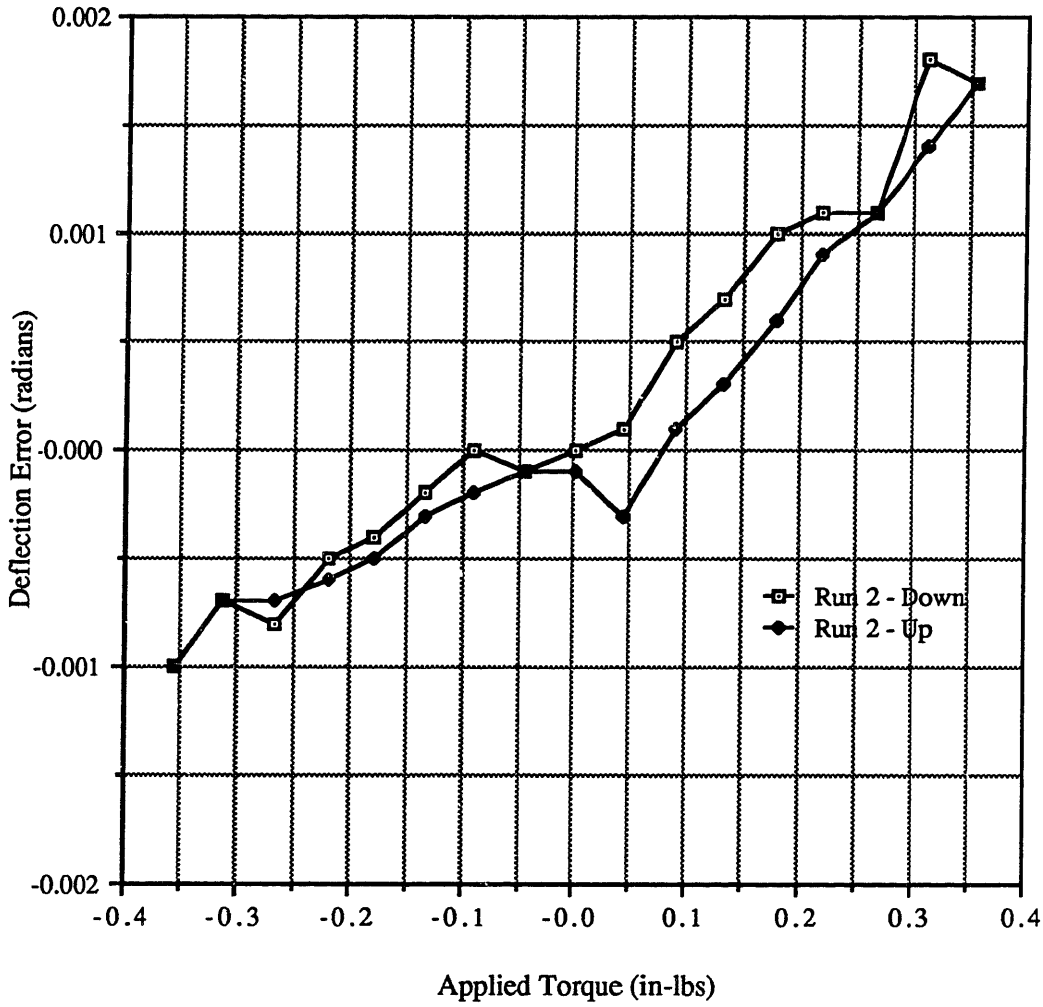

Figure A.21 - Deflection Error vs. Torque for a 45° Offset Axis of Flexure 2

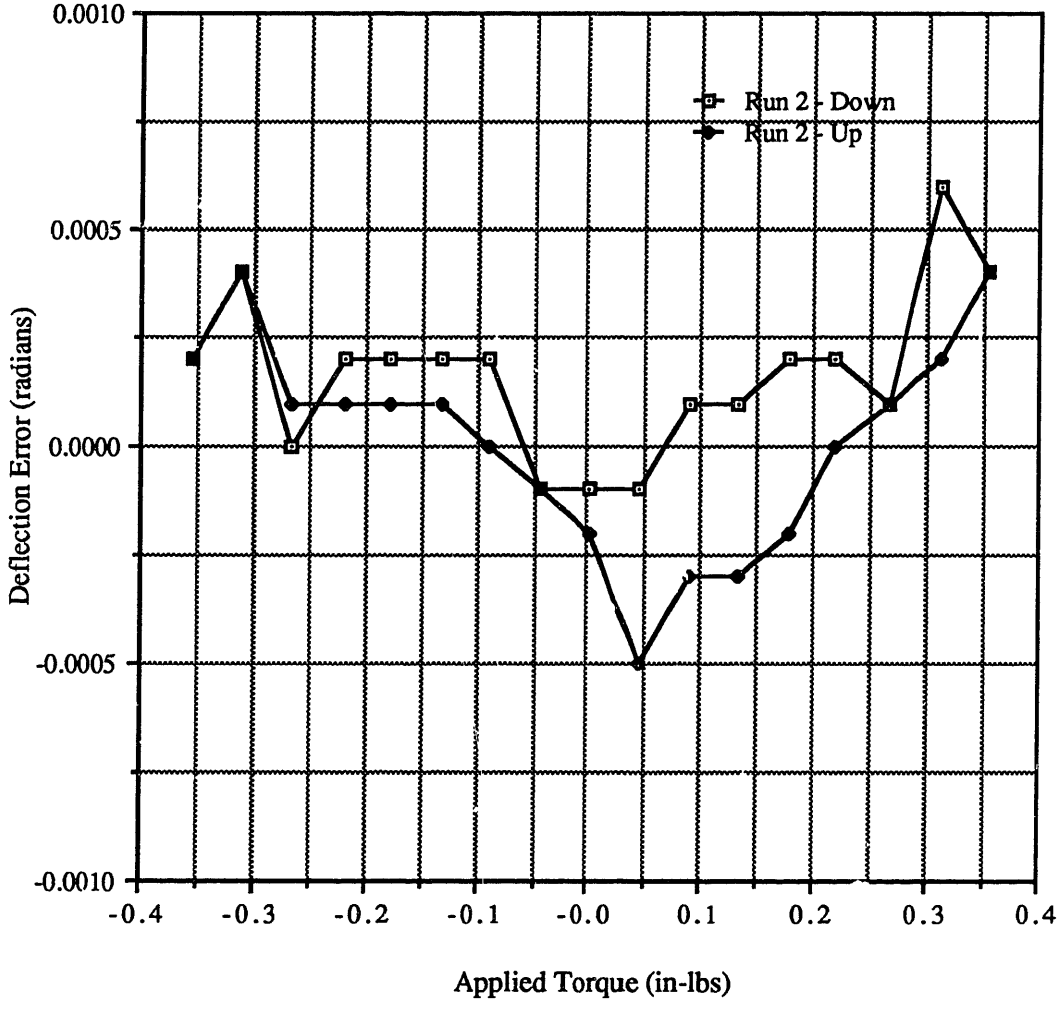

Figure A.22 - Normalized Error Curve for a 45° Offset Axis of Flexure 2

Table A.7 - Data from the Y Axis of Flexure 2

# of Nickels	Applied Torque (in-lbs)	Theoretical Deflection (radians)	Measured Stiffness Deflection (radians)	Deflection Run 1 - Down (radians)	Error from Theoretical Run 1 - Down (radians)	Error from Measured Stiffness Run 1 - Down (radians)	Deflection Run 1 - Up (radians)	Error from Theoretical Run 1 - Up (radians)	Error from Measured Stiffness Run 1 - Up (radians)
1	-0.0440	-0.0105	-0.0111	-0.0106	-0.0001	0.0005	-0.0117	-0.0012	-0.0006
2	-0.0886	-0.0211	-0.0220	-0.0214	-0.0003	0.0006	-0.0225	-0.0014	-0.0005
3	-0.1325	-0.0315	-0.0327	-0.0323	-0.0008	0.0004	-0.0331	-0.0016	-0.0004
4	-0.1785	-0.0424	-0.0440	-0.0437	-0.0013	0.0003	-0.0443	-0.0019	-0.0003
5	-0.2175	-0.0517	-0.0535	-0.0531	-0.0014	0.0004	-0.0536	-0.0019	-0.0001
6	-0.2656	-0.0632	-0.0652	-0.0651	-0.0019	0.0001	-0.0655	-0.0023	-0.0003
7	-0.3112	-0.0740	-0.0764	-0.0761	-0.0021	0.0003	-0.0764	-0.0024	0.0000
8	-0.3540	-0.0842	-0.0868	-0.0871	-0.0029	-0.0003	-0.0871	-0.0029	-0.0003
9	-0.3963	-0.0943	-0.0972	-0.0970	-0.0027	0.0002	-0.0970	-0.0027	0.0002
0	0.0000	0.0000	-0.0004	0.0000	0.0000	0.0004	-0.0011	-0.0011	-0.0007
1	0.0440	0.0105	0.0104	0.0106	0.0001	0.0002	0.0099	-0.0006	-0.0005
2	0.0886	0.0211	0.0213	0.0215	0.0004	0.0002	0.0208	-0.0003	-0.0005
3	0.1325	0.0315	0.0320	0.0322	0.0007	0.0002	0.0314	-0.0001	-0.0006
4	0.1785	0.0424	0.0432	0.0435	0.0011	0.0003	0.0429	0.0005	-0.0003
5	0.2175	0.0517	0.0528	0.0528	0.0011	0.0000	0.0526	0.0009	-0.0002
6	0.2656	0.0632	0.0645	0.0646	0.0014	0.0001	0.0644	0.0012	-0.0001
7	0.3112	0.0740	0.0756	0.0760	0.0020	0.0004	0.0756	0.0016	0.0000
8	0.3540	0.0842	0.0861	0.0861	0.0019	0.0000	0.0863	0.0021	0.0002
9	0.0396	0.0943	0.0964						

Table A.7 (cont'd) - Data from the Y Axis of Flexure 2

# of Nickels	Applied Torque (in-lbs)	Theoretical Deflection (radians)	Measured Stiffness Deflection (radians)	Deflection Run 2 - Down (radians)	Error from Theoretical Run 2 - Down (radians)	Error from Measured Stiffness Run 2 - Down (radians)	Deflection Run 2 - Up (radians)	Error from Theoretical Run 2 - Up (radians)	Error from Measured Stiffness Run 2 - Up (radians)
1	-0.0440	-0.0105	-0.0111	-0.0106	-0.0001	0.0005	-0.0117	-0.0012	-0.0006
2	-0.0886	-0.0211	-0.0220	-0.0214	-0.0003	0.0006	-0.0225	-0.0014	-0.0005
3	-0.1325	-0.0315	-0.0327	-0.0323	-0.0008	0.0004	-0.0330	-0.0015	-0.0003
4	-0.1785	-0.0424	-0.0440	-0.0434	-0.0010	0.0006	-0.0444	-0.0020	-0.0004
5	-0.2175	-0.0517	-0.0535	-0.0529	-0.0012	0.0006	-0.0538	-0.0021	-0.0003
6	-0.2656	-0.0632	-0.0652	-0.0650	-0.0018	0.0002	-0.0655	-0.0023	-0.0003
7	-0.3112	-0.0740	-0.0764	-0.0758	-0.0018	0.0006	-0.0764	-0.0024	0.0000
8	-0.3540	-0.0842	-0.0868	-0.0871	-0.0029	-0.0003	-0.0871	-0.0029	-0.0003
9	-0.3963	-0.0943	-0.0972	-0.0970	-0.0027	0.0002	-0.0970	-0.0027	0.0002
0	0.0000	0.0000	-0.0004	0.0000	0.0000	0.0004	-0.0011	-0.0011	-0.0007
1	0.0440	0.0105	0.0104	0.0106	0.0001	0.0002	0.0099	-0.0006	-0.0005
2	0.0886	0.0211	0.0213	0.0215	0.0004	0.0002	0.0208	-0.0003	-0.0005
3	0.1325	0.0315	0.0320	0.0322	0.0007	0.0002	0.0316	0.0001	-0.0004
4	0.1785	0.0424	0.0432	0.0435	0.0011	0.0003	0.0429	0.0005	-0.0003
5	0.2175	0.0517	0.0528	0.0530	0.0013	0.0002	0.0525	0.0008	-0.0003
6	0.2656	0.0632	0.0645	0.0646	0.0014	0.0001	0.0642	0.0010	-0.0003
7	0.3112	0.0740	0.0756	0.0760	0.0020	0.0004	0.0757	0.0017	0.0001
8	0.3540	0.0842	0.0861	0.0863	0.0021	0.0002	0.0863	0.0021	0.0002
9	0.3963	0.0943	0.0964						

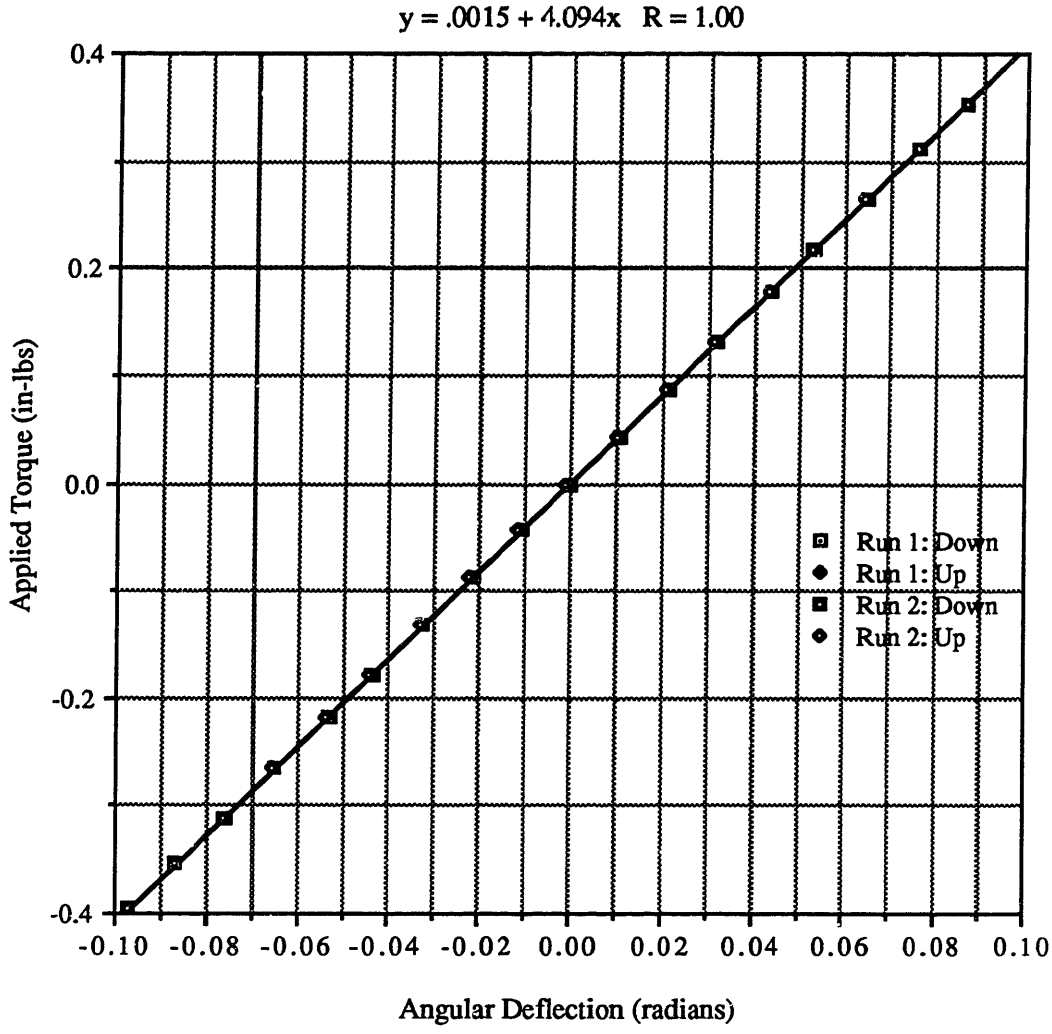

Figure A.23 - Torque vs. Angular Deflection for the Y Axis of Flexure 2

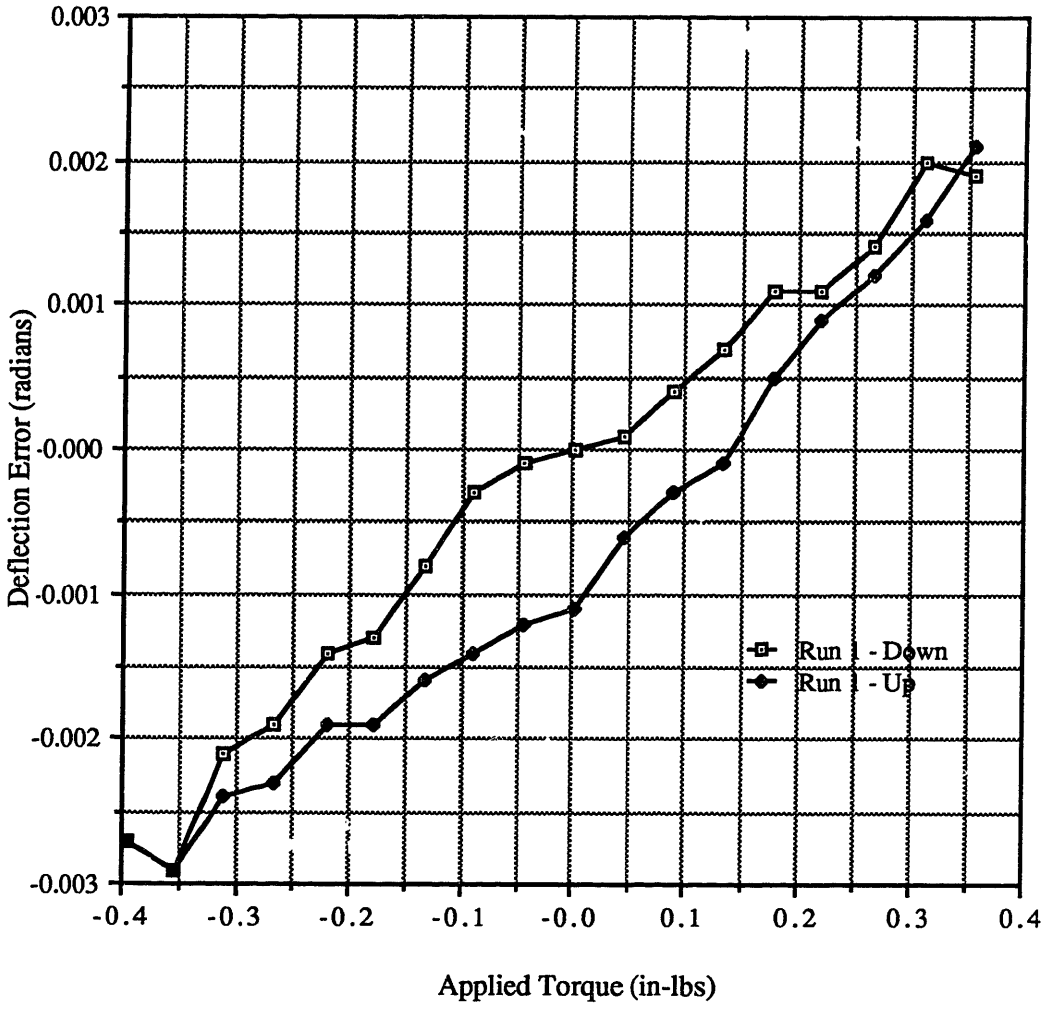

Figure A.24 - Deflection Error vs. Torque for the Y Axis of Flexure 2

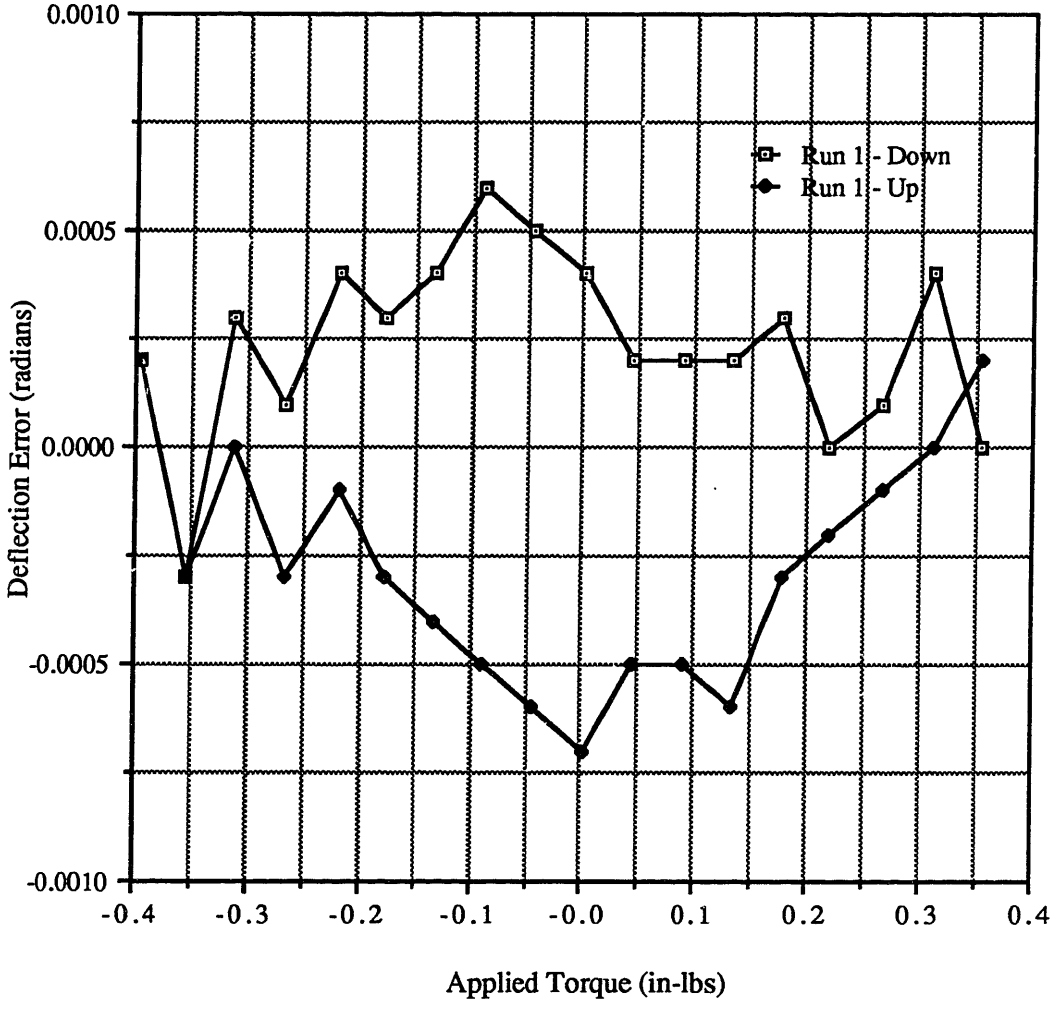

Figure A.25 - Normalized Error Curve for the Y Axis of Flexure 2

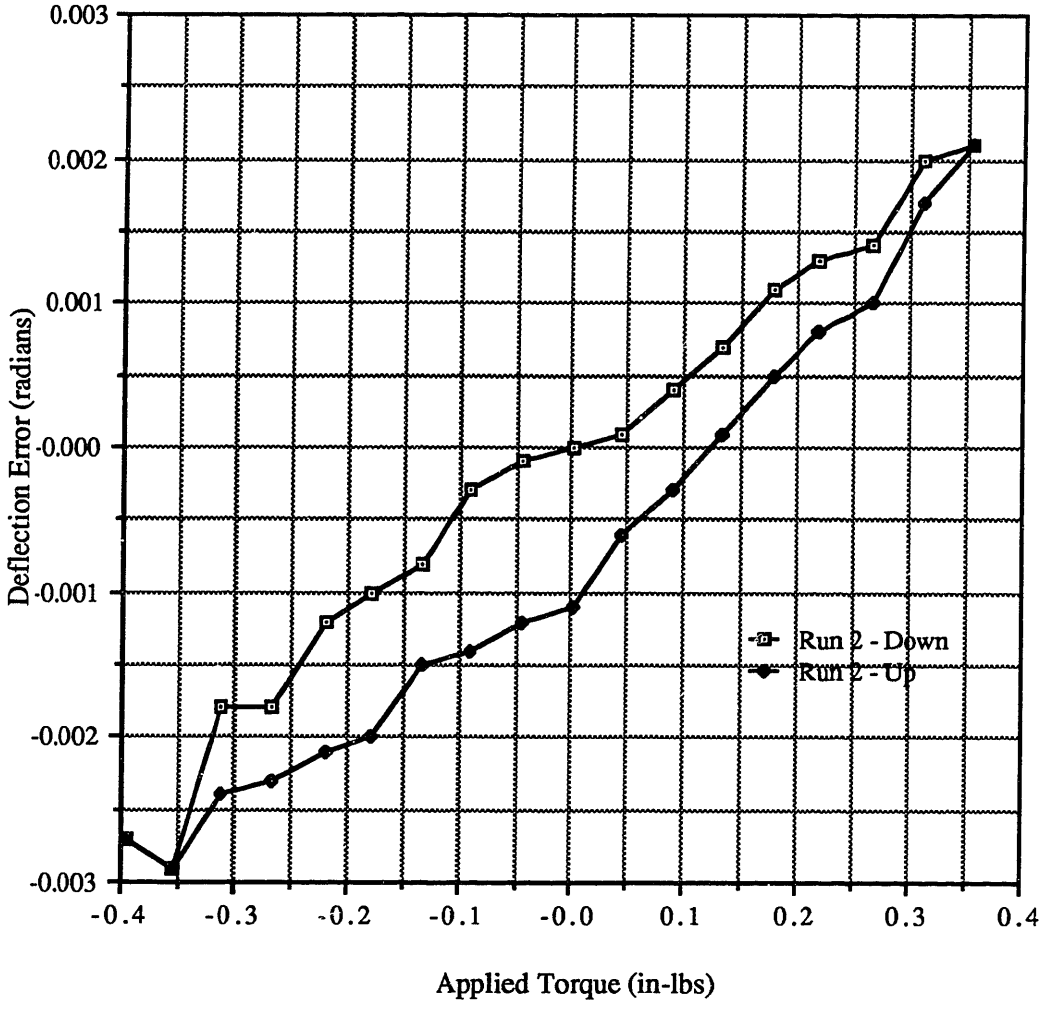

Figure A.26 - Deflection Error vs. Torque for the Y Axis of Flexure 2

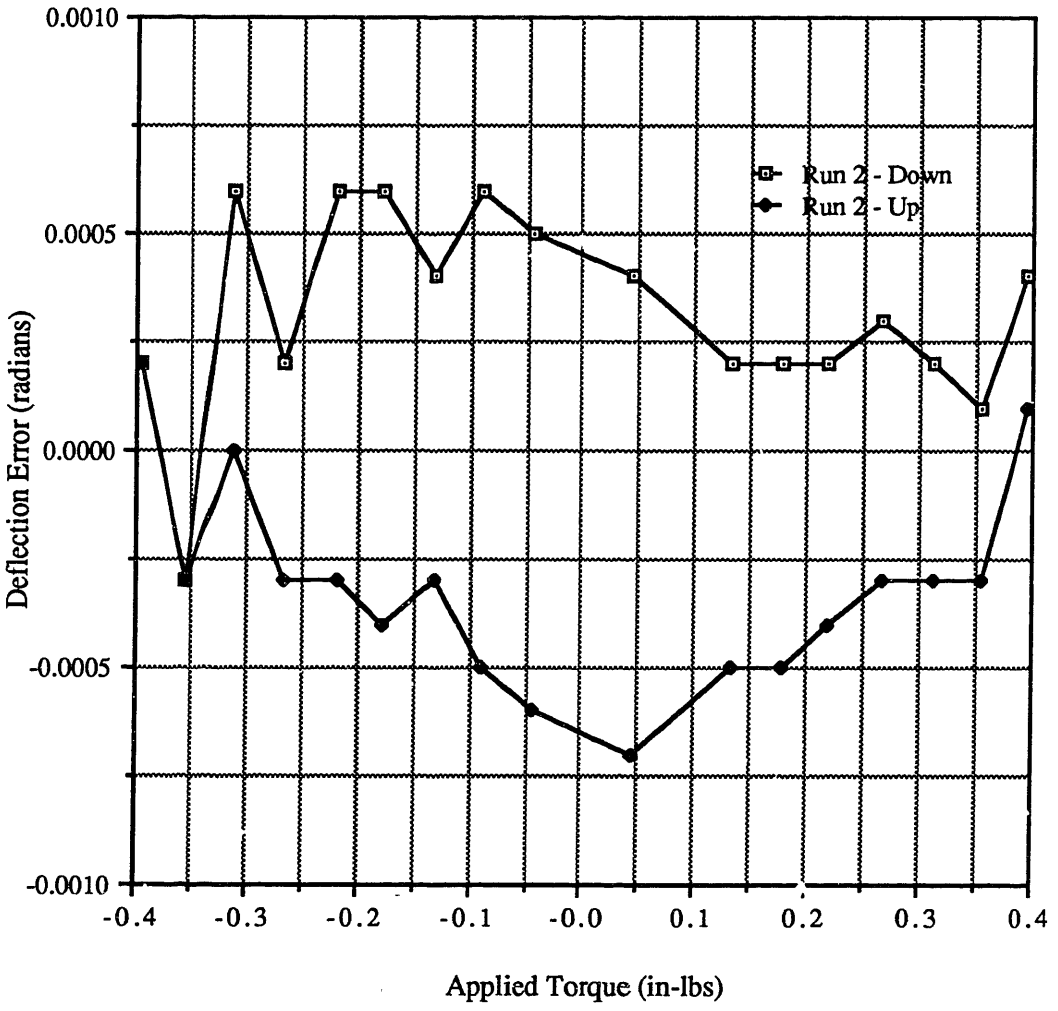

Figure A.27 - Normalized Error Curve for the Y Axis of Flexure 2

Table A.8 - Data from a 45° Offset Axis of Flexure 2

# of Nickels	Applied Torque (in-lbs)	Theoretical Deflection (radians)	Measured Stiffness Deflection (radians)	Deflection Run 1 - Down (radians)	Error from Theoretical Run 1 - Down (radians)	Error from Measured Stiffness Run 1 - Down (radians)	Deflection Run 1 - Up (radians)	Error from Theoretical Run 1 - Up (radians)	Error from Measured Stiffness Run 1 - Up (radians)
1	-0.0440	-0.0105	-0.0106	-0.0106	-0.0001	0.0000	-0.0108	-0.0003	-0.0002
2	-0.0886	-0.0211	-0.0214	-0.0214	-0.0003	0.0000	-0.0215	-0.0004	-0.0001
3	-0.1325	-0.0315	-0.0320	-0.0321	-0.0006	-0.0001	-0.0321	-0.0006	-0.0001
4	-0.1785	-0.0424	-0.0432	-0.0430	-0.0006	0.0002	-0.0432	-0.0008	0.0000
5	-0.2175	-0.0517	-0.0526	-0.0525	-0.0008	0.0001	-0.0527	-0.0010	-0.0001
6	-0.2656	-0.0632	-0.0643	-0.0645	-0.0013	-0.0002	-0.0645	-0.0013	-0.0002
7	-0.3112	-0.0740	-0.0754	-0.0751	-0.0011	0.0003	-0.0752	-0.0012	0.0002
8	-0.3540	-0.0842	-0.0857	-0.0860	-0.0018	-0.0003	-0.0860	-0.0018	-0.0003
9	-0.3963	-0.0943	-0.0960	-0.0958	-0.0015	0.0002	-0.0958	-0.0015	0.0002
0	0.0000	0.0000	0.0001	0.0000	0.0000	-0.0001	-0.0002	-0.0002	-0.0003
1	0.0440	0.0105	0.0108	0.0108	0.0003	0.0000	0.0106	0.0001	-0.0002
2	0.0886	0.0211	0.0216	0.0217	0.0006	0.0001	0.0216	0.0005	0.0000
3	0.1325	0.0315	0.0322	0.0324	0.0009	0.0002	0.0322	0.0007	0.0000
4	0.1785	0.0424	0.0434	0.0435	0.0011	0.0001	0.0437	0.0013	0.0003
5	0.2175	0.0517	0.0528	0.0531	0.0014	0.0003	0.0534	0.0017	0.0006
6	0.2656	0.0632	0.0645	0.0646	0.0014	0.0001	0.0649	0.0017	0.0004
7	0.3112	0.0740	0.0756	0.0760	0.0020	0.0004	0.0760	0.0020	0.0004
8	0.3540	0.0842	0.0859	0.0849			0.0849		
9	0.0396	0.0943	0.0962						

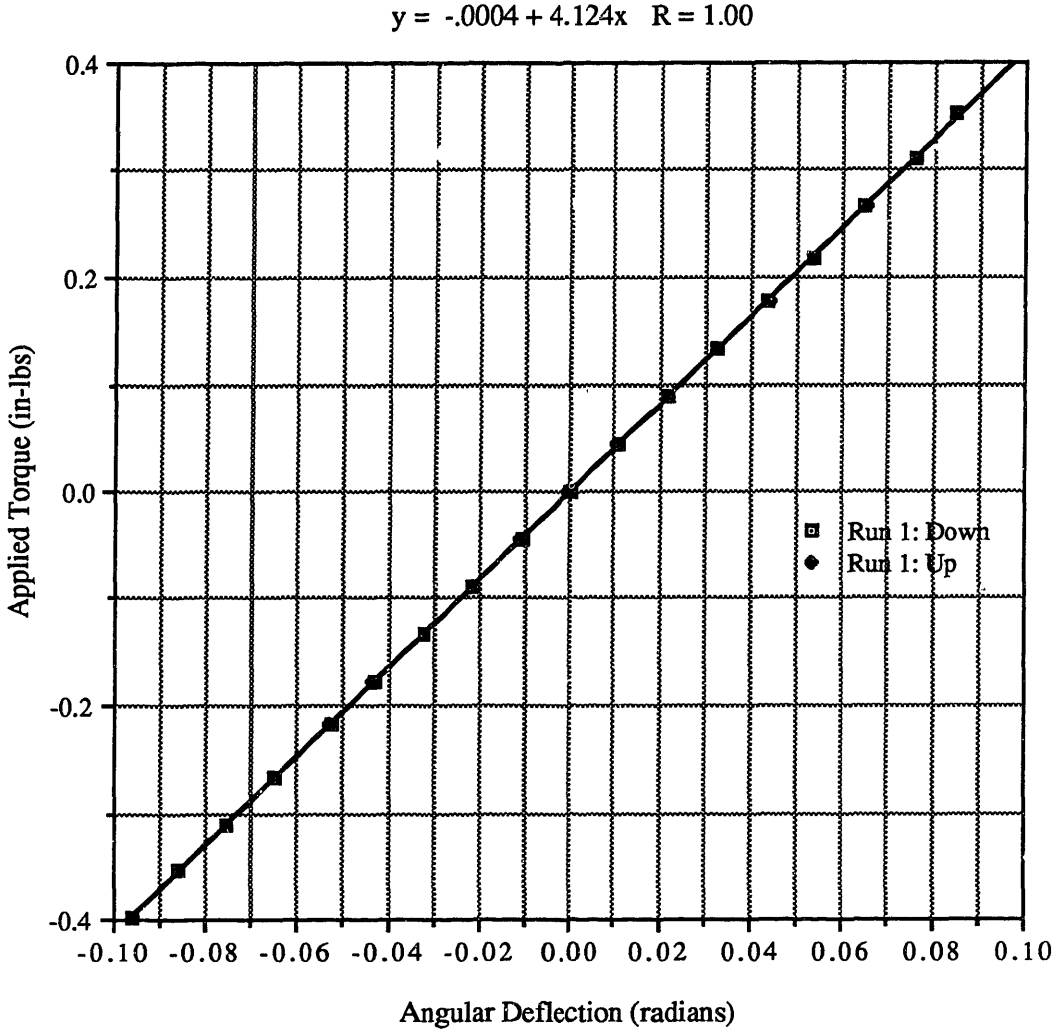

Figure A.28 - Torque vs. Angular Deflection for a 45° Offset Axis of Flexure 2

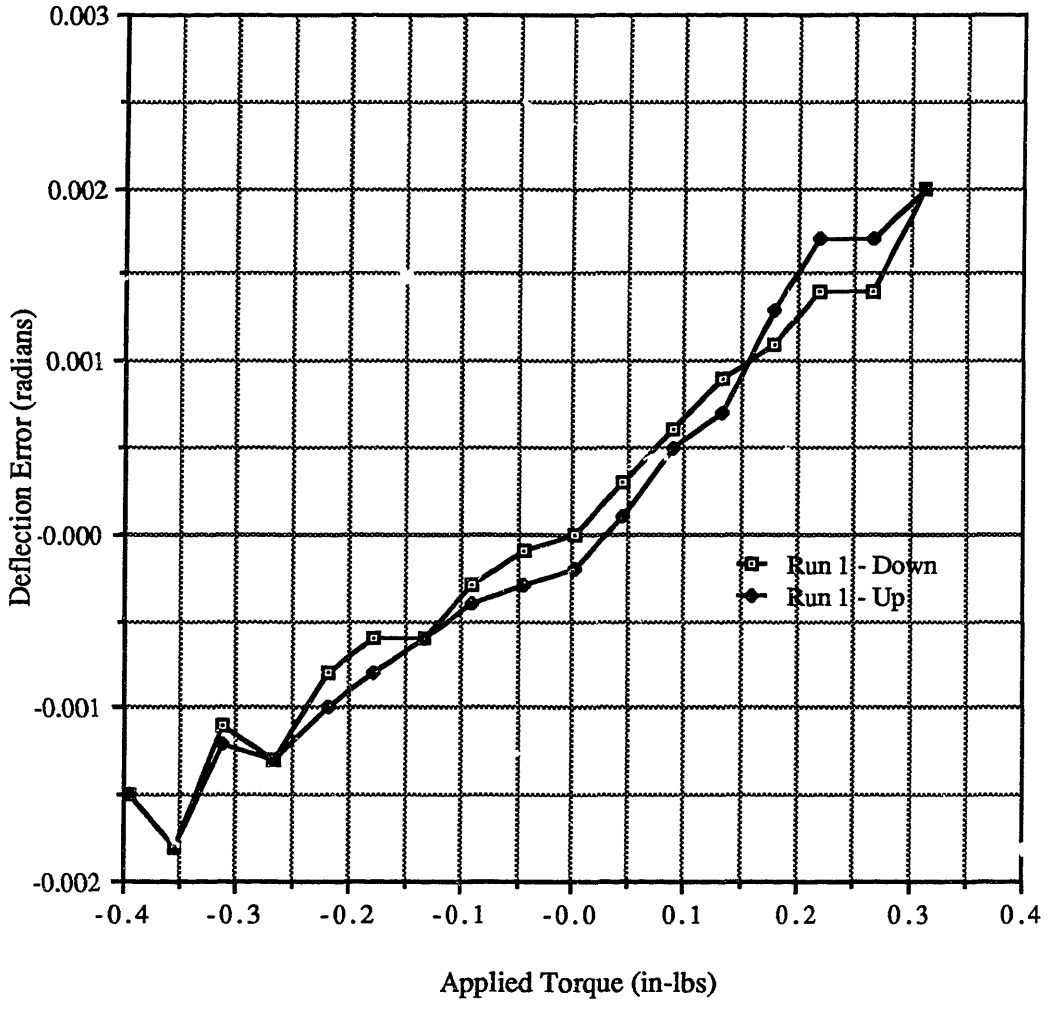

Figure A.29 - Deflection Error vs. Torque for a 45° Offset Axis of Flexure 2

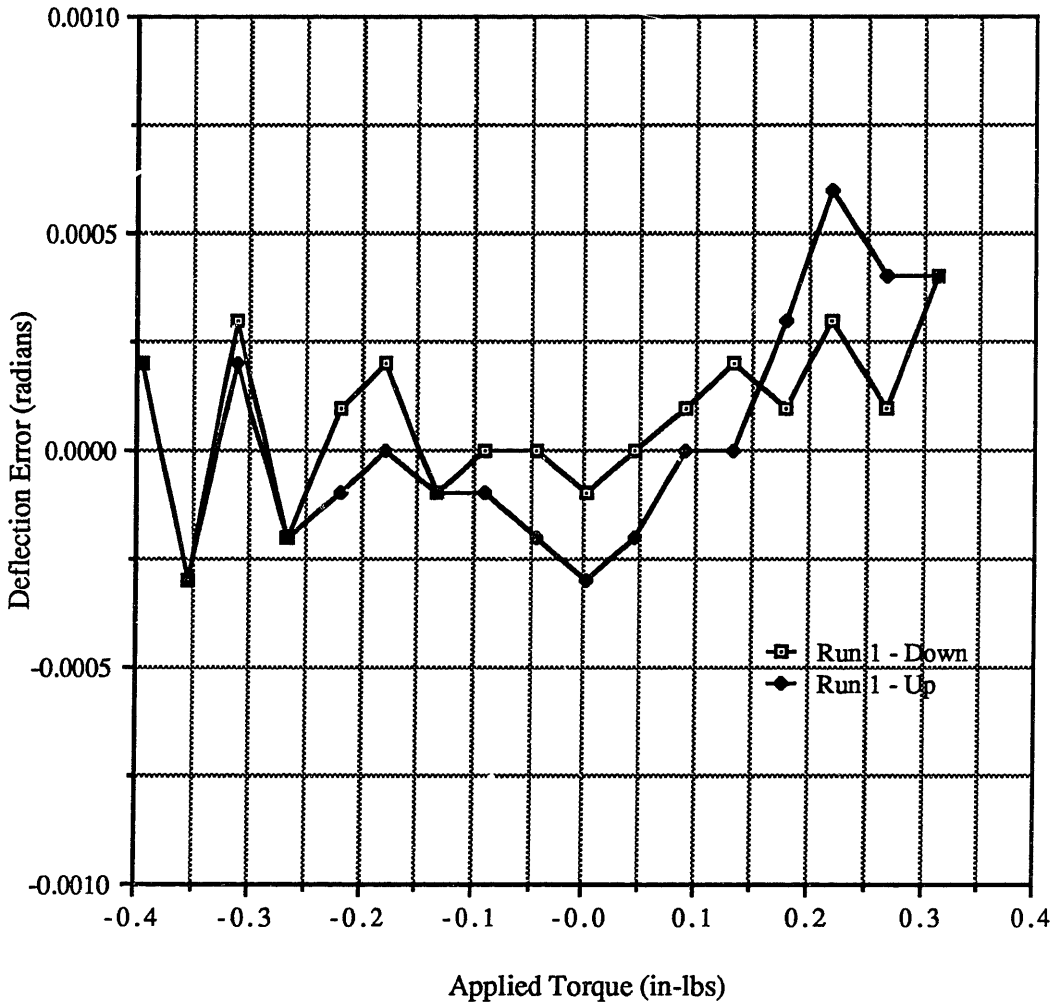

Figure A.30 - Normalized Error Curve for a 45° Offset Axis of Flexure 2

Table A.9 - Data from the X Axis of Flexure 3

# of Nickels	Applied Torque (in-lbs)	Theoretical Deflection (radians)	Measured Stiffness Deflection (radians)	Deflection Run 1 - Down (radians)	Error from Theoretical Run 1 - Down (radians)	Error from Measured Stiffness Run 1 - Down (radians)	Deflection Run 1 - Up (radians)	Error from Theoretical Run 1 - Up (radians)	Error from Measured Stiffness Run 1 - Up (radians)
1	-0.0440	-0.0105	-0.0120	-0.0115	-0.0010	0.0005	-0.0118	-0.0013	0.0002
2	-0.0886	-0.0211	-0.0241	-0.0237	-0.0026	0.0004	-0.0238	-0.0027	0.0003
3	-0.1325	-0.0315	-0.0360	-0.0356	-0.0041	0.0004	-0.0356	-0.0041	0.0004
4	-0.1785	-0.0424	-0.0484	-0.0480	-0.0056	0.0004	-0.0480	-0.0056	0.0004
5	-0.2175	-0.0517	-0.0590	-0.0585	-0.0068	0.0005	-0.0586	-0.0069	0.0004
6	-0.2656	-0.0632	-0.0720	-0.0714	-0.0082	0.0006	-0.0716	-0.0084	0.0004
7	-0.3112	-0.0740	-0.0844	-0.0839	-0.0099	0.0005	-0.0839	-0.0099	0.0005
8	-0.3540	-0.0842	-0.0960	-0.0958	-0.0120	0.0002	-0.0958	-0.0120	0.0002
9	-0.3963	-0.0943	-0.1074						
0	0.0000	0.0000	-0.0001	0.0009	0.0009	0.0010	0.0000	0.0000	0.0001
1	0.0440	0.0105	0.0118	0.0126	0.0021	0.0008	0.0119	0.0014	0.0001
2	0.0886	0.0211	0.0239	0.0248	0.0037	0.0009	0.0240	0.0029	0.0001
3	0.1325	0.0315	0.0358	0.0366	0.0051	0.0008	0.0359	0.0044	0.0001
4	0.1785	0.0424	0.0482	0.0492	0.0068	0.0010	0.0481	0.0057	-0.0001
5	0.2175	0.0517	0.0588	0.0596	0.0079	0.0008	0.0589	0.0072	0.0001
6	0.2656	0.0632	0.0718	0.0726	0.0094	0.0008	0.0720	0.0088	0.0002
7	0.3112	0.0740	0.0842	0.0848	0.0110	0.0006	0.0848	0.0110	0.0006
8	0.3540	0.0842	0.0957	0.0958	0.0120	0.0001	0.0958	0.0120	0.0001
9	0.0396	0.0943	0.1072						

Table A.9 (cont'd) - Data from the X Axis of Flexure 3

# of Nickels	Applied Torque (in-lbs)	Theoretical Deflection (radians)	Measured Stiffness Deflection (radians)	Deflection Run 2 - Down (radians)	Error from Theoretical Run 2 - Down (radians)	Error from Measured Stiffness Run 2 - Down (radians)	Deflection Run 2 - Up (radians)	Error from Theoretical Run 2 - Up (radians)	Error from Measured Stiffness Run 2 - Up (radians)
1	-0.0440	-0.0105	-0.0120	-0.0120	-0.0015	0.0000	-0.0127	-0.0022	-0.0007
2	-0.0886	-0.0211	-0.0241	-0.0240	-0.0029	0.0001	-0.0240	-0.0029	0.0001
3	-0.1325	-0.0315	-0.0360	-0.0359	-0.0044	0.0001	-0.0367	-0.0052	-0.0007
4	-0.1785	-0.0424	-0.0484	-0.0485	-0.0061	-0.0001	-0.0490	-0.0066	-0.0006
5	-0.2175	-0.0517	-0.0590	-0.0591	-0.0074	-0.0001	-0.0595	-0.0078	-0.0005
6	-0.2656	-0.0632	-0.0720	-0.0724	-0.0092	-0.0004	-0.0726	-0.0094	-0.0006
7	-0.3112	-0.0740	-0.0844	-0.0848	-0.0110	-0.0004	-0.0848	-0.0110	-0.0004
8	-0.3540	-0.0842	-0.0960	-0.0968	-0.0130	-0.0008	-0.0969	-0.0130	-0.0009
9	-0.3963	-0.0943	-0.1074						
0	0.0000	0.0000	-0.0001	0.0000	0.0000	0.0001	-0.0008	-0.0008	-0.0007
1	0.0440	0.0105	0.0118	0.0117	0.0012	-0.0001	0.0110	0.0005	-0.0008
2	0.0886	0.0211	0.0239	0.0238	0.0027	-0.0001	0.0230	0.0019	-0.0009
3	0.1325	0.0315	0.0358	0.0356	0.0041	-0.0002	0.0350	0.0035	-0.0008
4	0.1785	0.0424	0.0482	0.0480	0.0056	-0.0002	0.0472	0.0048	-0.0010
5	0.2175	0.0517	0.0588	0.0587	0.0070	-0.0001	0.0580	0.0063	-0.0008
6	0.2656	0.0632	0.0718	0.0717	0.0085	-0.0001	0.0711	0.0079	-0.0007
7	0.3112	0.0740	0.0842	0.0841	0.0100	-0.0001	0.0839	0.0099	-0.0003
8	0.3540	0.0842	0.0957	0.0951	0.0110	-0.0006	0.0950	0.0110	-0.0007
9	0.3963	0.0943	0.1072						

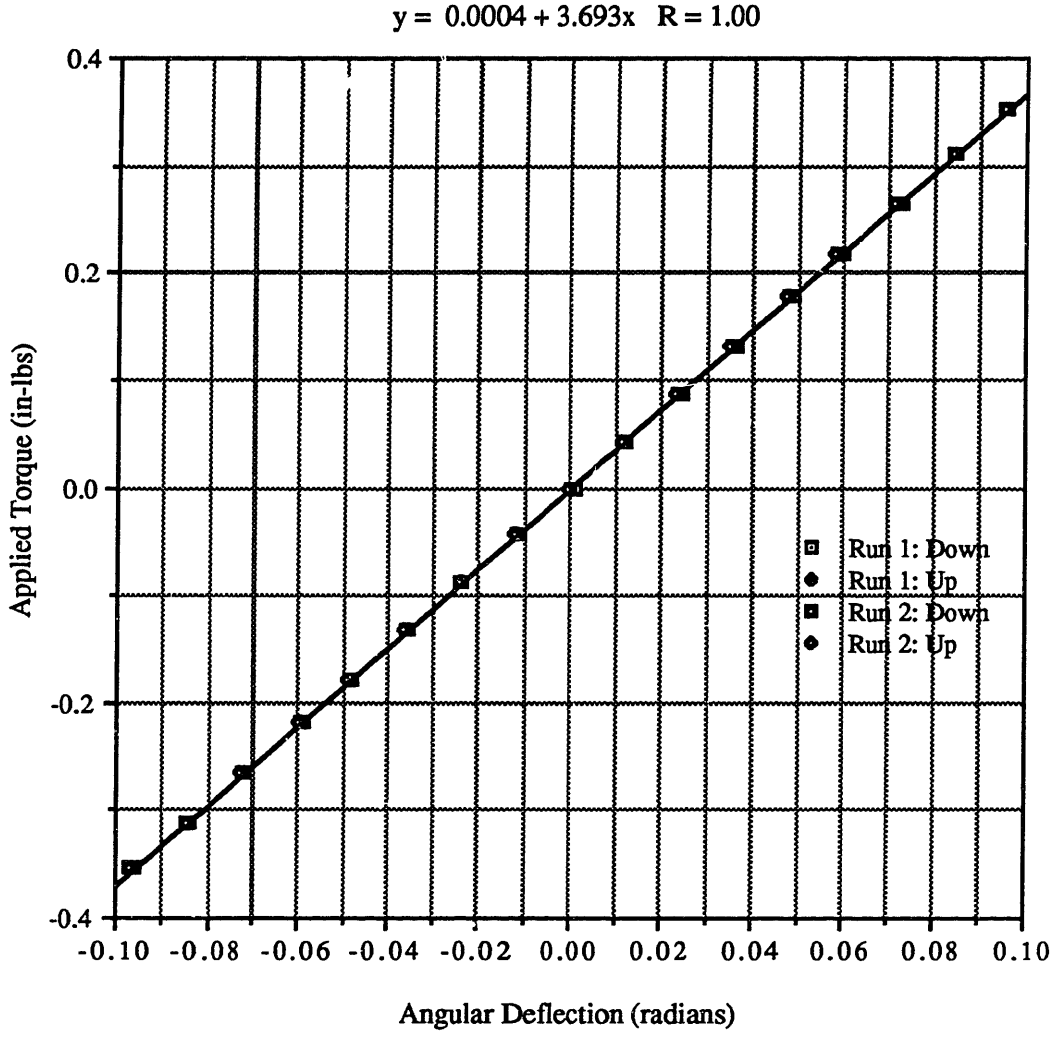

Figure A.31 - Torque vs. Angular Deflection for the X Axis of Flexure 3

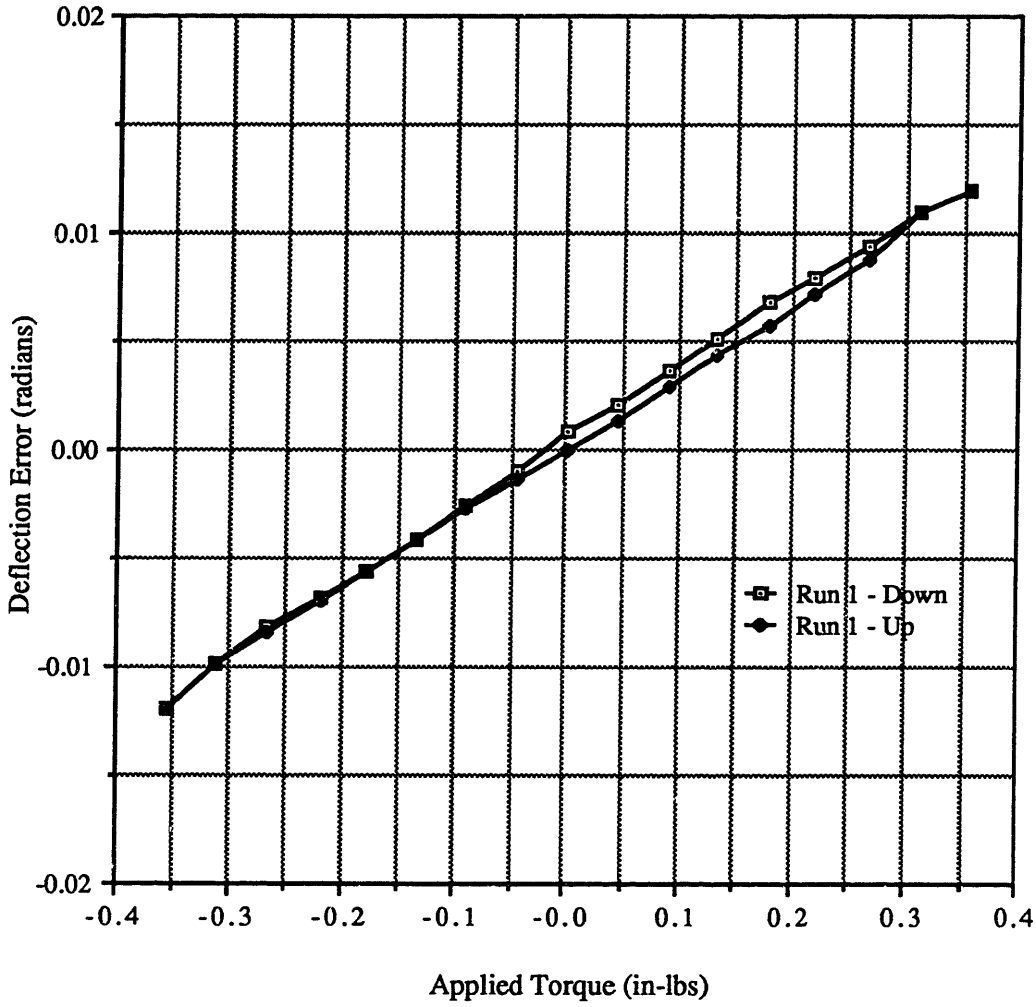

Figure A.32 - Deflection Error vs. Torque for the X Axis of Flexure 3

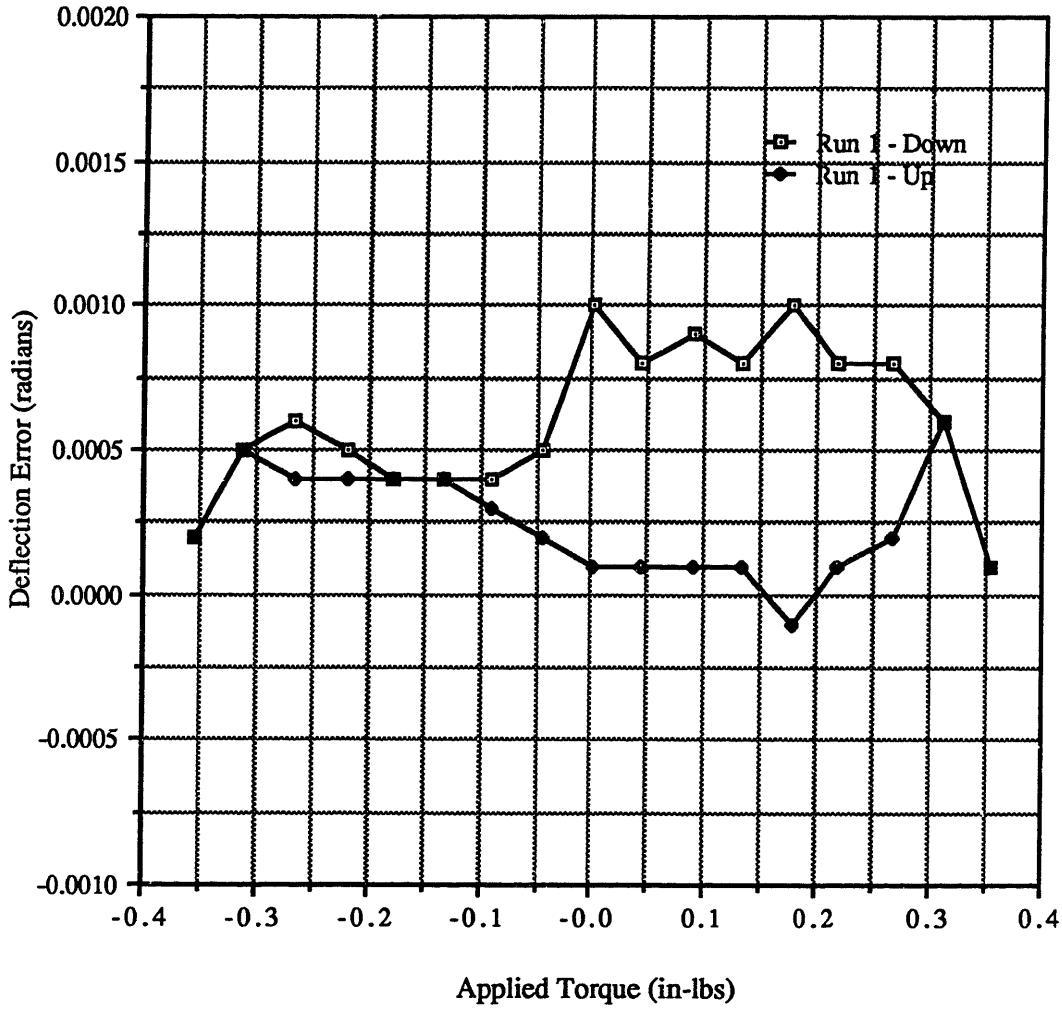

Figure A.33 - Normalized Error Curve for the X Axis of Flexure 3

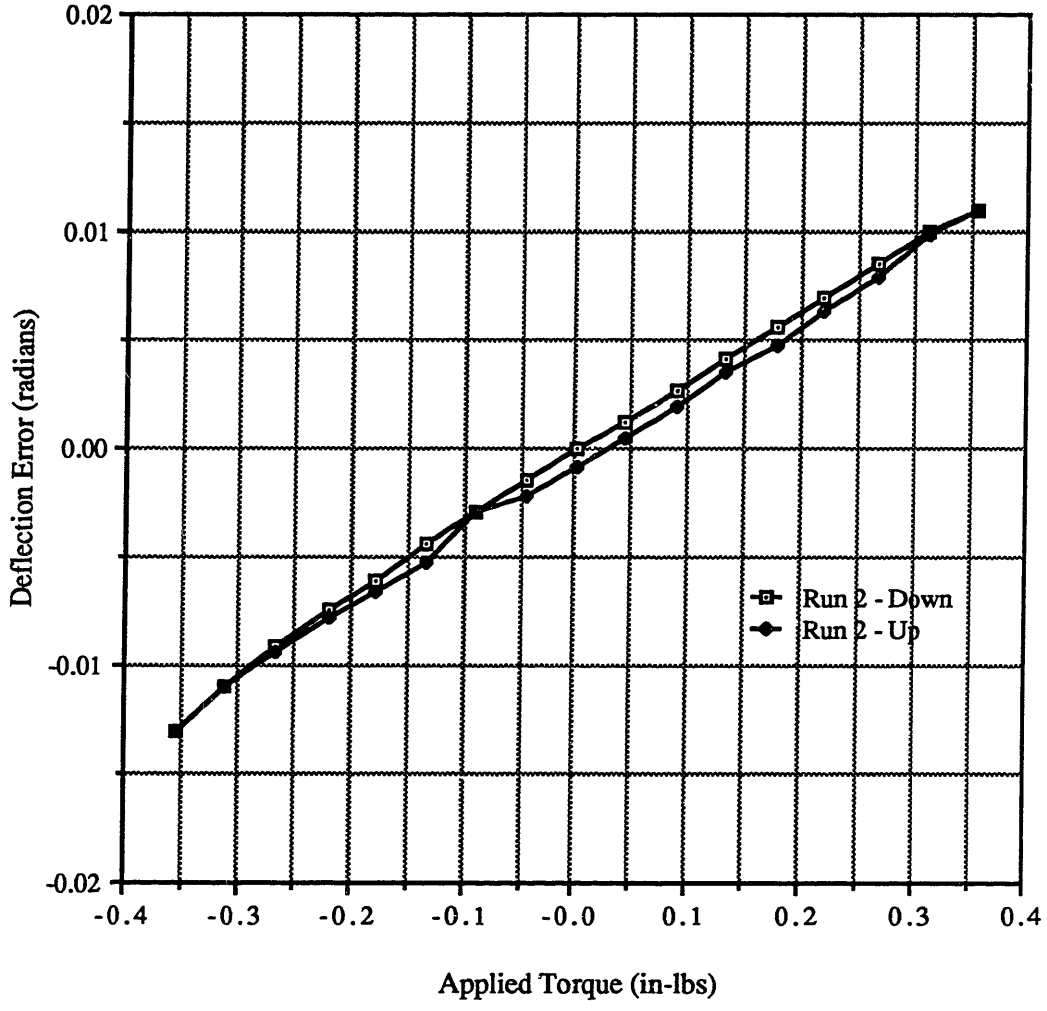

Figure A.34 - Deflection Error vs. Torque for the X axis of Flexure 3

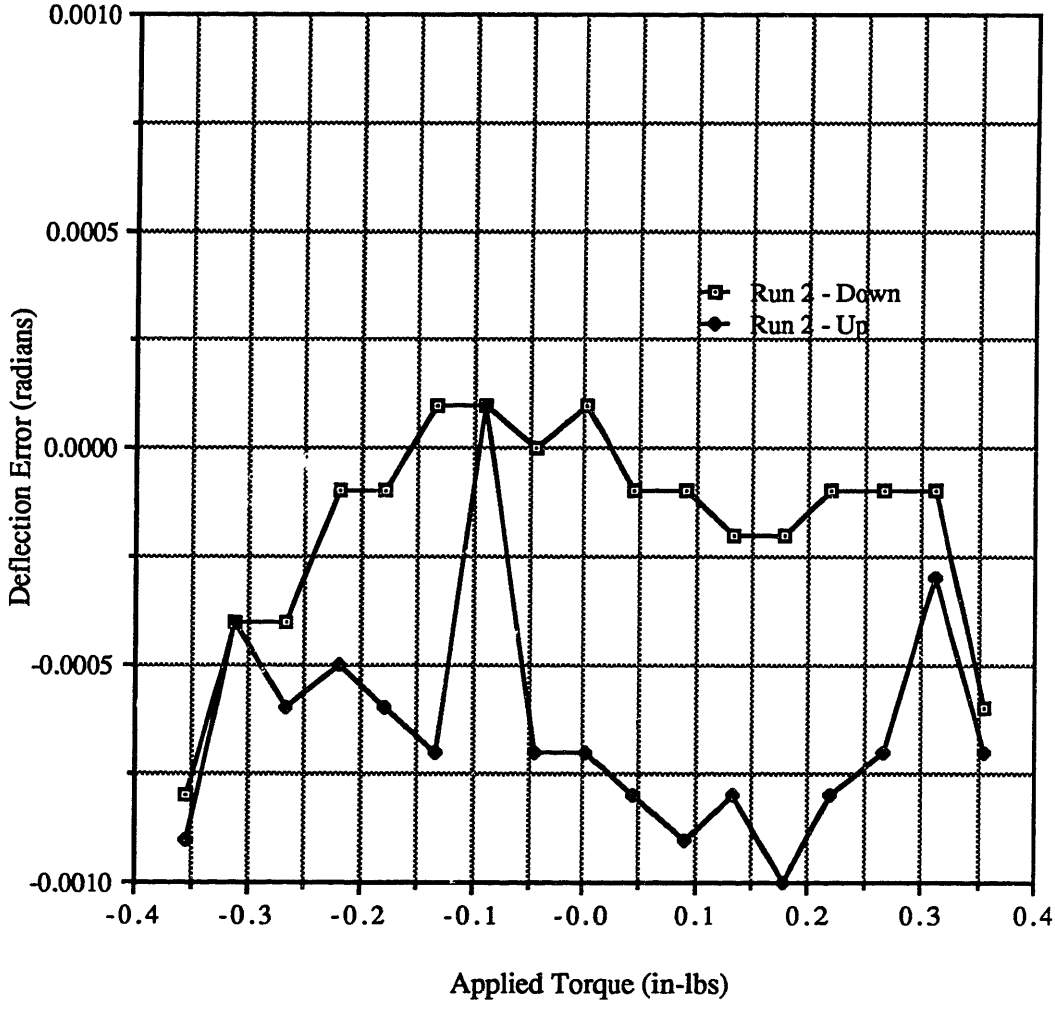

Figure A.35 - Normalized Error Curve for the X Axis of Flexure 3

Table A.10 - Data from a 45° Offset Axis of Flexure 3

# of Nickels	Applied Torque (in-lbs)	Theoretical Deflection (radians)	Measured Stiffness Deflection (radians)	Deflection Run 1 - Down (radians)	Error from Theoretical Run 1 - Down (radians)	Error from Measured Stiffness Run 1 - Down (radians)	Deflection Run 1 - Up (radians)	Error from Theoretical Run 1 - Up (radians)	Error from Measured Stiffness Run 1 - Up (radians)
1	-0.0440	-0.0105	-0.0114	-0.0112	-0.0007	0.0002	-0.0121	-0.0016	-0.0007
2	-0.0886	-0.0211	-0.0228	-0.0226	-0.0015	0.0002	-0.0233	-0.0022	-0.0005
3	-0.1325	-0.0315	-0.0340	-0.0336	-0.0021	0.0004	-0.0344	-0.0029	-0.0004
4	-0.1785	-0.0424	-0.0457	-0.0454	-0.0030	0.0003	-0.0461	-0.0037	-0.0004
5	-0.2175	-0.0517	-0.0556	-0.0555	-0.0038	0.0001	-0.0563	-0.0046	-0.0007
6	-0.2656	-0.0632	-0.0679	-0.0677	-0.0045	0.0002	-0.0684	-0.0052	-0.0005
7	-0.3112	-0.0740	-0.0795	-0.0796	-0.0056	-0.0001	-0.0796	-0.0056	-0.0001
8	-0.3540	-0.0842	-0.0905	-0.0910	-0.0068	-0.0005	-0.0910	-0.0068	-0.0005
9	-0.3963	-0.0943	-0.1013	-0.1011	-0.0068	0.0002	-0.1011	-0.0068	0.0002
0	0.0000	0.0000	-0.0002	0.0000	0.0000	0.0002	-0.0009	-0.0009	-0.0007
1	0.0440	0.0105	0.0111	0.0111	0.0006	0.0000	0.0106	0.0001	-0.0005
2	0.0886	0.0211	0.0224	0.0226	0.0015	0.0002	0.0221	0.0010	-0.0003
3	0.1325	0.0315	0.0336	0.0339	0.0024	0.0003	0.0333	0.0018	-0.0003
4	0.1785	0.0424	0.0454	0.0455	0.0031	0.0001	0.0453	0.0029	-0.0001
5	0.2175	0.0517	0.0553	0.0556	0.0039	0.0003	0.0551	0.0034	-0.0002
6	0.2656	0.0632	0.0676	0.0678	0.0046	0.0002	0.0674	0.0042	-0.0002
7	0.3112	0.0740	0.0792	0.0795	0.0055	0.0003	0.0794	0.0054	0.0002
8	0.3540	0.0842	0.0902	0.0900	0.0058	-0.0002	0.0900	0.0058	-0.0002
9	0.0396	0.0943	0.1009	0.1009	0.0066	0.0000	0.1009	0.0066	0.0000

Table A.10 (cont'd) - Data from a 45° Offset Axis of Flexure 3

# of Nickels	Applied Torque (in-lbs)	Theoretical Deflection (radians)	Deflection Run 2 - Up (radians)
1	-0.0440	-0.0105	
2	-0.0886	-0.0211	
3	-0.1325	-0.0315	
4	-0.1785	-0.0424	
5	-0.2175	-0.0517	
6	-0.2656	-0.0632	
7	-0.3112	-0.0740	
8	-0.3540	-0.0842	
9	-0.3963	-0.0943	
0	0.0000	0.0000	0.0000
1	0.0440	0.0105	0.0112
2	0.0886	0.0211	0.0226
3	0.1325	0.0315	0.0339
4	0.1785	0.0424	0.0455
5	0.2175	0.0517	0.0556
6	0.2656	0.0632	0.0678
7	0.3112	0.0740	0.0796
8	0.3540	0.0842	0.0899
9	0.3963	0.0943	0.1009

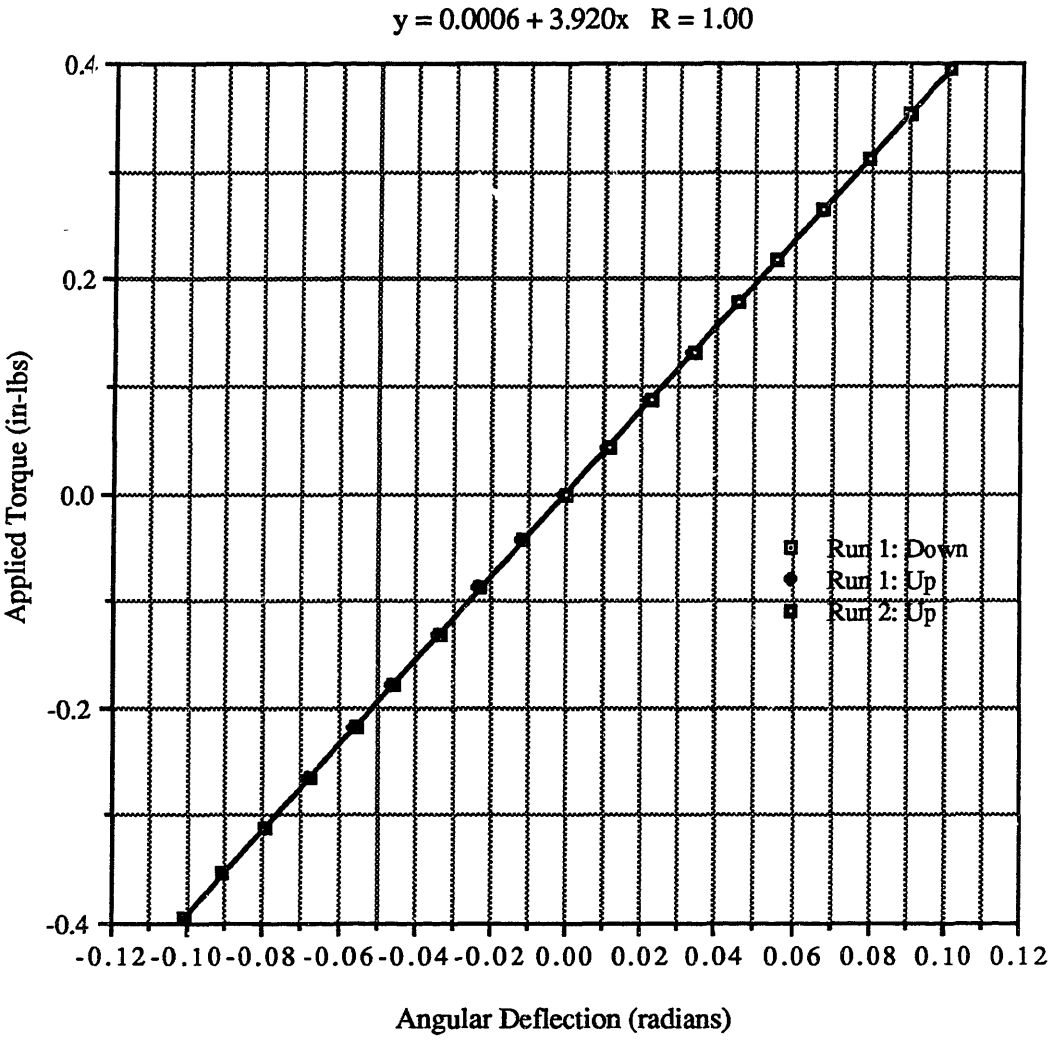

Figure A.36 - Torque vs. Angular Deflection for a 45° Offset Axis of Flexure 3

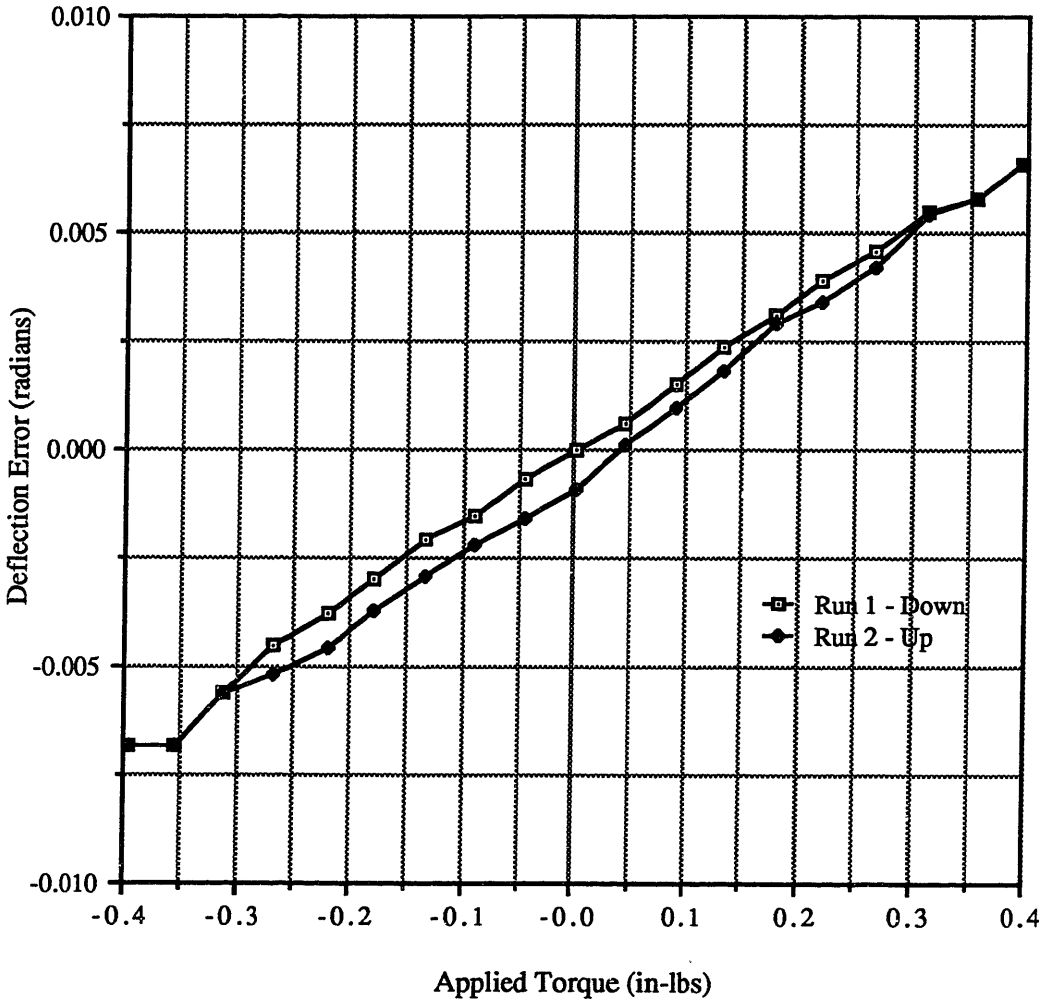

Figure A.37 - Deflection Error vs. Torque for the 45° Offset Axis of Flexure 3

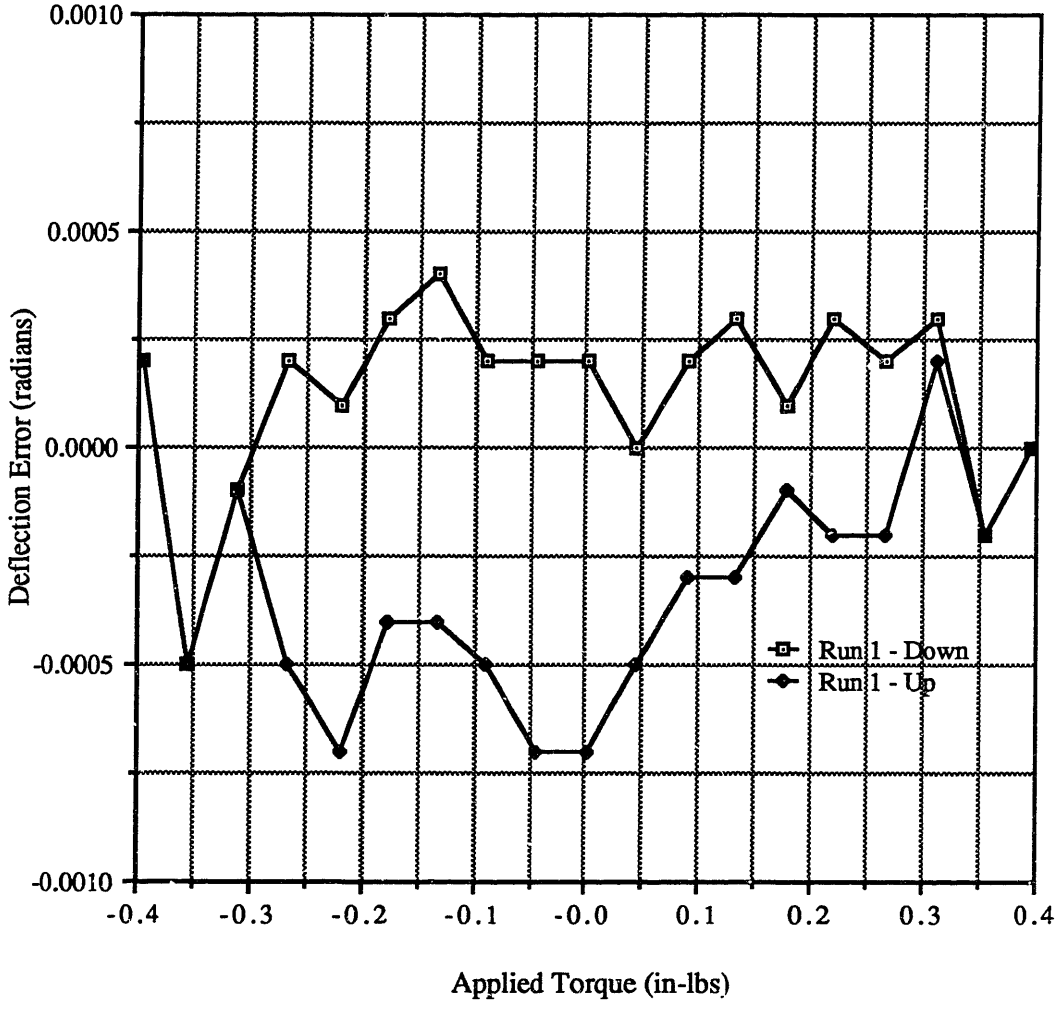

Figure A.38 - Normalized Error Curve for a 45° Offset Axis of Flexure 3

Table A.11 - Data from the Y Axis of Flexure 3

# of Nickels	Applied Torque (in-lbs)	Theoretical Deflection (radians)	Measured Stiffness Deflection (radians)	Deflection Run 1 - Down (radians)	Error from Theoretical Run 1 - Down (radians)	Error from Measured Stiffness Run 1 - Down (radians)	Deflection Run 1 - Up (radians)	Error from Theoretical Run 1 - Up (radians)	Error from Measured Stiffness Run 1 - Up (radians)
1	-0.0440	-0.0105	-0.0110	-0.0107	-0.0002	0.0003	-0.0118	-0.0013	-0.0008
2	-0.0886	-0.0211	-0.0219	-0.0222	-0.0011	-0.0003	-0.0225	-0.0014	-0.0006
3	-0.1325	-0.0315	-0.0327	-0.0328	-0.0013	-0.0001	-0.0333	-0.0018	-0.0006
4	-0.1785	-0.0424	-0.0439	-0.0439	-0.0015	0.0000	-0.0446	-0.0022	-0.0007
5	-0.2175	-0.0517	-0.0534	-0.0533	-0.0016	0.0001	-0.0539	-0.0022	-0.0005
6	-0.2656	-0.0632	-0.0652	-0.0651	-0.0019	0.0001	-0.0657	-0.0025	-0.0005
7	-0.3112	-0.0740	-0.0763	-0.0761	-0.0021	0.0002	-0.0766	-0.0026	-0.0003
8	-0.3540	-0.0842	-0.0868	-0.0877	-0.0035	-0.0009	-0.0876	-0.0034	-0.0008
9	-0.3963	-0.0943	-0.0971						
0	0.0000	0.0000	-0.0003	0.0000	0.0000	0.0003	-0.0012	-0.0012	-0.0009
1	0.0440	0.0105	0.0105	0.0104	-0.0001	-0.0001	0.0095	-0.0010	-0.0010
2	0.0886	0.0211	0.0213	0.0213	0.0002	0.0000	0.0205	-0.0006	-0.0008
3	0.1325	0.0315	0.0321	0.0322	0.0007	0.0001	0.0312	-0.0003	-0.0009
4	0.1785	0.0424	0.0433	0.0432	0.0008	-0.0001	0.0424	0.0000	-0.0009
5	0.2175	0.0517	0.0528	0.0526	0.0009	-0.0002	0.0521	0.0004	-0.0007
6	0.2656	0.0632	0.0646	0.0644	0.0012	-0.0002	0.0637	0.0005	-0.0009
7	0.3112	0.0740	0.0757	0.0758	0.0018	0.0001	0.0752	0.0012	-0.0005
8	0.3540	0.0842	0.0862	0.0856	0.0014	-0.0006	0.0851	0.0009	-0.0011
9	0.0396	0.0943	0.0965	0.0963	0.0020	-0.0002	0.0963	0.0020	-0.0002

Table A.11 (cont'd) - Data from the Y Axis of Flexure 3

# of Nickels	Applied Torque (in-lbs)	Theoretical Deflection (radians)	Measured Stiffness Deflection (radians)	Deflection Run 2 - Down (radians)	Error from Theoretical Run 2 - Down (radians)	Error from Measured Stiffness Run 2 - Down (radians)	Deflection Run 2 - Up (radians)	Error from Theoretical Run 2 - Up (radians)	Error from Measured Stiffness Run 2 - Up (radians)
1	-0.0440	-0.0105	-0.0110	-0.0108	-0.0003	0.0002	-0.0111	-0.0006	-0.0001
2	-0.0886	-0.0211	-0.0219	-0.0216	-0.0005	0.0003	-0.0220	-0.0009	-0.0001
3	-0.1325	-0.0315	-0.0327	-0.0323	-0.0008	0.0004	-0.0326	-0.0011	0.0001
4	-0.1785	-0.0424	-0.0439	-0.0433	-0.0009	0.0006	-0.0438	-0.0014	0.0001
5	-0.2175	-0.0517	-0.0534	-0.0529	-0.0012	0.0005	-0.0534	-0.0017	0.0000
6	-0.2656	-0.0632	-0.0652	-0.0648	-0.0016	0.0004	-0.0650	-0.0018	0.0002
7	-0.3112	-0.0740	-0.0763	-0.0756	-0.0016	0.0007	-0.0759	-0.0019	0.0004
8	-0.3540	-0.0842	-0.0868	-0.0869	-0.0027	-0.0001	-0.0868	-0.0026	0.0000
9	-0.3963	-0.0943	-0.0971						
0	0.0000	0.0000	-0.0003	0.0000	0.0000	0.0003	-0.0005	-0.0005	-0.0002
1	0.0440	0.0105	0.0105	0.0114	0.0009	0.0009	0.0101	-0.0004	-0.0004
2	0.0886	0.0211	0.0213	0.0222	0.0011	0.0009	0.0210	-0.0001	-0.0003
3	0.1325	0.0315	0.0321	0.0328	0.0013	0.0007	0.0318	0.0003	-0.0003
4	0.1785	0.0424	0.0433	0.0439	0.0015	0.0006	0.0430	0.0006	-0.0003
5	0.2175	0.0517	0.0528	0.0536	0.0019	0.0008	0.0527	0.0010	-0.0001
6	0.2656	0.0632	0.0646	0.0651	0.0019	0.0005	0.0645	0.0013	-0.0001
7	0.3112	0.0740	0.0757	0.0765	0.0025	0.0008	0.0760	0.0020	0.0003
8	0.3540	0.0842	0.0862	0.0865	0.0023	0.0003	0.0863	0.0021	0.0001
9	0.3963	0.0943	0.0965	0.0968	0.0025	0.0003	0.0968	0.0025	0.0003

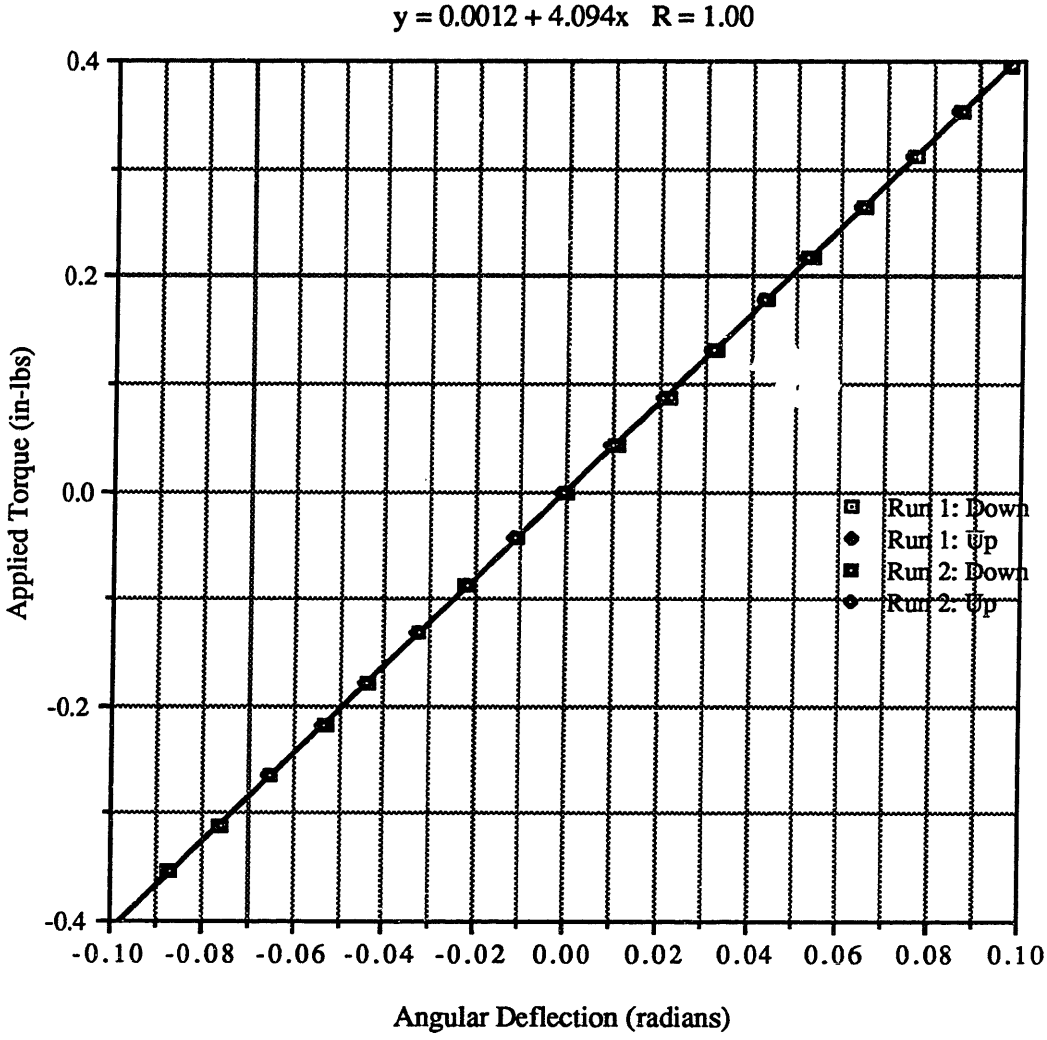

Figure A.39 - Torque vs. Angular Deflection for the Y Axis of Flexure 3

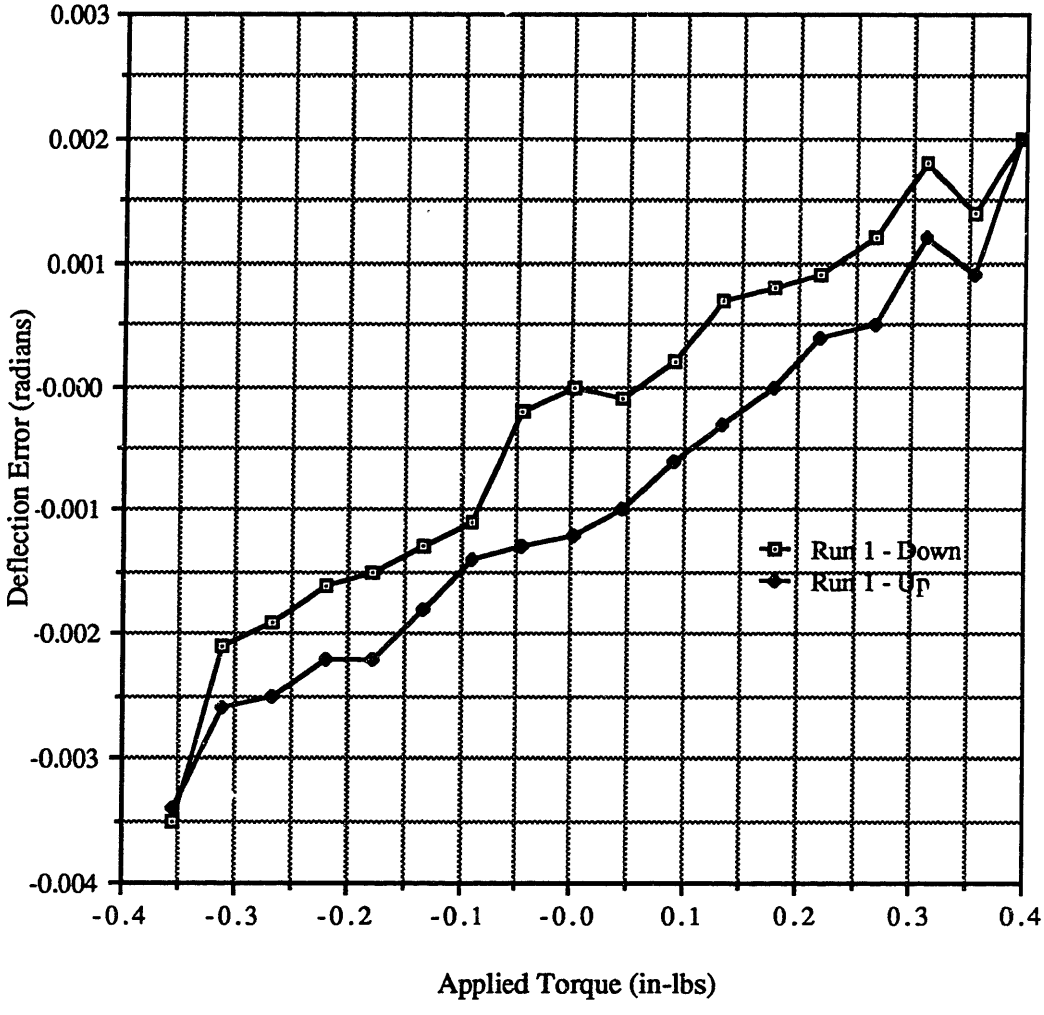

Figure A.40 - Deflection Error vs. Torque for the Y Axis of Flexure 3

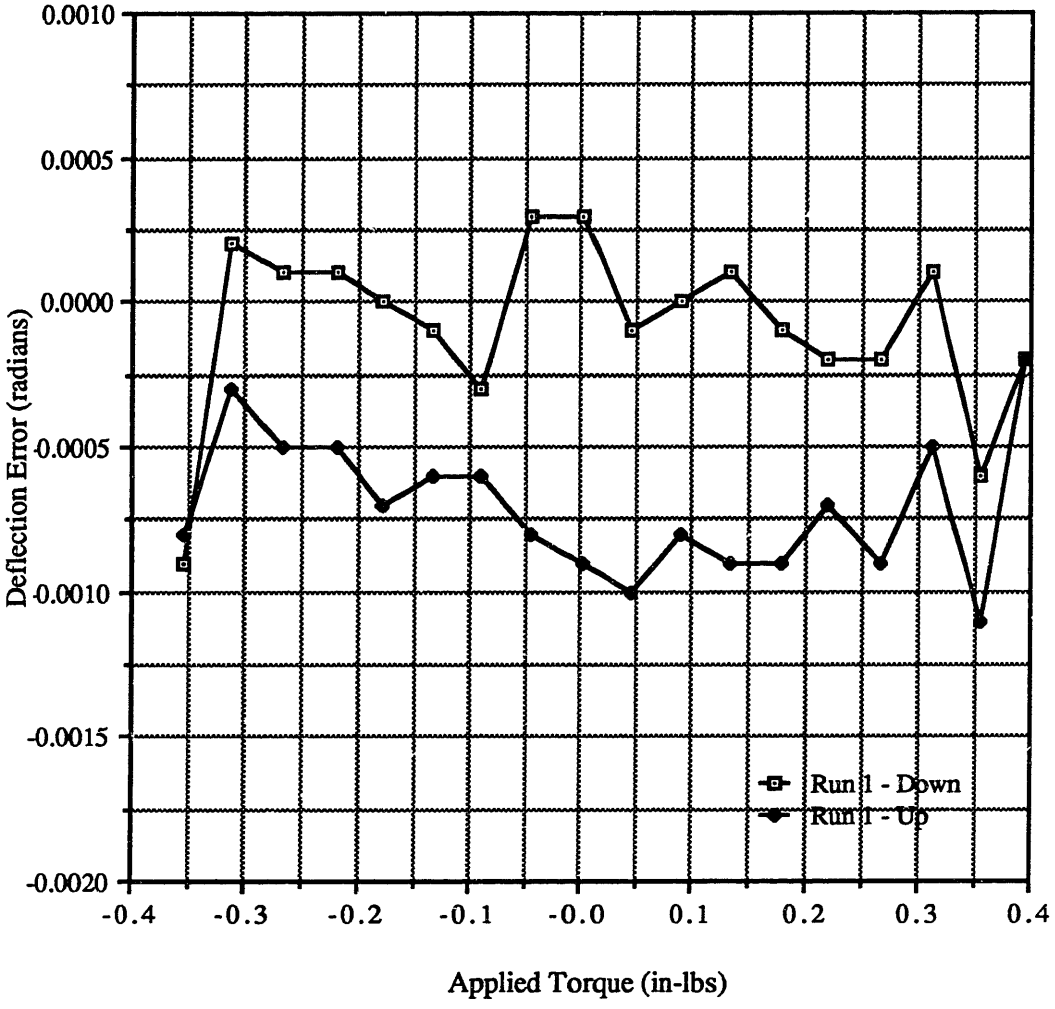

Figure A.41 - Normalized Error Curve for the Y Axis of Flexure 3

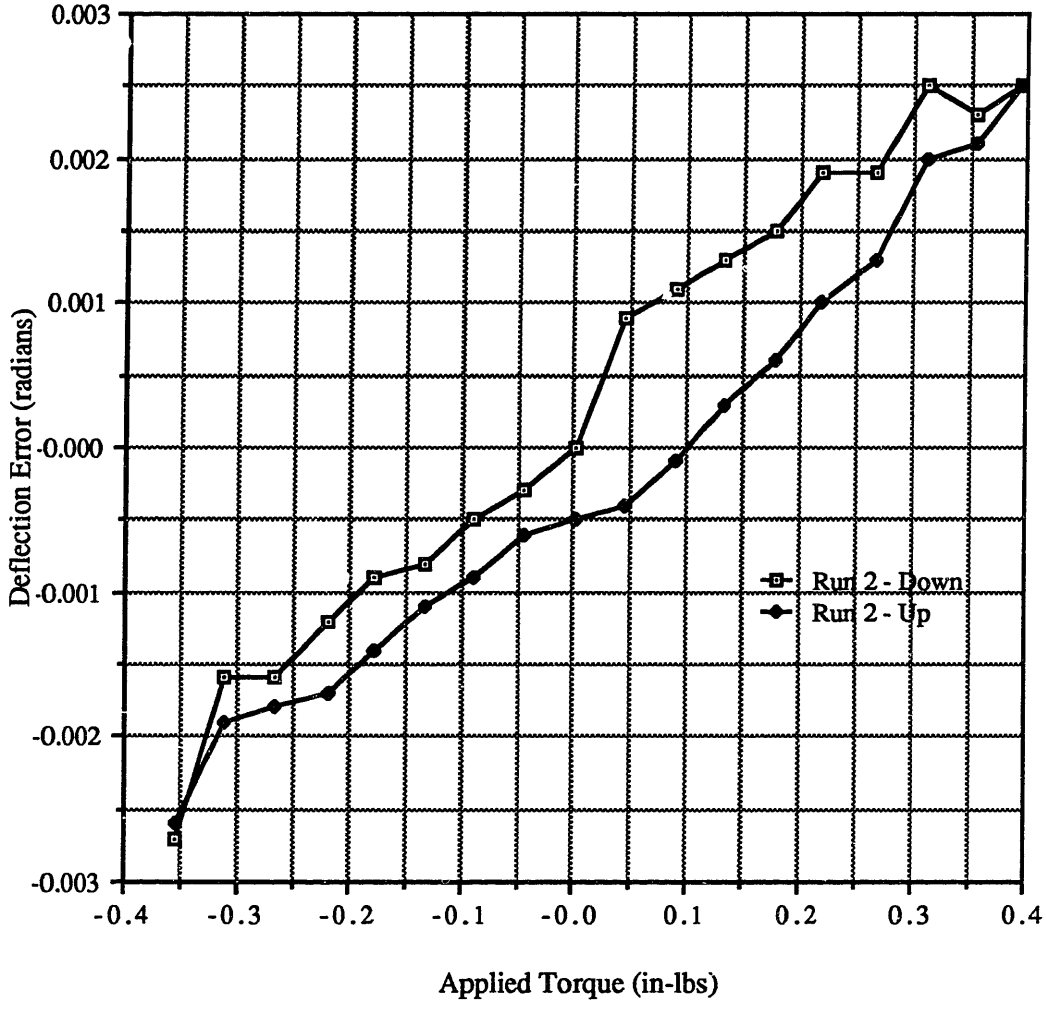

Figure A.42 - Deflection Error vs. Torque for the Y axis of Flexure 3

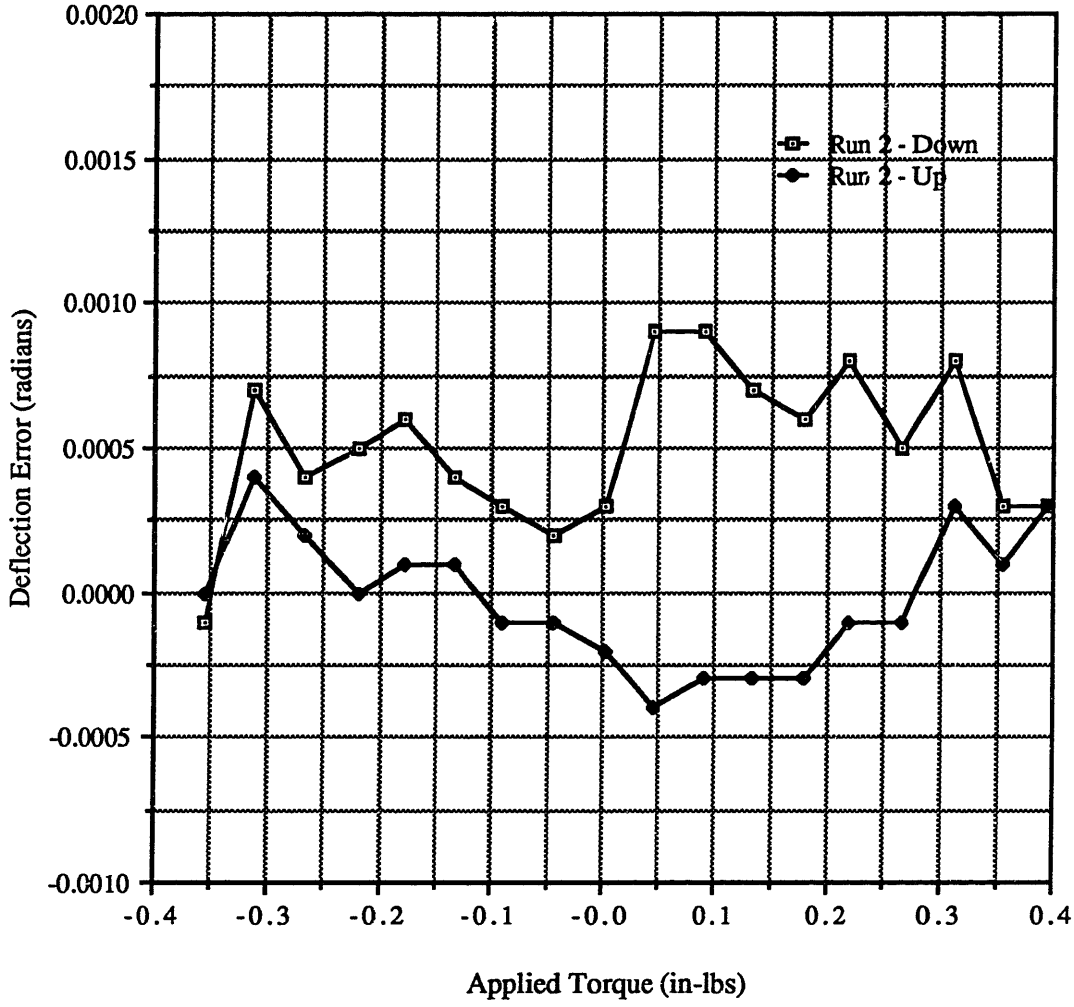

Figure A.43 - Normalized Error Curve for the Y Axis of Flexure 3

Table A.12 - Data from a 45° Offset Axis of Flexure 3

# of Nickels	Applied Torque (in-lbs)	Theoretical Deflection (radians)	Measured Stiffness Deflection (radians)	Deflection Run 1 - Down (radians)	Error from Theoretical Run 1 - Down (radians)	Error from Measured Stiffness Run 1 - Down (radians)	Deflection Run 1 - Up (radians)	Error from Theoretical Run 1 - Up (radians)	Error from Measured Stiffness Run 1 - Up (radians)
1	-0.0440	-0.0105	-0.0114	-0.0114	-0.0009	0.0000	-0.0114	-0.0009	0.0000
2	-0.0886	-0.0211	-0.0229	-0.0228	-0.0018	0.0001	-0.0229	-0.0018	0.0000
3	-0.1325	-0.0315	-0.0342	-0.0340	-0.0026	0.0002	-0.0341	-0.0026	0.0001
4	-0.1785	-0.0424	-0.0460	-0.0459	-0.0036	0.0001	-0.0460	-0.0036	0.0000
5	-0.2175	-0.0517	-0.0561	-0.0558	-0.0044	0.0003	-0.0561	-0.0044	0.0000
6	-0.2656	-0.0632	-0.0685	-0.0683	-0.0052	0.0002	-0.0684	-0.0052	0.0001
7	-0.3112	-0.0740	-0.0802	-0.0798	-0.0059	0.0004	-0.0799	-0.0059	0.0003
8	-0.3540	-0.0842	-0.0913	-0.0913	-0.0073	0.0000	-0.0915	-0.0073	-0.0002
9	-0.3963	-0.0943	-0.1022	-0.1022	-0.0079	0.0000	-0.1022	-0.0079	0.0000
0	0.0000	0.0000	0.0000	0.0000	-0.0004	0.0000	-0.0004	-0.0004	-0.0004
1	0.0440	0.0105	0.0113	0.0116	0.0007	0.0003	0.0112	0.0007	-0.0001
2	0.0886	0.0211	0.0228	0.0232	0.0015	0.0004	0.0226	0.0015	-0.0002
3	0.1325	0.0315	0.0341	0.0344	0.0027	0.0003	0.0342	0.0027	0.0001
4	0.1785	0.0424	0.0460	0.0463	0.0037	0.0003	0.0461	0.0037	0.0001
5	0.2175	0.0517	0.0560	0.0565	0.0045	0.0005	0.0562	0.0045	0.0002
6	0.2656	0.0632	0.0684	0.0686	0.0052	0.0002	0.0684	0.0052	0.0000
7	0.3112	0.0740	0.0802	0.0809	0.0065	0.0007	0.0805	0.0065	0.0003
8	0.3540	0.0842	0.0912	0.0914	0.0069	0.0002	0.0911	0.0069	-0.0001
9	0.0396	0.0943	0.1021	0.1023	0.0080	0.0002	0.1023	0.0080	0.0002

Table A.12 (cont'd) - Data from a 45° Offset Axis of Flexure 3

# of Nickels	Applied Torque (in-lbs)	Theoretical Deflection (radians)	Deflection Run 2 - Down (radians)	Deflection Run 2 - Up (radians)
1	-0.0440	-0.0105	-0.0113	-0.0117
2	-0.0886	-0.0211	-0.0228	-0.0230
3	-0.1325	-0.0315	-0.0341	-0.0344
4	-0.1785	-0.0424	-0.0459	-0.0462
5	-0.2175	-0.0517	-0.0559	-0.0560
6	-0.2656	-0.0632	-0.0684	-0.0684
7	-0.3112	-0.0740	-0.0799	-0.0801
8	-0.3540	-0.0842	-0.0915	-0.0916
9	-0.3963	-0.0943	-0.1025	-0.1025
0	0.0000	0.0000	0.0000	-0.0004
1	0.0440	0.0105		
2	0.0886	0.0211	0.0228	
3	0.1325	0.0315		
4	0.1785	0.0424		0.0457
5	0.2175	0.0517		
6	0.2656	0.0632	0.0683	
7	0.3112	0.0740		
8	0.3540	0.0842		0.0909
9	0.3963	0.0943	0.1019	0.1019

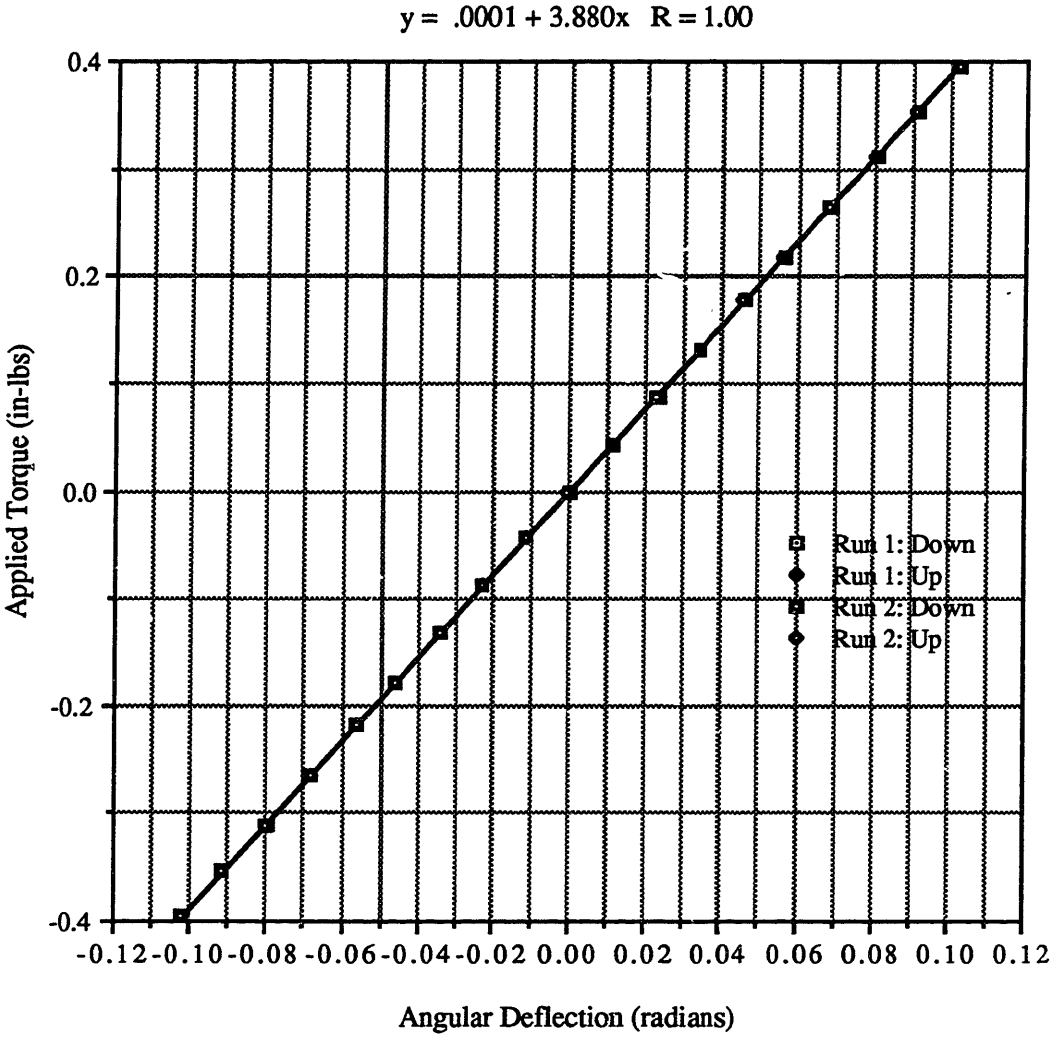

Figure A.44 - Torque vs. Angular Deflection for a 45° Offset Axis of Flexure 3

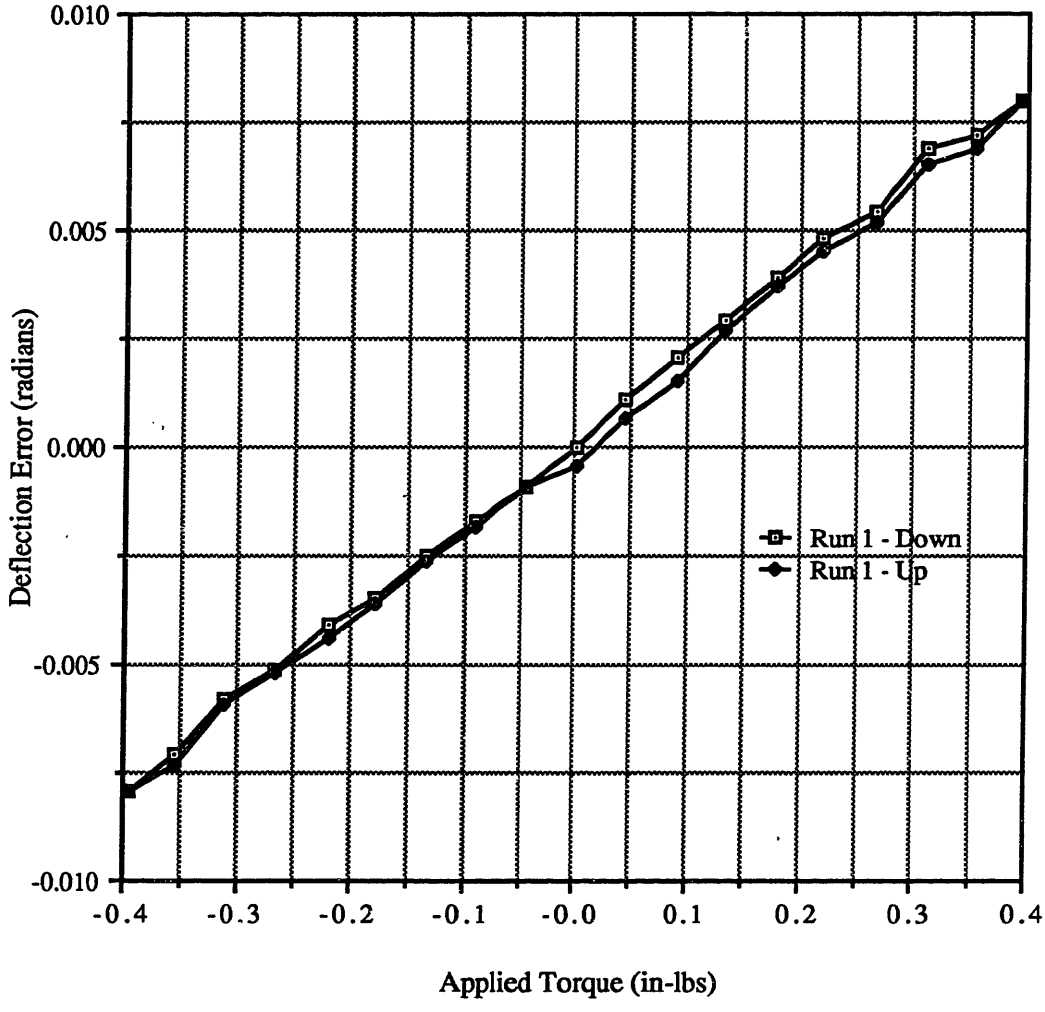

Figure A.45 - Deflection Error vs. Torque for the 45° Offset Axis of Flexure 3

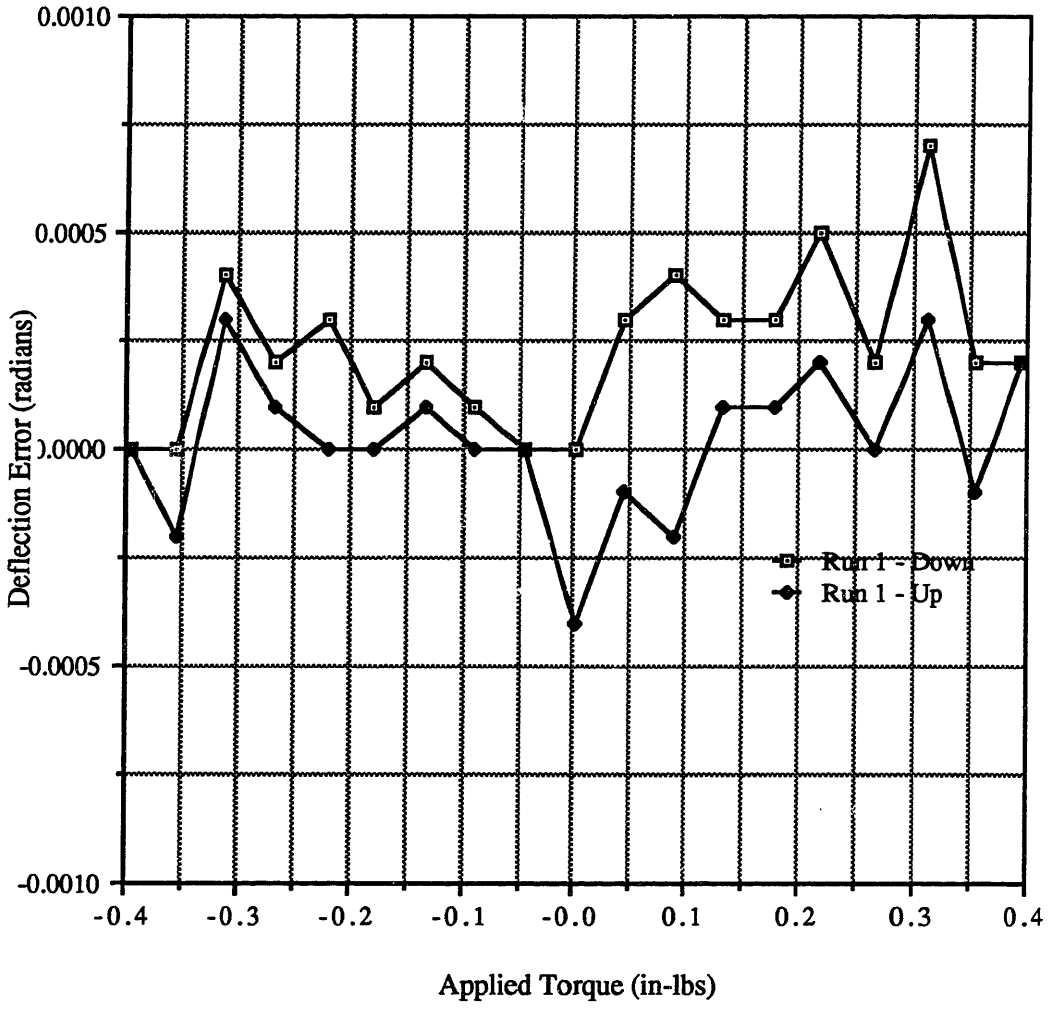

Figure A.46 - Normalized Error Curve for a 45° Offset Axis of Flexure 3

Appendix B
Detail Drawings

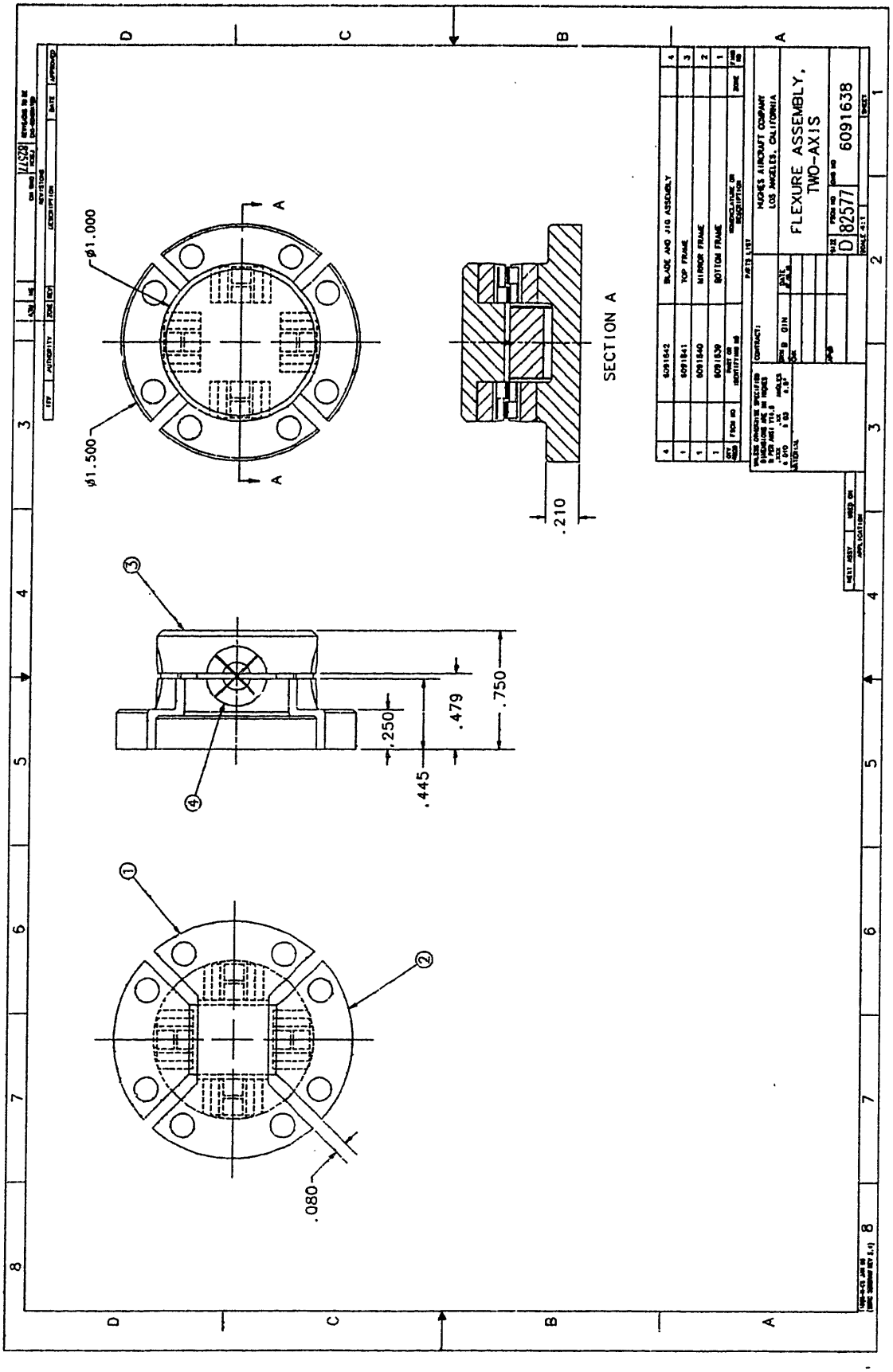
FLEXURE ASSEMBLY, TWO-AXIS
D 82577
6091638
MOOG'S AIRCRAFT COMPANY
LOS ANGELES, CALIFORNIA
SECTION A
ø1.000
ø1.500
.210
.250
.445
.479
.750
.080

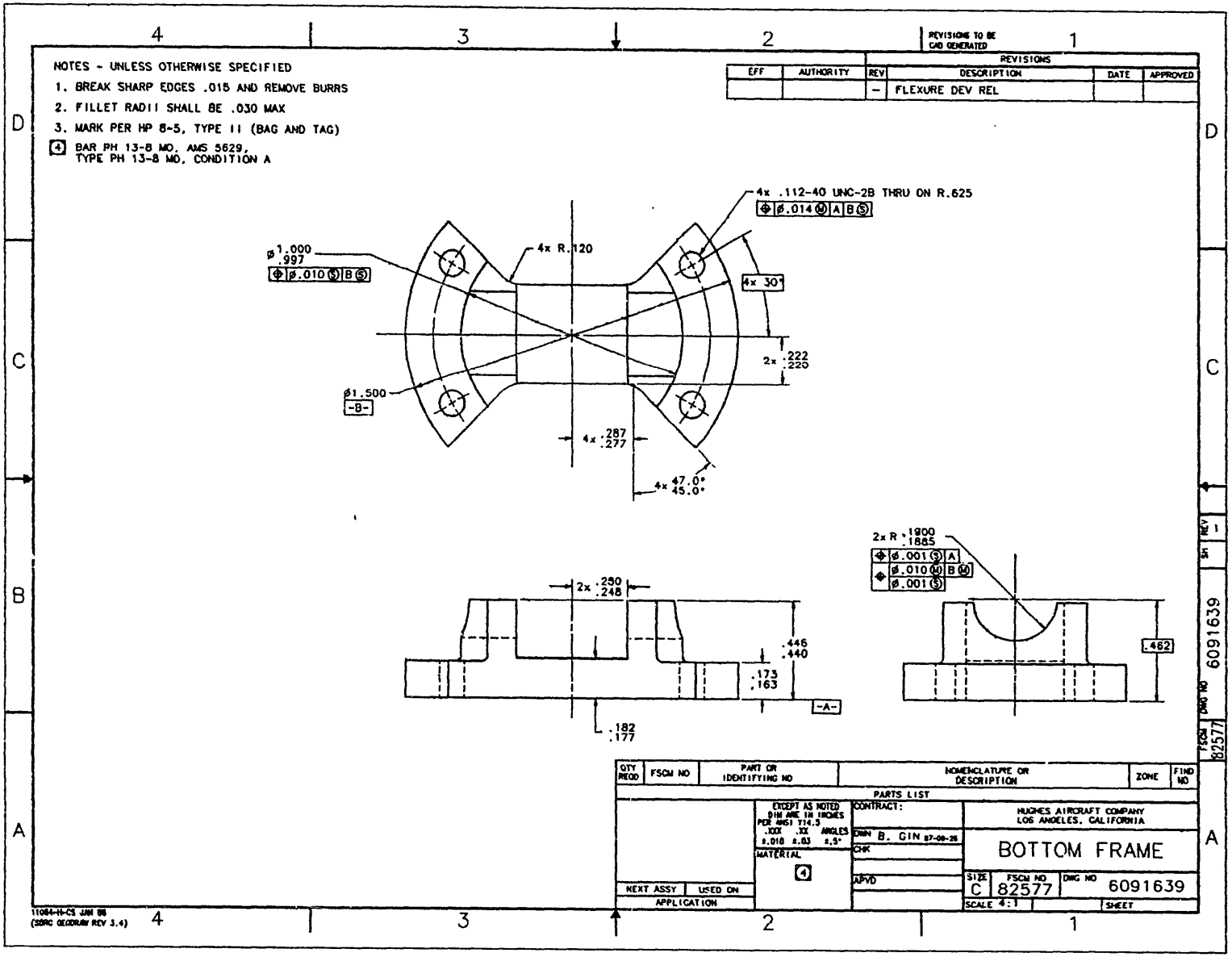
NOTES - UNLESS OTHERWISE SPECIFIED
1. BREAK SHARP EDGES .015 AND REMOVE BURRS
2. FILLET RADII SHALL BE .030 MAX
3. MARK PER MP 8-5, TYPE II (BAG AND TAG)
4 BAR PH 13-8 MO, AMS 5629, TYPE PH 13-8 MO, CONDITION A
REVISIONS
EFF | AUTHORITY | REV | DESCRIPTION | DATE | APPROVED
– FLEXURE DEV REL
4x .112-40 UNC-2B THRU ON R.625
ø.014 M A B S
ø 1.000 .997
ø.010 S B S
4x R.120
4x 30°
2x .222 .220
ø1.500
-B-
4x .287 .277
4x 47.0° 45.0°
2x R .1900 .1885
ø.001 S A
ø.010 M B M
ø.001 S
2x .250 .248
.446 .440
.173 .163
-A-
.182 .177
.462
QTY REQD | FSCM NO | PART OR IDENTIFYING NO | NOMENCLATURE OR DESCRIPTION | ZONE | FIND NO
PARTS LIST
EXCEPT AS NOTED DIM ARE IN INCHES PER ANSI Y14.5
.XXX ±.010 .XX ±.03 ANGLES ±.5°
MATERIAL
4
NEXT ASSY | USED ON
APPLICATION
CONTRACT:
DWN B. GIN 87-08-28
CHK
APVD
HUGHES AIRCRAFT COMPANY
LOS ANGELES, CALIFORNIA
BOTTOM FRAME
SIZE C | FSCM NO 82577 | DWG NO 6091639
SCALE 4:1 | SHEET
SH | REV | DWG NO 6091639 | FSCM 82577
11084-H-CS JAN 88
(SDRC GEODRAW REV 3.4)

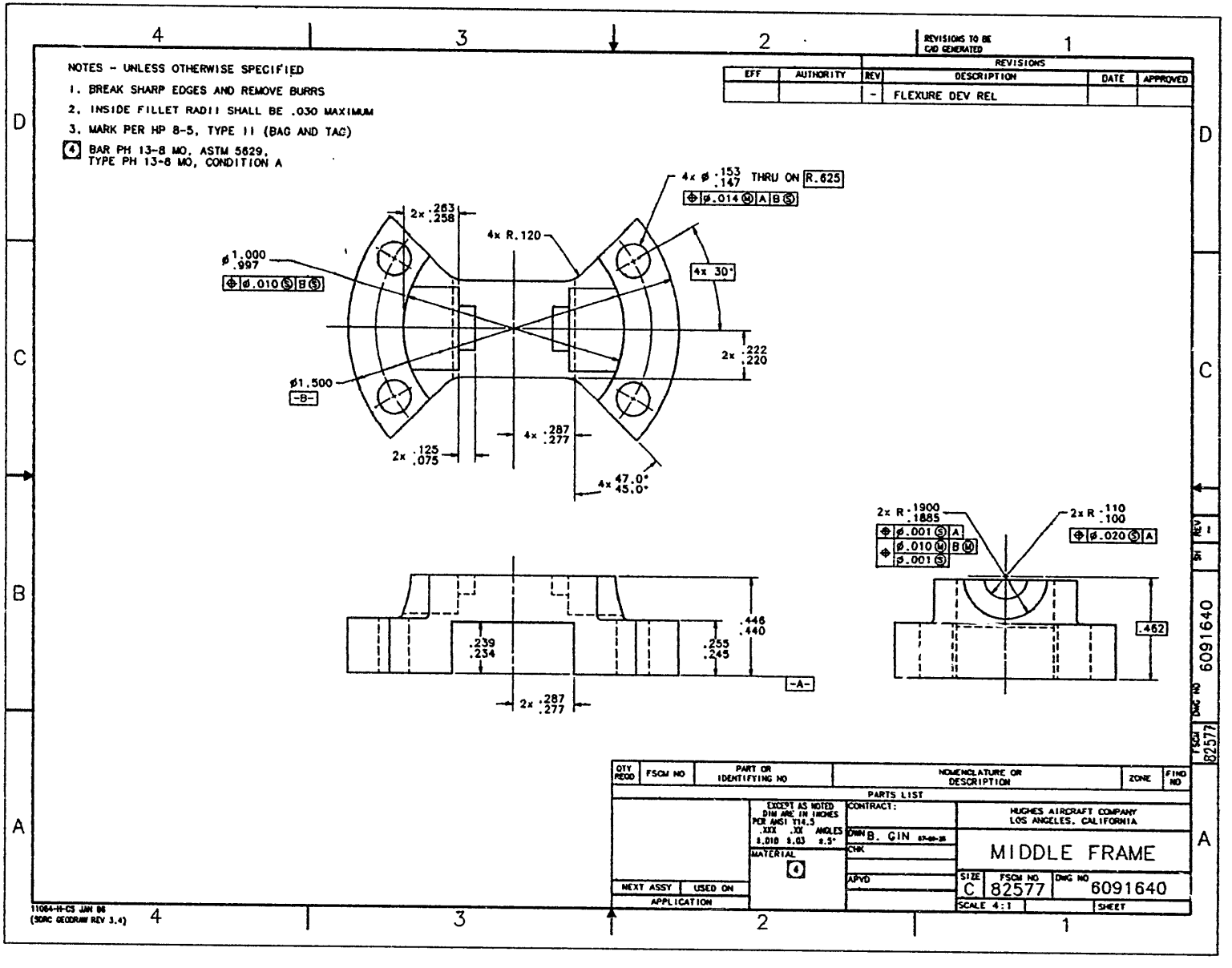
NOTES - UNLESS OTHERWISE SPECIFIED
1. BREAK SHARP EDGES AND REMOVE BURRS
2. INSIDE FILLET RADII SHALL BE .030 MAXIMUM
3. MARK PER MP 8-5, TYPE II (BAG AND TAG)
4 BAR PH 13-8 MO, ASTM 5629, TYPE PH 13-8 MO, CONDITION A
REVISIONS TO BE CAD GENERATED
REVISIONS
EFF | AUTHORITY | REV | DESCRIPTION | DATE | APPROVED
- FLEXURE DEV REL
4x ø .153 .147 THRU ON R.625
ø.014 M A B S
2x .263 .258
4x R.120
ø1.000 .997
ø.010 S B S
4x 30°
2x .222 .220
ø1.500
-B-
2x .125 .075
4x .287 .277
4x 47.0° 45.0°
.446 .440
.239 .234
.255 .245
-A-
2x .287 .277
2x R .1900 .1885
ø.001 S A
ø.010 M B M
ø.001 S
2x R .110 .100
ø.020 S A
.462
QTY REQD | FSCM NO | PART OR IDENTIFYING NO | NOMENCLATURE OR DESCRIPTION | ZONE | FIND NO
PARTS LIST
EXCEPT AS NOTED DIM ARE IN INCHES PER ANSI Y14.5
XXX ±.010 XX ±.03 ANGLES ±.5°
MATERIAL 4
CONTRACT:
DWN B. GIN
CHK
APVD
HUGHES AIRCRAFT COMPANY LOS ANGELES, CALIFORNIA
MIDDLE FRAME
SIZE C | FSCM NO 82577 | DWG NO 6091640
SCALE 4:1 | SHEET
NEXT ASSY | USED ON
APPLICATION
11084-H-C3 JAN 86 (SDRC GEODRAW REV 3.4)
REV -
DWG NO 6091640
FSCM 82577

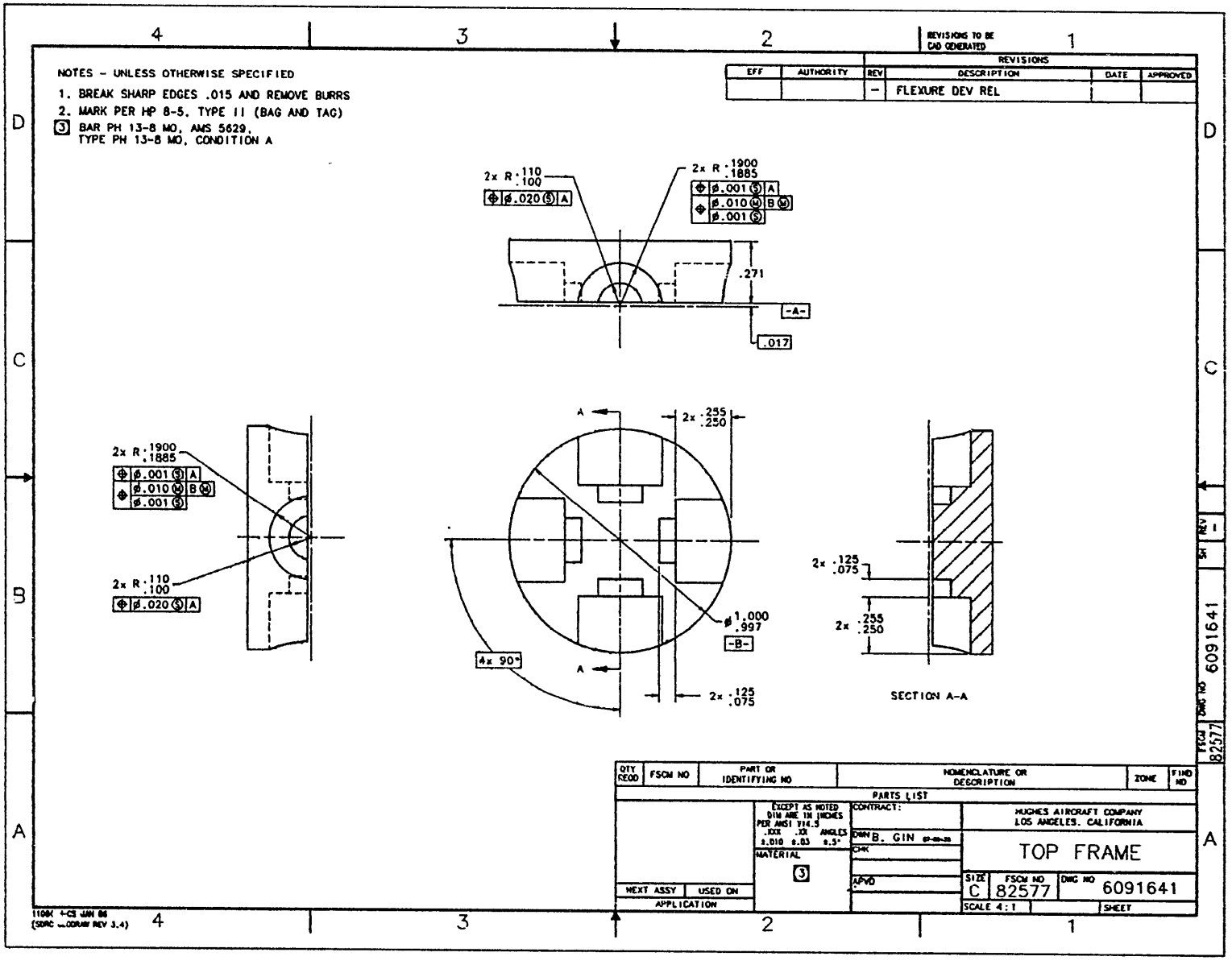
REVISIONS TO BE CAD GENERATED
REVISIONS
EFF | AUTHORITY | REV | DESCRIPTION | DATE | APPROVED
– | FLEXURE DEV REL
NOTES – UNLESS OTHERWISE SPECIFIED
1. BREAK SHARP EDGES .015 AND REMOVE BURRS
2. MARK PER MP 8-5, TYPE II (BAG AND TAG)
3 BAR PH 13-8 MO, AMS 5629, TYPE PH 13-8 MO, CONDITION A
2x R .110 .100
⌖ ø.020 Ⓢ A
2x R .1900 .1885
⌖ ø.001 Ⓢ A
ø.010 Ⓜ B Ⓜ
ø.001 Ⓢ
.271
-A-
.017
2x R .1900 .1885
⌖ ø.001 Ⓢ A
ø.010 Ⓜ B Ⓜ
ø.001 Ⓢ
2x R .110 .100
⌖ ø.020 Ⓢ A
A
2x .255 .250
ø 1.000 .997
-B-
4x 90°
2x .125 .075
2x .125 .075
2x .255 .250
SECTION A-A
QTY REQD | FSCM NO | PART OR IDENTIFYING NO | NOMENCLATURE OR DESCRIPTION | ZONE | FIND NO
PARTS LIST
EXCEPT AS NOTED DIM ARE IN INCHES PER ANSI Y14.5
.XXX .XX ANGLES
±.010 ±.03 ±.5°
MATERIAL
3
CONTRACT:
DWN B. GIN
CHK
APVD
HUGHES AIRCRAFT COMPANY LOS ANGELES, CALIFORNIA
TOP FRAME
SIZE C | FSCM NO 82577 | DWG NO 6091641
SCALE 4:1 | SHEET
NEXT ASSY | USED ON
APPLICATION
FSCM 82577 DWG NO 6091641 SH – REV –

NOTES - UNLESS OTHERWISE SPECIFIED

1. BRAZE PER MIL-B-7883, TYPE II, GRADE B USING FILLER METAL BAU-3 PER AWS A5.8

REVISIONS TO BE CAD GENERATED

REVISIONS					
EFF	AUTHORITY	REV	DESCRIPTION	DATE	APPROVED
		-	FLEXURE DEV REL		

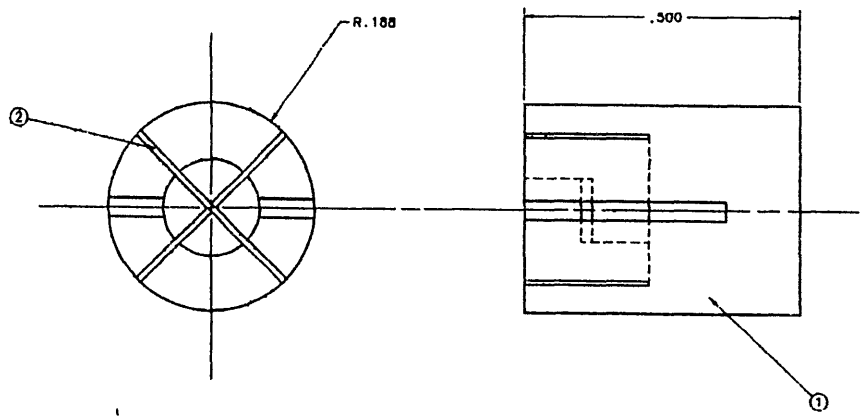

QTY REQD	FSCM NO	PART OR IDENTIFYING NO	NOMENCLATURE OR DESCRIPTION	ZONE	FIND NO
2		6091643	FLEXURE BLADE		2
1		6091644	BLADE JIG		1

PARTS LIST

EXCEPT AS NOTED DIM ARE IN INCHES PER ANSI Y14.5
.XXX ±.010 .XX ±.03 ANGLES ±.5°

MATERIAL

NEXT ASSY | USED ON
APPLICATION

CONTRACT:

DWN B. GIN

CHK

APVD

HUGHES AIRCRAFT COMPANY
LOS ANGELES, CALIFORNIA

BLADE AND JIG ASSEMBLY

SIZE C | FSCM NO 82577 | DWG NO 6091642

SCALE 8:1 | SHEET

DWG NO 6091642 | REV - | SH | FSCM 82577

11084-H-CS JAN 88
(SDRC GEODRAW REV 3.4)

NOTES - UNLESS OTHERWISE SPECIFIED

1. BREAK SHARP EDGES AND REMOVE BURRS
2. MARK PER HP 8-5, TYPE II (BAG AND TAG)
3. BAR PH-13-8 MO, AMS 5629, TYPE PH 13-8 MO, CONDITION A

REVISIONS					
EFF	AUTHORITY	REV	DESCRIPTION	DATE	APPROVED
		–	FLEXURE DEV REL		

REVISIONS TO BE CAD GENERATED

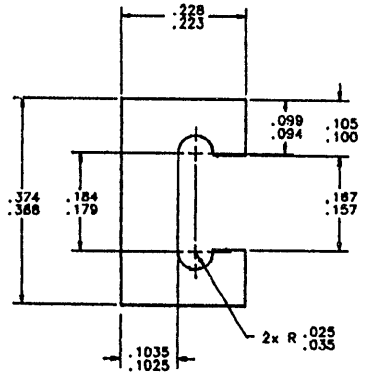

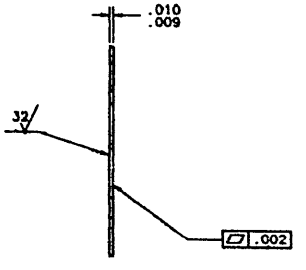

QTY REQD	FSCM NO	PART OR IDENTIFYING NO	NOMENCLATURE OR DESCRIPTION	ZONE	FIND NO

PARTS LIST

EXCEPT AS NOTED DIM ARE IN INCHES PER ANSI Y14.5
.XXX ±.010 .XX ±.03 ANGLES ±.5°

MATERIAL 3

NEXT ASSY | USED ON
APPLICATION

CONTRACT:

DWN B. GIN

CHK

APVD

HUGHES AIRCRAFT COMPANY
LOS ANGELES, CALIFORNIA

FLEXURE BLADE

SIZE	FSCM NO	DWG NO
C	82577	6091643

SCALE 8:1 SHEET

11084-H-CS JAN 88
(BORG GEODRAW REV 3.4)

FSCM 82577 DWG NO 6091643 REV – SH

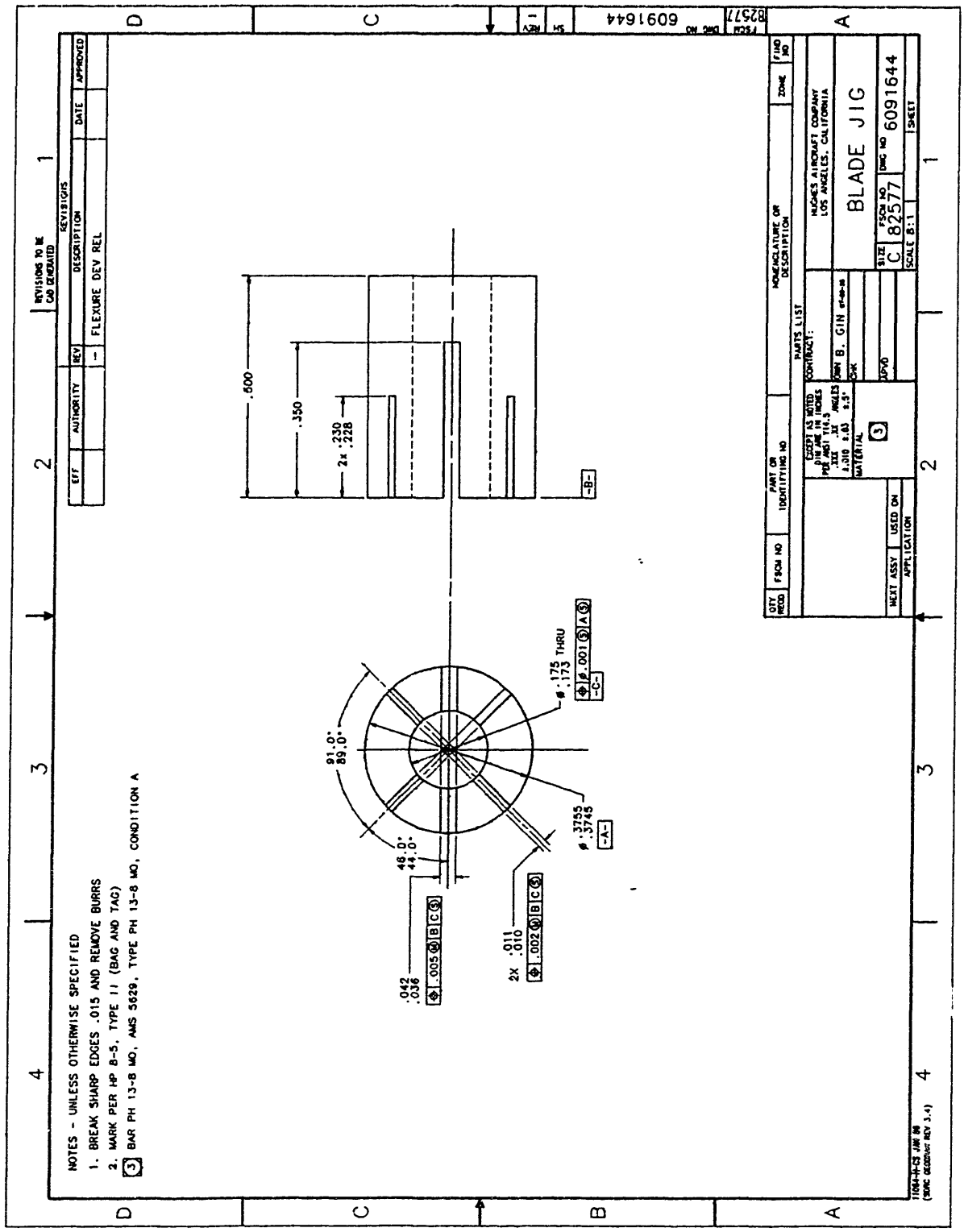
BLADE JIG
6091644
C
82577
HUGHES AIRCRAFT COMPANY
LOS ANGELES, CALIFORNIA
NOTES - UNLESS OTHERWISE SPECIFIED
1. BREAK SHARP EDGES .015 AND REMOVE BURRS
2. MARK PER MP 8-5, TYPE II (BAG AND TAG)
3 BAR PH 13-8 MO, AMS 5629, TYPE PH 13-8 MO, CONDITION A
.600
.350
2x .230
.228
.175 THRU
.173
.3755
.3745
2X .011
.010
.042
.036
46.0°
44.0°
91.0°
89.0°
-A-
-B-
-C-